Global renormalization group theoretic studies on liquid vapor phase transitions

By

A. Sai Venkata Ramana

PHYS01201104012

Bhabha Atomic Research Centre, Trombay, Mumbai.

A thesis submitted to the

Board of Studies in Physical Sciences

In partial fulfillment of requirements

For the Degree of

DOCTOR OF PHILOSOPHY

of

HOMI BHABHA NATIONAL INSTITUTE

2016

Homi Bhabha National Institute
Recommendations of the Viva Voce Board

As members of Viva Voce Board, we certify that we have read the dissertation prepared by "**A. Sai Venkata Ramana**" entitled "**Global renormalization group theoretic studies on liquid vapor phase transitions**" and recommend that it may be accepted as fulfilling the thesis requirement for the award of Degree of Doctor of Philosophy.

Chairman- Dr N. K. Gupta
Bhabha Atomic Research Centre
Trombay, Mumbai, Maharashtra - 400085, India

_____ **Date:**

Guide- Dr D. M. Gaitonde
Bhabha Atomic Research Centre
Trombay, Mumbai, Maharashtra - 400085, India

_____ **Date:**

Examiner- Dr Surajit Sengupta
Tata Institute of Fundamental Research, Centre for Interdisciplinary sciences,
21, Brindavan Colony,Gandipeta Road, Hyderabad, Telangana - 500075, India

_____ **Date:**

Member- Dr Dibyendu Das
Indian Institute of Technology Bombay
Mumbai, Maharashtra, India

_____ **Date:**

Member- Dr Aditi Ray
Bhabha Atomic Research Centre
Trombay, Mumbai - 400085, Maharashtra, India

_____ **Date:**

Final approval and acceptance of this dissertation is contingent upon the candidate's submission of the final copies of the dissertation to HBNI.
I hereby certify that I have read this dissertation prepared under my direction and recommend that it may be accepted as fulfilling the dissertation requirement.

Guide-

Date: **Place: Mumbai**

STATEMENT BY AUTHOR

This dissertation has been submitted in partial fulfillment of requirements for an advanced degree at Homi Bhabha National Institute (HBNI) and is deposited in the Library to be made available to borrowers under rules of the HBNI.

Brief quotations from this dissertation are allowable without special permission, provided that accurate acknowledgement of source is made. Requests for permission for extended quotation from or reproduction of this manuscript in whole or in part may be granted by the Competent Authority of HBNI when in his or her judgment the proposed use of the material is in the interests of scholarship. In all other instances, however, permission must be obtained from the author.

A. Sai Venkata Ramana

DECLARATION

I, *A. Sai Venkata Ramana*, hereby declare that the investigation presented in the thesis has been carried out by me. The work is original and has not been submitted earlier as a whole or part for a degree/diploma at this or any other Institution/University.

A. Sai Venkata Ramana

List of publications

International Journals

Publications related to Thesis :

1. A. S. V. Ramana, and S. V. G. Menon. "Generalized approach to global renormalization-group theory for fluids." **Physical Review E** 85.4 (2012): 041108.

2. A. S. V. Ramana, and S. V. G. Menon. "Coupling-parameter expansion in thermodynamic perturbation theory." **Physical Review E** 87.2 (2013): 022101.

3. A. S. V. Ramana, "Generalized coupling parameter expansion: Application to square well and Lennard-Jones fluids." **The Journal of chemical physics** 139.4 (2013): 044106.

4. A. S. V. Ramana, "On equivalence of high temperature series expansion and coupling parameter series expansion in thermodynamic perturbation theory of fluids." **The Journal of Chemical Physics** 140.15 (2014): 154106.

5. A. S. V. Ramana, "Molecular dynamics simulation of liquidvapor phase diagrams of metals modeled using modified empirical pair potentials." **Fluid Phase Equilibria** 361 (2014): 181-187.

6. A. S. V. Ramana, "Application of renormalization group corrected coupling parameter expansion method to square well fluids." **Physica A: Statistical Mechanics and its Applications** 442 (2016), 137-148.

Other Publications :

1. A. S. V. Ramana, and S. V. G. Menon. "Application of the EnglertSchwinger model to the equation of state and the fullerene molecule." **Physica A: Statistical Mechanics and its Applications** 390.9 (2011): 1575-1584.

2. A. S. V. Ramana, "Molecular Dynamics Simulation of Liquid-Vapor Coexistence Curves of Metals." **Journal of Physics: Conference Series**. Vol. 377. No. 1. IOP Publishing, 2012.

3. Shukla, N., Tripathi, S. K., Banerjee, A., Ramana, A. S. V., Rajput, N. S., Kulkarni, V. N. . Study of temperature rise during focused Ga ion beam irradiation using nanothermo-probe. **Applied Surface Science**, 256, 475(2009).

4. A. S. V. Ramana, "An OrbitalFree Quantum Hypernetted Chain Model Based Perturbation Theory for Equation of State of Hydrogen and Helium in Warm Dense Regime", **Contributions to Plasma Physics** 55(2015), 606-618.

To my parents

A Rama Murthy and *A Ahalya Devi*

.

Acknowledgements

I am grateful to Dr. S. V. G. Menon for mentoring me as a researcher. My confidence in attacking problems comes from the training I received from him. I am extremely thankful to my guide Dr. D. M. Gaitonde for the support, guidance and encouragement he gave me. I acknowledge the interesting discussions we had. I thank my doctoral committee chairman Dr. N. K. Gupta, members Dr. Swapan Ghosh, Dr. Aditi Ray and Dr. Dibyendu Das and dean Physics Dr. Saibal Basu for support. I thank Dr. D. Biswas, Dr. Raghwendra Kumar and Dr. H. D. Parab for stimulating discussions.

I pay obeisance to my parents Shri A. Rama Murthy and Smt. A. Ahalya devi and dedicate the thesis to them. I thank my brother Sarath Kumar, sisters Durga Bhavani and Savitri Devi for their encouragement. Most importantly, I thank my wife Madhuri Priyanka for her support at home without which I could not have completed my thesis. All through academic career I have been guided, helped and motivated by many teachers, friends, relatives and well-wishers. I remember each one of them and express my gratitude to them.

Synopsis

Introduction

Equations of state(EOS) of fluids have wide applications in the fields of high energy density physics, astrophysics and in chemical physics. For example, in high energy density physics experiments, the system passes through states with widely varying densities and temperatures which include the fluid state of the material. Hydrodynamic simulation of those experiments requires EOS of the materials involved. Another example is the fluid extraction process in chemical technology which requires the liquid vapor phase diagrams of the fluids. Because of such applications, an accurate knowledge of EOS and phase transitions of materials in the fluid state is an important requirement.

The available theoretical methods to obtain thermodynamic properties of fluids can be broadly divided into two categories. They are, (i) computer simulations (molecular dynamics and Monte Carlo methods) and (ii) semi-analytical methods based on classical statistical mechanics (e.g. perturbation theory, integral equation theory etc). The ab-initio simulations, like ab-initio molecular dynamics[1,2], although accurate, require huge computational time and it is currently impossible to generate EOS data libraries using these methods. The classical molecular dynamics or Monte-Carlo simulations[3] which require the interaction potential between the particles as input are relatively much faster than ab-initio simulations but even so it is still impractical to use the classical simulation methods to generate EOS data libraries. However, the results obtained using these methods may be used for comparison purposes as a benchmark to assess the reliability of semi-analytical methods.

Among the semi-analytical methods based on classical statistical mechanics, two different approaches are prominent. One is based on a self-consistent solution of the Ornstein-Zernike equation and an approximate closure, both of which relate the radial distribution function and the direct correlation func-

tion. This approach, called the integral equation theory[4], gives the structural properties of the fluid like radial distribution function etc. at a given temperature and density. Using the knowledge of structural properties, the EOS can be obtained either in virial route relating pressure to radial distribution function, or in energy route relating internal energy to radial distribution function or in the compressibility route relating the isothermal compressibility to direct correlation function. However, it has been observed that the EOSs obtained using these three routes are inconsistent with one another because of the approximate closure used. It has also been found that the Ornstein-Zernike equation doesn't have a solution in the phase transition region[5]. The second kind of approach is the thermodynamic perturbation theory[4] in which a system whose properties are known is taken as reference and the properties of the system under consideration are obtained as a perturbation over those of the reference system. Thus a given thermodynamic quantity, for example, the Helmholtz free energy is written as a series in which each term depends on the distribution functions of the reference system. This series is called the high temperature series. The n^{th} term in the series depends on distribution functions up to order $2n$. Since it is not possible to obtain distribution functions of order more than two, only the first term of the series can be calculated exactly if the radial distribution function of the reference system is known. To calculate the second order term approximately, Barker and Henderson suggested an approximation called the local compressibility approximation[6]. However, for potentials with short range, the local compressibility approximation method was not accurate[7]. Apart from this, the thermodynamic perturbation theory and the integral equation theory, being mean field theories, do not account for fluctuations which become important close to the critical region. Also, the isotherms obtained using these methods are unphysical in the coexistence region and have to be corrected. In the recent past, a method has been proposed by White[8] to include the fluctuation contribution to the Helmholtz free energy of a fluid. The method, which is called Global Renormalization Group

Theory (GRGT), takes the mean field free energy as input and improves over it by adding contributions from fluctuations in a step-by-step manner. It was claimed that the method improved the accuracy of EOS throughout the liquid vapor phase diagram apart from giving correct description in the critical region. However , the method required some parameters to be adjusted and lacked a rigorous formulation.

In spite of the deficiencies in the theories described above, the calculations are simpler and faster than the simulations by orders of magnitude. This advantage makes the methods suitable for large scale EOS calculations. However, there is scope for improvement of accuracy of the methods which forms the basis of our work. We found that the GRGT is a suitable starting point for our study as the method attempts to evaluate the partition function in a more accurate manner and gives a qualitatively correct description of physics throughout the phase diagram.

Brief account of work done

The aim of our study is to develop and implement accurate methods to obtain the EOS of fluids. In a nutshell, the study we carried out is the following:

1. The GRGT is derived in a generalized way starting from the square-gradient functional for the Helmholtz free energy[9] and using Wilson's phase space cell approach[10]. The method is applied to square-well and Lennard-Jones fluids. It is observed that the isotherms become flat in the two-phase region after GRGT correction. Also an improvement in accuracy is observed in the obtained liquid vapor phase diagrams in the critical region. However, the applications showed that the results obtained using GRGT are sensitive to the assumed initial coarse-graining length scale in the method[11]. We concluded that the mean field Helmholtz free energy and the coefficient of the square-gradient term in the Helmholtz free energy functional (called influence parameter) used in the GRGT calculations were inaccurate and their inaccu-

racy was the reason for sensitivity of GRGT results to the initial coarse-graining length scale.

2. We combined the ideas of thermodynamic perturbation theory and integral equation theory and developed a method to obtain a perturbation series for the mean field Helmholtz free energy , radial distribution function and other structure related functions. The method is based on introducing a coupling parameter [1] in the pair potential and expanding the correlation functions and Helmholtz free energy as a series in the coupling parameter. The terms in the Coupling Parameter Expansion (CPE) are obtained using the integral equation theory. In this work, we assumed that the bridge function[4] required to solve the Ornstein-Zernike equation does not depend on the coupling parameter. We applied our method to the square-well fluid with hard-sphere fluid as the reference system assuming an empirical form for the closure given by Malijevsky and Labik[12] to solve the Ornstein-Zernike equation. Using the new method, we obtained the radial distribution function and the Helmholtz free energy of square-well fluids of various ranges at various temperatures and densities and also their liquid vapor phase diagrams. The new method improved the results enormously over those obtained using existing perturbation methods[13] when compared with available simulation data. However, we observed that the coexistence region becomes too narrow close to the critical region as compared to the simulation data.

3. The perturbation method we developed is generalized[14] by relaxing the assumptions mentioned in point 2 so that it can be applied to any pair potential. The method is applied to square-well and Lennard-Jones fluids and liquid vapor phase diagrams are obtained. We also obtained the influence parameter and calculated the surface tension of square-well fluids of various ranges as a function of temperature. The obtained results are compared with available simulation data and are found to improve the agreement over the earlier calculations in point 2.

[1] The coupling parameter switches on and off the perturbation when varied from 1 to 0.

4. We showed the equivalence of the CPS obtained within our method to that of high temperature series [4,15] for pairwise additive interaction potentials[18]. As a consequence of the equivalence, we showed that the terms of the coupling parameter series scale inversely with temperature if the repulsive part of the potential has a hard-core.

5. We used the improved Helmholtz free energy and influence parameter, obtained using the perturbation theory we developed, in the GRGT and applied it to square-well fluids. We obtained the critical exponents using our method and observed that they are non-classical (differing from mean field) and belong to the Ising universality class, conforming to the earlier observations[8]. We also studied the Yang-Yang anomaly[16,17] in square-well fluids using the GRGT. All the obtained results[19] were found to be an improvement with respect to the perturbation method outlined in points 2 and 3 in the critical region when compared with available simulation data.

6. Application of the GRGT to realistic systems requires the inter-atomic pair potentials to be known. We obtained the parameters of empirical pair potentials of simple metals (Sodium and Potassium) using the cold curve[20]. The cold curves have been obtained using the density functional theory based code VASP[2]. The same potentials have been studied in GRGT as well as classical molecular dynamics and the obtained liquid vapor phase diagrams have been compared with experiments. The results of GRGT were found to be in good agreement with simulation results validating the GRGT method. GRGT and simulation results with our emiprical potentials were found to be in closer agreement with expriments than results from other pair potentials existing in the literature[21].

Organization of thesis

The thesis is organized as follows:
In chapter 1, we discuss the various existing liquid state theories(integral equation theory, thermodynamic perturbation theory and renormalization group theory) in detail. The current status of the methods is briefly reviewed and a basis is set for the study we carry out in further chapters. An outline of the thesis is given.

In chapter 2, we derive the GRGT starting from the square gradient functional using Wilson's phase space approach[10]. Numerical implementation of the method is described with application to square-well and Lennard-Jones fluids. The obtained results are compared with simulation data from literature and analyzed.

We discuss the method we developed to obtain terms of the CPE in chapter 3. Initially, a simplified version of the method is discussed and applied to square-well fluids. The results are compared with those of simulations from literature and are analyzed. Later, a generalized version is described and applied to square-well and Lennard-Jones fluids. The results of generalized version are compared with available simulation data and earlier results. Also, application of the method to obtain surface tension is explained and applied to square-well fluids.

In chapter 4, we show that the CPE and the perturbation series obtained by Zwanzig are equivalent in the case of pairwise additive interaction potentials. The consequences of equivalence are discussed.

The CPE method is combined with the GRGT and applied to square-well fluids in chapter 5. Application of the CPE+GRGT to study equation of state, critical exponents and Yang-Yang anomaly is discussed and the results are analyzed.

In chapter 6, we describe a method to obtain parameters of pair potentials of simple metals using their ab-initio cold curves. Details of obtaining the cold

curve from ab-initio calculations are provided. The potentials have been obtained for Potassium and Sodium. Details of the classical molecular dynamics simulations we did to obtain the liquid vapor coexistence data using the pair potentials are presented. Finally, application of the CPE+GRGT method to these metals using the above developed potentials is described. The results are compared with the simulation and experimental data and analyzed.

The thesis is concluded in chapter 7. Main conclusions of the thesis are summarized here. A discussion on future work is given.

1. 1 R. Car and M. Parrinello, Phys. Rev. Lett. 55, 2471 (1985);

2. 2 G. Kresse; J. Hafner, Phys. Rev. B 47, (1993) 558-561; G. Kresse, Furthmuller, J. Computat Mater Sci 6, (1996) 15-60; G. Kresse, Furthmuller, Phys. Rev. B 54, (1996) 11169-11186; G. Kresse,D. Joubert, Phys Rev B 59, (1999) 1758-1775.

3. 3 M. P. Allen and D. J. Tildesley, Computer Simulation of Liquids (Clarendon Press, Oxford, 1987; reprinted 1990).

4. 4 J. P. Hansen and I. R. McDonald, Theory of Simple Liquids (Academic Press, London, 2006).

5. 5 P. M. W. Cornelisse, C. J. Peters and J. de Swaan Arons, J. Chem. Phys. 106, 9820 (1997) and references therein.

6. 6 J. A. Barker and D. henderson, J. Chem. Phys. 47, 2856(1967); Rev. Mod. Phys., 48, 587, 1976.

7. 7 Praestgaard, E.; Toxvaerd, S. J. Chem. Phys. 1969, 51, 1895.

8. 8 J. A. White, J. Chem. Phys. 112, 3236 (2000), J. A. White, J. Chem. Phys. 113, 1580 (2000).

9. 9 R. Evans, Adv. in Phys. 28, 143(1979).

10. 10 S. V. G. Menon, "Renormalization Group Theory of Critical Phenomena, IPA Monographs in Physics, Wiley Eastern Ltd. 1995".

11. 11 A. S. V. Ramana and S. V. G. Menon. Phys Rev E 85 041108 (2012).

12. 12 A.Malijvesky and S. Labik, Mol. Phys. 60, 663 (1987).

13. 13 A. S. V. Ramana and S. V. G. Menon, Phys. Rev. E 87 022101 (2013).

14. 14 A. S. V. Ramana, J. Chem. Phys. 139, 044106 (2013).

15. 15 R. W. Zwanzig, J. Chem. Phys. 22, 1420(1954).

16. 16 C. N. Yang and C. P. Yang, Phys. Rev. Lett. 13, 303(1964).

17. 17 M. E. Fisher and G. Orkoulas, Phys. Rev. Lett. 85, 696(2000).

18. 18A. S. V. Ramana, J. Chem. Phys. 140, 154106 (2014).

19. 19 A. S. V. Ramana, Physica A 442 , 137(2016).

20. 20 A. S. V. Ramana, Fluid Phase Equilibria 361, 181 (2014).

21. 21 J. K. Singh , J. Adhikari , S. K. Kwak, Fluid Phase Equilibria 248, 1 (2006).

List of Acronyms

RDF - Radial Distribution Function

DCF - Direct Correlation Function

OZE - Ornstein-Zernike Equation

HNC - Hyper-Netted Chain

PY - Percus-Yevick

RHNC - Reference Hyper-Netted Chain

RY - Roger-Young

HMSA - Hybrid Mean Spherical Approximation

SCOZA - Self-Consistent Ornstein Zernike Approximation

TPT - Thermodynamic Perturbation Theory

HTSE - High Temperature Series Expansion

BH - Barker and Henderson

WCA - Weeks-Chandler-Anderson

RGT - Renormalization Group Theory

LVPD - Liquid Vapor Phase Diagram

GRGT - Global Renormalization Group Theory

HRT - Hierarchial Reference Theory

MSA - Mean Spherical Approximation

CPE - Coupling Parameter Expansion

IRSWEOS - Intermediate Range Square-Well Equation Of State

Contents

List of Figures

List of Tables

CHAPTER 1

Background

Liquid is a state of matter intermediate between solid and gas. A naive distinction between a solid and a liquid is the flowing property. Liquids have negligible shear modulus when compared to solids. From a microscopic viewpoint, Bragg diffraction pattern of a solid contains sharp peaks showing a long range order in arrangement of the atoms whereas the Bragg diffraction pattern of a fluid contains diffuse maxima indicating a short range ordering of the atoms. A liquid and a gas are indistinguishable in terms of the above mentioned properties. The liquid and the gas are distinguishable and coexist only between the triple point and the critical point. Below the triple point, the liquid ceases to exist and above the critical point, the distinction between them in terms of low and high density phases ceases to exist. A typical phase diagram of a simple liquid is shown in Fig.(1.1). Theoretical modeling of a fluid accounting for the liquid-vapor phase transition was originated by Van der Waals with his derivation of the famous Van der Waals equation in 1873. Since then the theoretical modeling of properties of a fluid has been a major topic of research which has seen many breakthroughs. The aim of this thesis is to develop an accurate method to obtain the thermodynamic properties of a simple classical fluid incorporating the effects of fluctuations which are generally neglected. Following is a brief discussion of the methods which are used in the study carried out in subsequent chapters.

1.1 Basic Definitions

The system we consider is a simple classical fluid which is a collection of N particles interacting with a given spherically symmetric pair potential $u(r)$ in

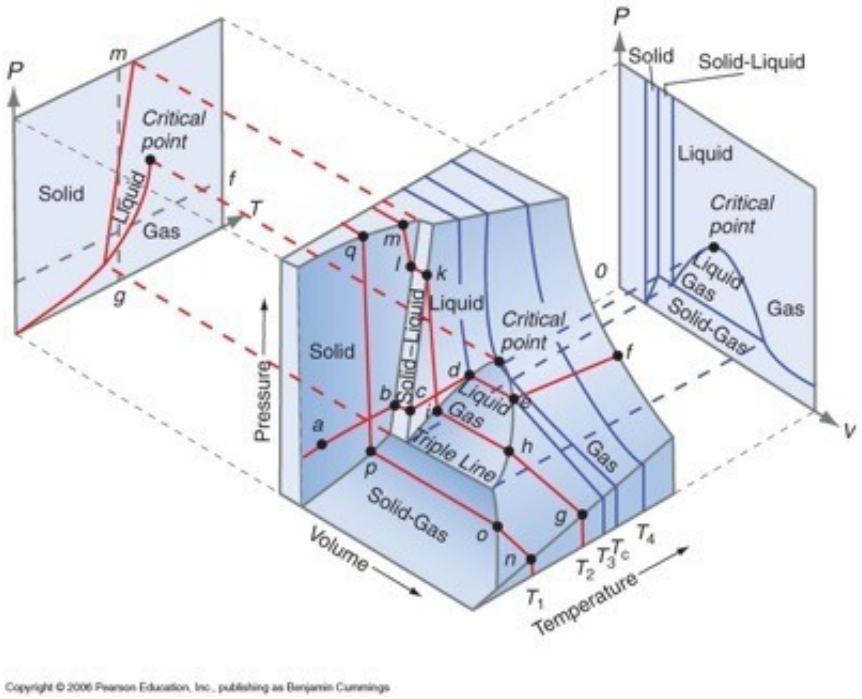

Figure 1.1: *Phase diagram of a simple fluid*

a volume V at an absolute temperature T. The system is assumed to be homogeneous and isotropic with a average (number) density $\rho = N/V$. Above assumptions remain valid throughout the thesis.

1.1.1 Canonical partition function

Canonical partition function $Q_N(V,T)$ of the system is defined as

$$Q_N(V,T) = \frac{1}{N!\lambda_D^{3N}} \int exp(-\beta U) d\vec{r}_1 d\vec{r}_2 ... d\vec{r}_N \tag{1.1}$$

where $\lambda_D = \hbar/\sqrt{2mk_BT}$ is the thermal De-Broglie wavelength and $\beta = 1/k_BT$. The term depending on λ_D is obtained by integrating out the momentum degrees of freedom. U is the total potential energy of the system obtained by summing over the positions of all the particles.

$$U = \frac{1}{2} \sum_i \sum_j u(|\vec{r}_i - \vec{r}_j|) \quad (i \neq j) \tag{1.2}$$

The integral in Eq.(1.1), leaving out the constant prefactor, is called the configuration integral and is denoted as $Z_N(V,T)$. It is understood that the integral is over the total volume for each particle co-ordinate.

1.1.2 *n*- particle density

The equilibrium $n-particle\ number\ density$ in canonical ensemble is defined as

$$\rho^n(\vec{r}_1,\vec{r}_2,..\vec{r}_n) = \frac{N!}{(N-n)!}\frac{1}{Z_N}\int exp(-\beta U(\vec{r}_1,\vec{r}_2,\ldots,\vec{r}_N)))d\vec{r}_{n+1}d\vec{r}_{n+2}...d\vec{r}_N \tag{1.3}$$

From the above definition, the single particle density is written as

$$\begin{aligned}\rho^1(\vec{r}) &= \frac{N}{Z_N}\int exp(-\beta U(\vec{r},\vec{r}_2,\ldots,\vec{r}_N))d\vec{r}_2...d\vec{r}_N \\ &= \left\langle \sum_j \delta(\vec{r}-\vec{r}_j)\right\rangle \end{aligned} \tag{1.4}$$

and

$$\int d\vec{r}\rho^1(\vec{r}) = N \tag{1.5}$$

Thus for a homogeneous and isotropic system, $\rho^1(\vec{r}) = \rho = N/V$. $\rho^1(\vec{r})$ may be related to the probability of finding a particle at a particular position. Along similar lines, the two particle density can be written as

$$\begin{aligned}\rho^2(\vec{r},\vec{r}') &= \frac{N(N-1)}{Z_N}\int exp(-\beta U(\vec{r},\vec{r}',\ldots,\vec{r}_N)))d\vec{r}_3d\vec{r}_4...d\vec{r}_N \\ &= \frac{1}{2}\left\langle \sum_i\sum_j \delta(\vec{r}-\vec{r}_j)\delta(\vec{r}'-\vec{r}_i)\right\rangle. \quad (i\neq j)\end{aligned} \tag{1.6}$$

$\rho^2(\vec{r},\vec{r}')$ is related to the probability of finding a particle at a particular position $\vec{r}_1$ and another particle at a position $\vec{r}_2$ which gives a sense of correlation between the two particles' positions. If the particles are un-correlated as in the case of ideal gas, then $\rho^2(\vec{r},\vec{r}') = \rho^1(\vec{r})\rho^1(\vec{r}')$.

A measure of the deviation from ideal(un-correlated) behavior may be ob-

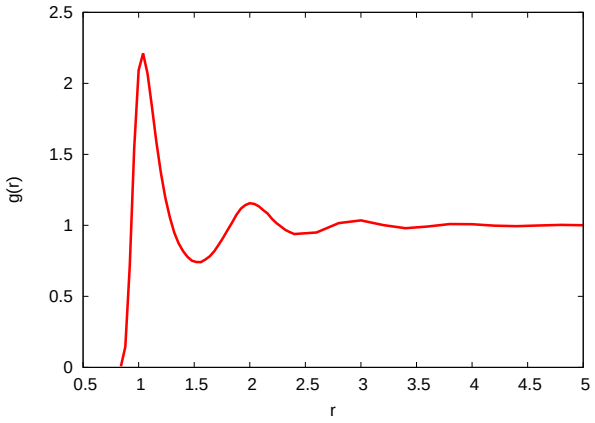

Figure 1.2: *Radial distribution function of Lennard-Jones fluid at temperature* 2.88 *and density* 0.85 *in reduced units.*

tained from the two particle correlation function defined as

$$h(\vec{r},\vec{r}') = \frac{\rho^2(\vec{r},\vec{r}') - \rho^1(\vec{r})\rho^1(\vec{r}')}{\rho^1(\vec{r})\rho^1(\vec{r}')} \tag{1.7}$$

The deviation from un-correlated ideal gas behavior may be viewed as correlation and thus the name pair correlation function to $h(r)$.

1.1.3 Radial Distribution Function (RDF)

From Eq.(1.7), we define two particle distribution function as

$$g(\vec{r},\vec{r}') = \frac{\rho^2(\vec{r},\vec{r}')}{\rho^1(\vec{r})\rho^1(\vec{r}')} \tag{1.8}$$

Thus $g(\vec{r},\vec{r}') = h(\vec{r},\vec{r}') + 1$. For a homogeneous and isotropic system, $g(\vec{r},\vec{r}') = g(|\vec{r}-\vec{r}'|)$ and is called the radial distribution function (RDF). The RDF plays a key role in describing the structure and thermodynamics of liquids. Fourier transform of $g(r)$ is called the structure factor and is experimentally measurable through scattering experiments[1]. A typical plot of RDF is shown in Fig.(1.2). Physical meaning to $g(r)$ may be given using Percus' interpretation of the single particle density $\rho^1(r)$ at a distance r as $\rho g(r)$ provided a particle of the fluid is located at the origin[1]. Thus the number of particles in the shell between r and $r+dr$ is given by $4\pi r^2 dr \rho g(r)$. Hence the peaks in $g(r)$ (see Fig(1.2)) represent shells of neighbors indicative of short range ordering

of atoms in the liquid state. It can be seen from Fig.(1.2) that $g(r)$ becomes zero as $r \to 0$. In-fact it practically dies down well before r approaches zero indicating a strong repulsive interaction between particles at smaller distances. The distance at which the RDF practically becomes zero may be taken as diameter of a particle for practical purposes. It can also be seen from Fig.(1.2) that the RDF tends to unity at large distances implying the dying down of correlations between widely separated particles, which is expected in the case of fluids.

1.1.4 Thermodynamic properties from RDF

If the RDF is known, thermodynamic properties of a fluid with particles interacting via a pairwise additive potential can be expressed as integrals involving the RDF[1]. The excess internal energy E^{ex}, which is the total internal energy E minus the ideal gas contribution E^{id}, is given by the *energy equation*

$$\frac{E^{ex}}{N} = 2\pi\rho \int_0^\infty u(r)g(r)r^2 dr. \tag{1.9}$$

The pressure P is related to $g(r)$ by the below equation called the *virial equation*:

$$\frac{\beta P}{\rho} = 1 - \frac{2\pi\beta\rho}{3} \int_0^\infty \frac{du(r)}{dr} g(r)r^3 dr. \tag{1.10}$$

Also, the isothermal compressibility χ may be obtained using $g(r)$ from the following equation

$$\frac{\rho\chi}{\beta} = 1 + 4\pi\rho \int_0^\infty (g(r) - 1)r^2 dr \tag{1.11}$$

Above equation is called the *compressibility equation*. Thus, with the knowledge of $g(r)$ for a given temperature and density, one can use any one of the above equations and obtain a thermodynamic potential and then calculate the other physical quantities using thermodynamic relations. The problem of calculating $g(r)$ theoretically is discussed in the next section.

1.2 Integral Equation Theory

In the previous section, the role played by $g(r)$ in describing the thermodynamic and structural properties of a fluid has been discussed. In this section we describe briefly the methods for obtaining the RDF and other structure related quantities.

1.2.1 Born-Green equation

One method to obtain RDF is by solving the Born-Green equation obtained by terminating the Yvon-Born-Green hierarchy of equations for particle densities using the Kirkwood superposition approximation[2, 3]. The Born-Green equation is the following

$$\begin{aligned} -\nabla_1 \left(lng(\vec{r}_1, \vec{r}_2) + \beta u(\vec{r}_1, \vec{r}_2) \right) = \\ \beta\rho \int \nabla_1 u(\vec{r}_1, \vec{r}_3) g(\vec{r}_1, \vec{r}_3) \left[g(\vec{r}_2, \vec{r}_3) - 1 \right] d\vec{r}_3 \end{aligned} \tag{1.12}$$

The results obtained using this method were seen to be accurate only at low densities [4].

1.2.2 Ornstein-Zernike equation and various approximate closures

A popular method to obtain $g(r)$ is the Integral Equation Theory based on solving the Ornstein-Zernike Equation(OZE) along with a closure relation[1, 5]. The OZE for a homogeneous and isotropic fluid is given by

$$h(r) = c(r) + \rho \int h(r')c(|r - r'|)d^3r' \tag{1.13}$$

Above equation basically is a separation of the pair correlation function into two parts: the first part $c(r)$ is called the direct correlation function and the remaining part on the $R.H.S.$ of the above equation is called the indirect correlation function (denoted as $y(r)$). The $c(r)$ is the correlation between two particles which are within the range of potential of interaction and thus di-

rectly interacting whereas the $y(r)$ is the correlation between particles whose interactions are not direct but mediated by other particles. Eq.(1.13) has two unknowns $h(r)$ and $c(r)$. To Solve OZE one more equation called the closure relation is required, the exact form of which is given by

$$c(r) = \exp(-\beta u(r) + y(r) + B(r)) - y(r) - 1 \tag{1.14}$$

Eq.(1.14) has been obtained using diagrammatic methods[1]. In the above equation $B(r)$ is called the bridge function. Eq.(1.13) and Eq.(1.14) can be self-consistently solved to obtain $g(r)$ and $c(r)$ if the $B(r)$ is known. However, the exact form of $B(r)$ is unknown. Thus the problem of obtaining $g(r)$ boils down to the problem of devising a form for $B(r)$.

The simplest approximation to $B(r)$ is taking it to be 0. This approximation is called the Hyper-Netted Chain(HNC) approximation[6]. Another simple approximation given by Percus and Yevick[7](PY) is the following

$$B(r) = ln[1 + y(r)] - y(r) \tag{1.15}$$

The PY approximation is basically a linearized form of HNC $w.r.t.\ y(r)$. Both the PY and HNC closures tend to the correct asymptotic form (i.e., $exp(-\beta u(r))$) in the low density limit($\rho \to 0$). Also, the closures give correct expressions for the second and third terms in the virial expansion of EOS. However, because the forms of $B(r)$ are approximate, it is found that the equations of state(EOS)s obtained using the three routes i.e., the energy equation (1.9), the virial equation (1.10) and the compressibility equation (1.11), differ from each other. This is a common problem with all the approximate closures. However, the HNC is a special case where the energy and virial routes are found to be equivalent.

The PY and HNC closures have been used to obtain solutions of OZE for various potentials. The PY approximation gives accurate results for the Hard Sphere fluid. Also it is analytically solvable in this case. Regarding the performance of these closures, it is found that the PY approximation is more accurate than HNC for strongly repulsive and short ranged potentials because of cancellation of errors. The accuracy of the closures is seen to decrease with

decrease in temperature.

Various advanced approximate forms for $B(r)$ are available in the literature. A good discussion of various forms of the bridge function and their performance is given in a review by Bomont[5]. As explained earlier, the inconsistency between the EOS obtained from various routes is a general problem for any approximate closure. Methods have been proposed in which the consistency between various routes is imposed by adjusting the parameters in the closure or a mixture of closures. Some examples are RHNC (Reference HNC), RY (Roger Young) closure, HMSA closure, SCOZA (Self consistent Ornstein Zernike Approximation) [8] etc.

With the improved closures, the accuracy of the calculated thermodynamic properties increased enormously. However, it was found that for each closure, there is a region in the thermodynamic phase space where solution to OZE does not exist. The self-consistency conditions make the numerical schemes complicated. Apart from this, it has been found that the methods become less accurate at low temperatures and for potentials with shorter ranges. In the next section, we discuss an alternate method to obtain the thermodynamic properties of fluids.

1.3 Thermodynamic Perturbation Theory

The basic idea of Thermodynamic Perturbation Theory (TPT) is the distinct role played by the repulsive and attractive parts of the pair potential[1, 9–11]. It has been observed that the structure factor of a fluid at a given temperature and density is mostly determined by the repulsive part of the pair potential which is steep and short ranged. The potential energy due to attractive part of the potential which is weak and long ranged forms a uniform background in which the particles move. It only adds corrections to the structure. This idea motivates splitting of the $u(r)$ into a reference part which is dominantly repulsive and an attractive part which is treated perturbatively. Assuming that the properties of the reference fluid like Helmholtz free energy, RDF etc. are known, the properties of the fluid under consideration are expressed in terms

of the properties of the reference fluid. The method briefly[1] is given below.

1.3.1 Basic derivation

Let the pair potential be split and written as follows

$$u(r,\zeta) = u_{ref}(r) + \zeta u_{per}(r) \tag{1.16}$$

where ζ is called the coupling parameter which when varied from 0 to 1 switches the potential $u(r)$ from the reference system potential to the potential of the system under consideration. ζ is a parameter introduced only for the ease of calculating the perturbation expansion and is set equal to 1 at the end of the calculation. Thus the total potential energy of the system for a given configuration of particles is $U = U_{ref} + \zeta U_{per}$ where each of the terms is a double sum of the corresponding potential over positions of the particles. The Helmholtz free energy of the system of particles interacting with potential of Eq.(1.16) is given by

$$F(\zeta,V,T) = -k_B T ln Q_N(\zeta,V,T) \tag{1.17}$$

where k_B is the Boltzmann constant and $Q_N(\zeta,V,T)$ is the canonical partition function of the system with coupling parameter ζ. Using Eq.(1.16), $F(\zeta,V,T)$ may be re-written as

$$\begin{aligned} F(\zeta,V,T) &= -k_B T\ lnQ_N(0,V,T) - k_B T\ ln\left(\frac{Q_N(\zeta,V,T)}{Q_N(0,V,T)}\right) \\ &= -k_B T\ lnQ_N(0,V,T) - k_B T\ ln\left\langle exp[-\beta\zeta U_{per}]\right\rangle_0 \end{aligned} \tag{1.18}$$

Angular brackets in the second term of above equation represent a canonical ensemble average and the subscript 0 indicates that the average is over the reference system ensemble.The first term represents the Helmholtz free energy of the reference system(denoted as F_0). Expanding the exponential term in the angular brackets as a Taylor series around $\zeta = 0$, we get

$$\left\langle exp[-\beta\zeta U_{per}]\right\rangle_{\zeta=0} = 1 - \beta\zeta\left\langle U_{per}\right\rangle_0 + \frac{\beta^2\zeta^2}{2!}\left\langle U_{per}^2\right\rangle_0 - \frac{\beta^3\zeta^3}{3!}\left\langle U_{per}^3\right\rangle_0 + ... \tag{1.19}$$

Substituting the above equation in Eq.(1.18) and expanding the logarithm (using $log(1+x)$ expansion), we get the so called cumulant expansion.

$$\begin{aligned} F(\zeta,V,T) &= F_0 - k_BT\ ln\left(1-\beta\zeta\left\langle U_{per}\right\rangle_0 + \frac{\beta^2\zeta^2}{2!}\left\langle U_{per}^2\right\rangle_0 - \frac{\beta^3\zeta^3}{3!}\left\langle U_{per}^3\right\rangle_0 + ...\right) \\ &= F_0 - k_BT\ \left(-\beta\zeta\left\langle U_{per}\right\rangle_0 + \frac{\beta^2\zeta^2}{2!}\left[\left\langle U_{per}^2\right\rangle_0 - \left\langle U_{per}\right\rangle_0^2\right] + ...\right) \quad (1.20) \end{aligned}$$

This is the perturbation expansion for the Helmholtz free energy. The Helmholtz free energy of the actual system can be obtained by setting $\zeta = 1$. In the above equation, the term inside the logarithm other than 1 is required to be less than 1 for the expansion to be convergent which is difficult to check. In practice, it is assumed that the series is convergent if $\langle \beta U_{per} \rangle << 1$ which is a less stringent condition and is valid for high temperatures. Thus the series is also called High Temperature Series Expansion(HTSE).

1.3.2 First order correction to Helmholtz free energy

Using the definition of RDF[1] denoted as $g(r)$, the first order correction term F_1 in the HTSE (Eq.(1.20)) is given by

$$F_1 = \left\langle U_{per}\right\rangle_0 = \frac{\rho N}{2}\int g_0(r)u_{per}(r)(4\pi r^2 dr) \quad (1.21)$$

1.3.3 Local compressibility approximation

The second order term in HTSE turns out to be a complicated functional of correlation functions of the reference system up to fourth order. It cannot be determined exactly as the correlation functions of order higher than two are unknown. Barker and Henderson[12] proposed local compressibility approximation to the second order term F_2 given by

$$F_2 = -\pi\rho N\left(\frac{\partial\rho}{\partial p}\right)_{\zeta=0}\frac{\partial}{\partial\rho}\left[\int \rho u_{per}^2(r)g_0(r)r^2dr\right] \quad (1.22)$$

A simplified version of local compressibility approximation is called the macroscopic compressibility approximation where $g_0(r)$ is assumed to be indepen-

dent of pressure p. It is observed that the local compressibility approximation and the macroscopic compressibility approximation do not improve much the estimated F with respect to the first order correction, for potentials of intermediate and short ranges[13, 14]. Using the macroscopic compressibility approximation, a method to sum the series was worked out by Preastgaard[14]. However, it has been seen that the contribution of higher order terms within the macroscopic compressibility approximation is found to be very small.

Thus within the method described above, the Helmholtz free energy of a simple classical liquid may be obtained from which other thermodynamic properties can be calculated. There are however two issues which have a crucial bearing on the accuracy of the obtained results. First is the choice of reference system. Second is the method used to separate the potential $u(r)$ into reference and perturbation parts. A brief discussion of these follows.

1.3.4 Choice of the reference system

There are only two reference systems for which analytical fitting formulae to the Helmholtz free energy which are in good agreement with the computer simulations are known. One is the hard sphere fluid[15] and the other is the One Component Plasma. Of these, the hard sphere fluid reference system is suitable for simple fluids with an empirical interaction potential(for e.g., Lennard Jones) which are of our concern while the one component plasma reference system is well suited for ionic fluids.

For fluids with inter particle interaction modeled using square-well potential, Yukawa potential etc., or in general any potential with a hard sphere repulsive part and a weak attractive tail, the hard sphere system is the natural reference system. However, for systems with inter-particle interactions modeled using potentials like Lennard-Jones potential for which the repulsive part is not a hard sphere potential, the separation is not immediately obvious. Various ways of separating $u(r)$ have been proposed in these cases. Most prominent of theses are the Barker and Henderson(BH) prescription[16] and the Weeks Chandler and Anderson(WCA) prescription[17]. The BH prescription is as fol-

lows

$$\begin{aligned} u_{ref}(r) &= u(r) \qquad r \leq \sigma \\ &= 0 \qquad r > \sigma \\ u_{per}(r) &= 0 \qquad r \leq \sigma \\ &= u(r) \qquad r > \sigma \end{aligned} \tag{1.23}$$

where σ is the distance at which $u(r)$ changes sign. The WCA prescription is

$$\begin{aligned} u_{ref}(r) &= u(r) + \epsilon \qquad r \leq b \\ &= 0 \qquad r > b \\ u_{per}(r) &= -\epsilon \qquad r \leq b \\ &= u(r) \qquad r > b \end{aligned} \tag{1.24}$$

where b is the separation at which the potential is minimum and ϵ is the depth of the potential. It can be seen that the above kind of separations do not naturally lead to hard sphere system as reference system. However BH and WCA, along with their prescriptions for separation of $u(r)$, have given methods to relate the properties of the reference system with potential $u_{ref}(r)$ to that of the hard sphere system.

In the BH method[16], the Helmholtz free energy F_0 and the RDF $g_0(r)$ of the reference system are approximated to be those of hard sphere reference system with the hard sphere diameter D_{HS} chosen to be

$$D_{HS} = \int_0^\sigma [exp(-\beta u(r)) - 1] dr \tag{1.25}$$

BH applied their theory to the Lennard-Jones fluid and found that the results are in excellent agreement with simulations when the Helmholtz free energy is calculated upto the second order perturbation term correction (F_2).

In the WCA method, F_0 is approximated by the free energy of the hard sphere system (F_{HS}) and $g_0(r)$ is assumed to be $g_0(r) = exp(-\beta u_{ref}(r)) y_{hs}(r)$, where $y_{hs}(r)$ is the cavity distribution function of the HS system. (The cavity

distribution function is defined as $exp(-\beta u(r))g(r)$). The diameter D_{HS} of the hard sphere is obtained by solving the equation

$$\int_0^b r^2 y_{hs}(r)dr = \int_0^b r^2 exp(-\beta u_0(r))y_{hs}(r)dr \tag{1.26}$$

Above equation has to be solved numerically using an iterative procedure. It was found that the convergence of the perturbation series with WCA prescription is faster as compared to the BH prescription. Subsequently, there have been many improvements over the WCA method[18, 19].

Apart from the BH and WCA methods and their improvements, Mansoori and Canfield developed a variational method based on the Gibbs-Bogoliubov inequality in which the HS diameter is treated as a variational parameter[20, 21]. Using the variational principle, Kerley developed a perturbation theory in which the zero temperature isotherm is used in lieu of the pairwise interaction potential[22].

Second order HTSE with local compressibility approximation or macroscopic compressibility approximation gave good results for fluids with interaction potentials with ranges varying from long to intermediate. However, the method was seen to become inaccurate for short ranged potentials and adding higher order corrections within the macroscopic compressibility approximation did not lead to a significant improvement with when compared with simulation results.

1.3.5 Zhou's method

A new method to obtain the Helmholtz free energy within TPT was developed by Zhou in 2006[23]. The perturbation series for Helmholtz free energy was obtained in an alternative way called the coupling parameter expansion(CPE). Differentiating $F(\zeta, V, T)$ in Eq.(1.17) $w.r.t.\ \zeta$ and re-writing it in terms of the RDF of system, Zhou obtained

$$F(\zeta, V, T) = F_0 + \frac{\rho N}{2}\int_0^1 d\zeta \int g_\zeta(r) u_{per}(r) d^3r \tag{1.27}$$

In the above equation, expanding $g_\zeta(r)$ (which is a function of V and T also) as a Taylor series in ζ around $\zeta = 0$ and integrating over ζ, we get

$$F(\zeta = 1, V, T) = F_0 + \frac{\rho N}{2} \int r^2 dr u_{per}(r) \left\{ g_0(r) + \frac{1}{2!} \frac{dg}{d\zeta}\bigg|_0 + \frac{1}{3!} \frac{d^2 g}{d\zeta^2}\bigg|_0 + ... \right\} \tag{1.28}$$

It can be seen that the first term in the above expansion is same as that of HTSE (see Eq.(1.21)). To obtain the n^{th} order term, $\frac{d^n g}{d\zeta^n}\Big|_0$ is required. Zhou obtained it by solving for $g(\zeta, r)$ using Integral Equation Theory for various values of ζ close to 0 and further calculating the numerical derivative at each r. Using this method, Zhou obtained the Helmholtz free energy upto fifth order[24]. Zhou's method, when applied to various simple fluids like the square-well fluid showed a remarkable improvement in the results as compared to those obtained using second order HTSE within macroscopic compressibility approximation. However, Zhou's method was exceedingly numerical and the derivatives obtained required further smoothing procedures to remove unwanted numerical fluctuations. In the subsequent chapters we describe a new method we developed for calculating terms of CPE, which is equivalent to the Zhou's method but is based on fundamental arguments and is much easier to implement.

1.4 Renormalization Group Theory

Theories described above are called mean field theories. Basic assumption of a mean field theory is that the potential (energy) experienced by a particle is the mean (a weighted average) of the potential due to the surrounding particles. Landau and Ginzburg gave a more general and unified way of understanding a mean field theory. According to Landau-Ginzburg theory, if the partition function is written as a functional integral over all possible configurations of the *order parameter*[1], then the mean field approximation amounts to approximating the functional integral as the maximum value of the inte-

[1]The concept of order parameter is explained below.

grand. It is also called the saddle point approximation[25, 26]. The mean field theories do not account for fluctuations in the order parameter which become especially important close to the critical point of a continuous phase transition (commonly known as second order phase transition). We first give below, a brief discussion of the experimental facts regarding continuous phase transitions. Then we give a brief review of theoretical developments for explaining the second order transitions ending up with a discussion on ideas of Renormalization Group Theory(RGT) put forward by Kenneth G. Wilson[27] which succeeded in explaining the observed experimental facts close to the second order transitions.

1.4.1 Continuous phase transitions

The study of continuous phase transitions started around the year 1869 with Thomas Andrews' experiments on CO_2 showing that a transition from the gaseous to liquid phase of CO_2 can be made in a continuous way without any sudden change in density. Andrews coined the term "critical point" which he meant as the point in the thermodynamic phase space (T, ρ, P space in case of fluids), where the distinction between a gas and a liquid disappears. A similar phenomenon has been observed in magnets (ferromagnetic materials) where the materials lost their magnetic properties above some temperature i.e., the material would be ferromagnetic (with non-zero net magnetization) below a certain temperature and paramagnetic (zero net magnetization) above that temperature. Analogous to the case of fluids, this temperature is also called the critical temperature. Again, in binary alloys, it was found that the ordered arrangement of atoms disappears above a particular temperature. In all of the above three examples, there is a continuous transition from one phase to other at a point in the thermodynamic phase space called the critical point. The most interesting fact is the experimentally observed *universality* in the behavior of the above apparently *unrelated* systems close to the critical point.

1.4.2 Critical exponents

It has been observed that systems undergoing a continuous phase transition follow certain *universal* scaling laws close to the critical regions, the exponents of which have been measured experimentally and are called critical exponents. They are the following:

Exponent β: The zero field magnetization m of a ferromagnet is found to scale as

$$|m| \propto (T_c - T)^{\beta} \qquad T \to T_c^- \tag{1.29}$$

Similarly, the difference between the liquid densityρ_l and vapor densityρ_v of a fluid scales as

$$\rho_l - \rho_v \propto (T_c - T)^{\beta} \qquad T \to T_c^-. \tag{1.30}$$

Also in the case of a binary mixture, the difference between concentrations of one of the compounds in the two phases close to critical temperature scales as

$$c_1 - c_2 \propto (T_c - T)^{\beta} \qquad T \to T_c^-. \tag{1.31}$$

Surprisingly, the value of β in all these cases has been found experimentally to be same and is close to 0.32.

Exponent α: The specific heat of a ferromagnet, a fluid and a binary alloy close to their corresponding critical points is found to diverge according to the scaling law,

$$\begin{aligned} C &\propto (T_c - T)^{-\alpha} \qquad T < T_c \\ &\propto (T - T_c)^{-\alpha} \qquad T > T_c \end{aligned} \tag{1.32}$$

Again, the value of α is close to 0.1 for all the above cases.

Exponent γ: This exponent is related to the divergence of zero-field susceptibility close to the critical temperature which follow the scaling law,

$$\begin{aligned} \chi &\propto (T_c - T)^{-\gamma} \qquad T < T_c \\ &\propto (T - T_c)^{-\gamma} \qquad T > T_c \end{aligned} \tag{1.33}$$

In the case of ferromagnetic materials, χ is the magnetic susceptibility whereas in the case of a fluid, χ is the isothermal compressibility. The measured value of γ for different materials is 1.2.

Exponent δ: This exponent is related to the variation of magnetization m with external magnetic field along the critical isotherm in the case of a ferromagnetic material. The corresponding scaling law is

$$m \propto h^{1/\delta} \tag{1.34}$$

In the case of a fluid, the exponent δ is related with the following scaling law

$$\rho - \rho_c \propto (P - P_c)^{1/\delta} \tag{1.35}$$

The exponent δ has been measured to be close to 4.8.

Apart from α, β, γ and δ, there are two more exponents ν and η which are related to the divergence of correlation length and the power-law decay of the correlation function.

As explained above, the puzzling fact is the *universality* exhibited close to the critical point. The various critical exponents are identical not just for various fluids or for various magnetic materials close to their corresponding critical point but between continuous transitions of completely different types, independent of materials involved. This in turn amounts to saying that the behaviour near the critical point is independent of microscopic Hamiltonians. The microscopic details of the system are irrelevant when the system is close to its critical point.

1.4.3 Landau - Ginzburg theory

The para-ferro transition in ferromagnetic materials was first explained by Weiss and Curie. The liquid-vapor transition was first explained by Van der Waals and the order-disorder transition in binary mixtures was first explained by Bragg and Williams[28, 29]. But these theories were based on microscopic Hamiltonians specific to the transition apart from being mean field theories.

Landau, in 1937, gave a unified (mean field) theory of continuous transitions which can be used for all the cases above. Landau also generalized the concept of *order parameter* originally introduced by Bragg and Williams for binary alloys.

The concept of *order parameter* is based on the following observation: When a system is taken from above the critical point to below, allowing the continuous transition to take place, there is a reduction of symmetry. For example, in a ferromagnetic system, above the critical point there is no net magnetization and the system is rotationally invariant. Below the critical temperature, a net magnetization pointing in a particular direction exists destroying the rotational invariance. Similar is the order-disorder transition in binary alloys. Thus there is a reduction of symmetry when a system passes from T_c^+ to T_c^- because of some "order" developing in the system. To capture this change in symmetry, a parameter called the *order parameter* has been introduced. In continuous phase transitions, the *order parameter* changes continuously from a non-zero value below the critical temperature to a zero value above the critical temperature. For a magnetic material, the magnetization m is the order parameter. For a fluid, $\rho_l - \rho_v$ is the order parameter.

Landau's theory was based on the understanding that the continuous phase transition is a collective phenomenon where the microscopic details of the interactions between the particles are integrated out i.e., they are *coarse grained*. Thus, the basic idea of Landau's theory[30] was to write the Gibbs free energy as a functional of coarse-grained order parameter density by Taylor expanding it around the critical point. The temperature dependence of coefficients of the expansion terms were obtained from symmetry considerations. Since Landau's theory has been extensively discussed in the literature[25, 26, 29], the detailed derivation of the Ginzburg-Landau free energy functional is omitted here. However, the obtained partition function and Landau free energy are given below for the sake of completeness.

The partition function is written as a functional integral

$$Q = \int \dots \int \prod_i Ds_i(\vec{r}) exp\left[-\frac{H[s]}{T}\right] \tag{1.36}$$

Table 1.1: critical exponents obtained using Landau theory

-	α	β	γ	δ	ν	η
Landau	0	1/2	1	3	1/2	0
Exact	0.1	0.32	1.2	4.8	0.6	0.05

where $s_i(\vec{r})$ is the i^{th} component of the order parameter field. $\int Ds_i(\vec{r})$ implies the functional integration over all possible functions(configurations) of the order parameter.

$$H[s] = \int_V \left\{ a_0 + a_2 \mathbf{s}^2(\vec{r}) + a_4 \mathbf{s}^4(\vec{r}) - h s_1(\vec{r}) + c|\nabla \mathbf{s}(\vec{r})|^2 \right\} \tag{1.37}$$

where $a_0 = -k_B T ln(2), \quad a_2 = const.(T - T_c), \quad a_4 = const.(k_B T)$. The expansion doesn't contain a first order gradient term as it violates the rotational symmetry of the underlying microscopic Hamiltonian.

As explained above, Landau's theory amounts to replacing the functional integral in the partition function(Eq.(1.36)) with the most probable functional form of $\mathbf{s}(\mathbf{x})$ which is a constant obtained by minimizing Eq.(1.37). The critical exponents obtained using the Landau's theory are given in Table.(1.1). Landau's theory brings out some important facts. It explains how singularities can arise in physical quantities even when the Hamiltonian is a regular function. It also explains the universality in the exponents as none of them depend on parameters of the model.

The values of exponents obtained in this way are called *classical* exponents. The exponents obtained using Landau's theory do not match with the experimental observations. According to Landau's theory, the exponent $\alpha = 0$. Thus the Landau's method could not predict the observed divergence in specific heat. The other calculated exponents also deviate from the experimental values. Apart from the small deviation from experimental exponents, there is another shortcoming in Landau's theory. The critical exponents are independent of the parameters in the model implying their universality. However, the universality is overstated; there is no dependence on spatial dimension in the exponents. As a result, the exponents do not satisfy some general scaling laws

(to be discussed later).

An improvement to Landau's theory was effected by adding the contribution of Gaussian fluctuations to the Landau free energy. The contribution of these fluctuations is such that the exponent α now depends on the spatial dimension d for $d < 4$ whereas other exponents remain unchanged. It is also seen that the effects of fluctuations are large for $d < 4$ and negligible for $d > 4$. Thus the dimension $d = 4$ above which the Landau theory becomes exact is called the upper critical dimension. The dimension $d = 1$ is called the lower critical dimension below which there is no phase transition.

Perturbation theory beyond the quadratic approximation proved unsuccessful as each term in the series diverges upon inclusion of fluctuations. Thus the mean field theories of Landau type turned out to be inadequate to calculate the observed critical exponents. However, the Landau theory brought out some facts giving a direction for further improvements.

1.4.4 Scaling Hypothesis

The critical exponents discussed in Section 1.4.2 are not independent as they are related to the thermodynamic quantities which are themselves related. Using the *scaling hypothesis*, it was shown that the critical exponents are actually related. The *scaling hypothesis* is basically the assumption that, near the critical point, the correlation length[1] (hereafter denoted as ξ) is exceedingly large and is the only characteristic length in the system so that the microscopic details are unimportant. The scaling approach has been developed independently by Widom, Domb and Hunter, Patashinkii and Pokrovskii in attempts to incorporate the non-classical exponents in the mean field theory.

As a result of scaling approach, out of the six exponents $\{\alpha, \beta, \gamma, \delta, \eta$ and $\nu\}$ only two are found to be independent while others are related by the following four equations called scaling laws.

[1]Correlation length is basically the length up to which the correlations in order parameter persist. The two point correlation function is defined as $\Gamma(\vec{r}) = \langle s(\vec{r})s(0)\rangle - \langle s(\vec{r})\rangle \langle s(0)\rangle$. Close to the critical point, Ornstein and Zernike showed that $\Gamma(\vec{r}) \approx e^{-r/\xi}/r$ which shows that the correlation function and hence the correlation length also diverges as critical point is approached.

$$Fisher: \quad \gamma = \nu(2-\eta) \tag{1.38}$$

$$Rushbrooke: \quad \alpha + 2\beta + \gamma = 2 \tag{1.39}$$

$$Widom: \quad \gamma = \beta(\delta - 1) \tag{1.40}$$

$$Josephson: \quad \nu d = 2 - \alpha \tag{1.41}$$

In the Josephson law(also called the hyper-scaling law), *d* is the spatial dimensionality. The derivation of above laws is given in standard text books[26, 29] and hence is not discussed here.

1.4.5 Renormalization Group Transformation

Kadanoff developed a generalized way of obtaining the scaling laws between the critical exponents using the block spin transformation[31] which was the first step towards the renormalization group theory(RGT) of critical phenomena. However, Kadanoff's ideas didn't lead to any rigorous calculation scheme and there were too many ad-hoc assumptions some of which were unjustified. A rigorous and complete formalism of effecting the *renormalization group transformation* was developed by K. G. Wilson[27] in 1971. The basic idea was that the (excessively large) correlation length ξ near the critical point being the only important length scale in the system, variations at length scales smaller than ξ do not effect the physics (large length scale behavior) of the system. Thus, the short wavelength fluctuations are systematically integrated out to obtain an effective Hamiltonian which contains only long wavelength modes approaching ξ. We briefly explain below the basic steps of the renormalization group transformation in a nutshell[32].

Coarse grain: This step is basically tantamount to decreasing the resolution by increasing the length scale of the system. One way of effecting the coarse graining procedure is to divide the system into blocks of certain length $a' << \xi$ in space and average out the microscopic variables in each block. $a' = la > a$,

the length scale of the original system. For example, in a ferromagnet, we average the magnetization $s(\vec{r})$ in each block so that we have a *coarse grained* system with length scale a' and magnetization $s'(\vec{r})$.

$$s'(\vec{r}) = \frac{1}{l^d} \int s(\vec{r'}) d^d r'$$

where d is the spatial dimension.

Rescale: The original resolution of the system is to be restored by rescaling all the lengths by a factor l.

$$r' = r/l$$

This is done so that the symmetries in the original system and the coarse grained system can be compared.

Renormalize: The order parameter is re-scaled so that the variations in the coarse-grained order parameter match with those of the original one. To effect this, a scaling factor α is introduced as below

$$s'(\vec{r}) = \frac{1}{\alpha l^d} \int s(\vec{r'}) d^d r'$$

We give below an example of an application of RGT using the Wilson's phase space approach. We chose the Gaussian model which is a convenient pedagogical tool.

The Hamiltonian of the Gaussian model is

$$\frac{H[s]}{T} = \int_V \left[a_2 s(\vec{r})^2 + c|\nabla s(\vec{r})|^2 \right] d^d r \tag{1.42}$$

where a_2 and c are temperature dependent parameters. The partition function is given by

$$Z = \int Ds(\vec{r}) e^{-H[s]/T} \tag{1.43}$$

We now carry out the above mentioned steps as follows

coarse grain: The above Hamiltonian with order parameter $s(\vec{r})$ (assumed to be having a single component) already contains effects of fluctuations up

to some wavelength λ. Thus $s(x)$ contains fluctuations of wavelengths greater than λ and can be written in terms of Fourier modes as

$$s(\vec{r}) = \frac{1}{L^{d/2}} \sum_{k \leq \Lambda} exp(i\mathbf{k} \cdot \mathbf{x}) s_{\vec{k}} \tag{1.44}$$

where $\Lambda = 2\pi/\lambda$ Now to coarse grain, the fluctuations of order parameter in the wave length band $(\lambda, q\lambda)$ where $q > 1$ are integrated out and an effective Hamiltonian is obtained. The partition function remains unchanged in the process.

We first write

$$s(\vec{r}) = s'(\vec{r}) + \phi(\vec{r}) \tag{1.45}$$

where

$$s'(\vec{r}) = \frac{1}{L^{d/2}} \sum_{k \leq \Lambda/q} exp(i\mathbf{k} \cdot \mathbf{x}) s_{\vec{k}} \tag{1.46}$$

$$\phi(\vec{r}) = \frac{1}{L^{d/2}} \sum_{\Lambda/q < k \leq \Lambda} exp(i\mathbf{k} \cdot \mathbf{x}) s_{\vec{k}}. \tag{1.47}$$

The partition function is then re-written as

$$\begin{aligned} Z &= \int Ds(\vec{r}) e^{-H[s'+\phi]/T} \\ &= \int Ds'(\vec{r}) e^{-H[s']/T} \int D\phi(\vec{r}) e^{-H[\phi]/T} \end{aligned} \tag{1.48}$$

where

$$\frac{H[\phi]}{T} = \int_V d^d r \left[a_2 \phi^2(\vec{r}) + c|\nabla \phi(\vec{r})|^2 \right]. \tag{1.49}$$

To partially integrate the partition function i.e., the part containing $\phi(x)$, Wilson introduced a function called the Wilson's function. The basic idea behind the Wilson's function ($w(x)$) was to capture the effect of fluctuations within a given wave-vector band $\Lambda/q < k < \Lambda$. Then the volume spanned in the Fourier space is given by

$$V_k = (2\Lambda)^d - (2\Lambda/q)^d = (2\Lambda)^d (1 - q^{-d}) \tag{1.50}$$

Thus the minimum volume Ω spanned by $w(x)$ in coordinate space is

$$\Omega = (2\pi)^d / V_k \tag{1.51}$$

The function $w(x)$ should satisfy the following properties:

$$\int_\Omega d^d r w_i(\vec{r}) = \int_V d^d r w_i(\vec{r}) = 0 \tag{1.52}$$

$$\int_\Omega d^d r w_i(\vec{r}) w_j(\vec{r}) = \int_V d^d r w_i(\vec{r}) w_j(\vec{r}) = \delta_{ij} \tag{1.53}$$

Wilson assumed that $w(x)$ is localized around $x = 0$ within Ω and is negligible outside. It is further assumed that gradients of w are orthogonal i.e.,

$$\int_\Omega d^d r \nabla w_i(\vec{r}) \nabla w_j(\vec{r}) = \int_V d\vec{r} \nabla w_i(\vec{r}) \nabla w_j(\vec{r}) \approx k_m^2 \delta_{ij} \tag{1.54}$$

where $k_m = \frac{2\pi}{\lambda_m}$ and λ_m is the mean wavelength in the band $(\lambda, \lambda/q)$.

A function which approximately satisfies these conditions, as chosen by Wilson is

$$w(\vec{r}) = \frac{\pm 1}{\sqrt{\Omega}} \tag{1.55}$$

where $+$ sign is for half of the volume and $-$ sign is for the other half volume.

Now, using $w(\vec{r})$ the partial integration in Eq.(1.48) is done as follows: First, we expand $\phi(\vec{r})$ as

$$\phi(\vec{r}) = \sum_l \phi_l(\vec{r}) w_l(\vec{r}). \tag{1.56}$$

Using above expansion and the properties of $w(\vec{r})$ in Eq.(1.48), we get

$$Z = \int Ds' e^{\frac{-H[s']}{T}} \prod_l \left[d\phi_l e^{-(a_2 + c k_m^2)\phi_l^2} \right] \tag{1.57}$$

which can be re-written as

$$Z = \int Ds' e^{\left\{ \frac{-H[s']}{T} + \frac{1}{\Omega} \int_V \, d^d r \; ln(I(0)) \right\}} \tag{1.58}$$

where

$$I(0) = \int d\phi_l e^{-(a_2+ck_m^2)\phi_l^2} \tag{1.59}$$

The fact that the above equation doesn't depend on $s'(\vec{r})$ is specific to the Gaussian model. The term containing $I(0)$ thus becomes irrelevant for the present study as it just adds a constant term to the free energy and doesn't contribute to the emergence of singularities and non-analyticites in the derived quantities.

We now perform the next steps of the transformation i.e., the *rescaling* and *renormalization* together,

$$\begin{aligned} \vec{r} \rightarrow \vec{r}' = \frac{\vec{r}}{q} \\ s'(\vec{r}) \rightarrow \alpha(q) s(\vec{r}') \end{aligned} \tag{1.60}$$

to the Hamiltonian $H[s']$ to obtain $H'[s]$. It can be shown that the factor $\alpha(q) = q^a$ where $a = 1 - \eta/2 - d/2$[25] (d is the dimensionality of the system.) The Hamiltonian after the RG transformation becomes

$$H'[s(\vec{r}')]/T = \int_V d\vec{r}' \left[a_2' s(\vec{r}') + c' |\nabla s(\vec{r}')|^2\right] \tag{1.61}$$

where

$$\begin{aligned} a_2' &= a_2 q^d q^{2-\eta-d} \\ c' &= c q^{-\eta} \end{aligned} \tag{1.62}$$

Above equation gives the relation between the parameters of the original Hamiltonian with those of the transformed Hamiltonian. It can be seen from Eq.(1.62) that by repeated application of the RG transformation (hereafter denoted as R_q), the parameter related to c becomes zero if $\eta \neq 0$ which implies that there is no gradient in the density and thus no correlations. Thus, in order to allow for correlations, we have to choose $\eta = 0$ which makes $c' = c$. With the choice of $\eta = 0$, we get $a_2' = a_2 q^2$. Also, existence of critical point (or fixed point of the transformation) implies that, at the critical point, the parameters reach a value

given by

$$R_q \{a_2^*, c^*\} = \{a_2^*, c^*\} \tag{1.63}$$

A non-trivial fixed point can be seen (by inspection) to occur if $a_2^* = 0$ with c being arbitrary.

With the above knowledge we may obtain the correlation length exponent ν as follows: The correlation length ξ of the original and the renormalized system are related as

$$\xi(a_2, c) = q\xi(a_2', c') = q\xi(a_2', c) \tag{1.64}$$

If $\tilde{a_2}$ is the parameter obtained from a_2 close to the critical region after l RG transformations, then it can be expanded as,

$$\tilde{a_2} = q^{2l}(A(T - T_c) + B(T - T_c)^2 + \dots) \tag{1.65}$$

Thus

$$\xi(\tilde{a_2}, c) = q^l \xi(Aq^{2l}(T - T_c) + \dots) \tag{1.66}$$

As $T \to T_c$ and for large l, for the ξ to diverge, we require

$$q^{2l} \approx (T - T_c)^{-1} \tag{1.67}$$

which implies (as $T \to T_c$)

$$\xi(\tilde{a_2}, c) \approx (T - T_c)^{-1/2} \xi(A + \dots). \tag{1.68}$$

Thus $\nu = 1/2$.

Knowing the values of the exponents ν and η, the other exponents can be obtained using the scaling laws described above. The other exponents turn out

to be

$$\begin{aligned} \alpha &= (4-d)/2 \qquad d \leq 4 \\ \beta &= (d-2)/4 \\ \gamma &= \nu(2-\eta) \\ \delta &= (d+2)/(d-2) \end{aligned} \tag{1.69}$$

The Gaussian model is exactly solvable and the exact exponents are the same as those obtained above. Wilson's method is able to obtain the exact critical exponents for the Gaussian model.

The above discussion is just to illustrate the RG transformation as done using the Wilson's phase cell approach. The above method has been found to be useful to obtain the correct critical exponents. But to obtain the critical point and improved phase diagrams, the microscopic Hamiltonian of the system is required. White[33] developed a way of implementing the Wilson's RG transformation method in fluids. Our work is a development (generalization) of White's method which will be discussed in the next chapter.

1.4.6 Outline of the Thesis

In the Chapter II, we describe White's implementation of Wilson's RG followed by our generalized derivation of the RG theory for fluids. We apply our method to square-well fluids and Lennard-Jones fluids and analyze the results. The analysis paves the way for improvement in the mean field theory which is an input into the RG theory for fluids.

In Chapter III, we describe the perturbation theory we have developed to obtain the Helmholtz free energy. The method is applied to square-well fluids and compared with simulation results.

In Chapter IV, we show the equivalence of the perturbation theory we have developed with that developed by Zwanzig's method in the case of pair potential. We also discuss the advantages of our method in terms of ease in implementation.

In Chapter V, we combine the perturbation method we described in Chap-

ter III and the RG method described in Chapter I and apply the method to square-well fluids to obtain Liquid Vapor Phase Diagrams(LVPDs). We also obtain the critical exponents using our method and study the Yang-Yang anomaly using the method.

In Chapter VI, we apply our method to liquid metals and obtain the liquid vapor phase diagrams which are compared with simulation results.

The thesis is concluded in Chapter VII with a discussion of the results that have been obtained, possible short comings of our study and directions for future improvements.

CHAPTER 2

Global Renormalization Group Theory For Simple Fluids

As explained in Chapter 1, the mean field theories fail to accurately describe the thermodynamics of fluids near the critical point and predict classical critical exponents. The renormalization group theory (RGT) developed by Wilson [27] takes into account fluctuations at all length scales and thus predicts non-classical critical exponents and the observed universal features near the critical point. However, the method evolved by Wilson is suitable only asymptotically close to the critical point in a regime determined by the Ginsberg criterion. Recently, theories have been developed for fluids which tend to a mean field theory away from the critical point and crossover to RGT as the critical point is approached. One of the developments along these lines is the global renormalization group theory (GRGT) originated by White [33–35] and modified by Tang et. al. [36, 37] and Lue and Prausnitz [38]. The other methods include HRT developed by Parola and Reatto [39], the non-perturbative renormalization group techniques [40], and the self consistent solutions to Ornstein-Zernike approximation for special form (screened Coulomb) of potentials [8, 41].

The basic aim of GRGT is to calculate Helmholtz free energy of a fluid by including all contributions from density fluctuations. The mean field free energy density (f_0) includes effects of fluctuations at length scales less than and of the order of the range of the potential. One way of representing the density fluctuations is to expand them in terms of Fourier modes, each mode corresponding to a particular wavelength. If λ_0 is the wavelength up to which fluctuations are accounted for in f_0, then density fluctuations beyond mean field theory will contain only longer wavelengths. GRGT starts with f_0 as reference free energy density and contributions from fluctuations of wavelength

greater than λ_0 are added in a recursive manner. In the first step, the contribution δf_1 arising from the wavelength band (λ_0, λ_1) is calculated and added to f_0 to obtain a new free energy density f_1, thereby accounting for fluctuations up to λ_1. In the next step, f_1 takes the place of f_0 and δf_2 from fluctuations in the band (λ_1, λ_2) is calculated and added to f_1 to obtain f_2. This process is repeated until the free energy density converges to a well defined function of mean density. All the above calculations are done at a constant temperature T. In published approaches to GRGT[33], the density fluctuations within a phase cell are assumed to vary as a cosine function. The GRGT method has a basic free parameter which is the the initial wavelength (λ_0) up to which fluctuations are accounted for in mean field theory. White introduced another parameter z which is a scale factor used to multiply the phase cell volume. Apart from these, White and other workers introduced additional parameters which have been adjusted in order to get good agreement with experimental / simulation data for critical constants i.e., critical temperature T_c, critical density ρ_c and critical pressure P_c.

In the present work[42] we start with the square-gradient approximation to (Helmholtz) free energy functional[43]. We then show that the scheme for computing contributions to free energy density δf_n at n^{th} iteration can be obtained in a more rigorous and general way than the derivation of White. The present method has the advantage that it allows us to incorporate any mean field free energy density and direct correlation function into GRGT. The assumption of cosine variation of density fluctuations is relaxed by using Wilson's functions. We also suggest a qualitative way of inferring the two parameters λ_0 and z. In Sec 2.1 we discuss the new theory in detail. Sec 2.2 shows its relationship to earlier approaches. In Sec 2.3 the theory is applied to square-well and Lennard-Jones fluids. We discuss the need to use accurate mean field theories for obtaining accurate liquid-vapor phase diagram (LVPD). The chapter is concluded in Sec 2.4.

2.1 Theory

The square-gradient approximation for the Helmholtz free energy functional[43] for a system of particles interacting with a spherically symmetric pair potential and occupying a volume V at a temperature T is given by

$$F[\rho(\vec{r})] = \int d\vec{r}\,\{f_0[T,\rho(\vec{r})] + f_G[T,\rho(\vec{r})]|\nabla\rho(\vec{r})|^2\} \tag{2.1}$$

where f_0 is the coarse-grained free energy density. The second term f_G arises only due to contributions from density fluctuations. $\rho(\vec{r})$ is the number density in an infinitesimal volume around $\vec{r}$. A simple approximation to f_0 for a fluid described by a pair potential is the first order TPT result. Using the hard sphere reference system, the free energy density functional can be expressed as

$$f_0[\rho(\vec{r})] = f_{HS}[\rho(\vec{r})] + \frac{\rho^2(\vec{r})}{2}\int d\vec{r}' u_{att}(r')g_{HS}[\rho(\vec{r}),r'] \tag{2.2}$$

where $f_{HS}[\rho(\vec{r})]$ is the free energy density functional of a hard sphere reference fluid, $u_{att}(r)$ is the attractive part of the potential and $g_{HS}[\rho,r]$ is the RDF[1] of the hard sphere system. The coefficient f_G of gradient term is given by

$$f_G[\rho(\vec{r})] = \frac{1}{12\beta}\int d\vec{r}' r'^2 c[\rho(\vec{r}),r'] \tag{2.3}$$

where $\beta = 1/k_BT$ and $c[\rho(\vec{r}),r]$ is the DCF.

To set up a consistent notation, we will continue to denote the total fluctuating density by $\rho(\vec{r})$. The mean density will be written as $\bar{\rho}$ without any arguments. As said earlier, we expand the density fluctuations into Fourier modes, each mode corresponding to a specific wavelength. Then the total range of wavelengths can be divided into bands with endpoints $\lambda_0, \lambda_1, \lambda_2, \ldots$, etc. The coarse grained mean field theory free energy density $f_0(\bar{\rho})$ contains effects of all fluctuations up to λ_0. In other words, fluctuations of wavelengths less than λ_0 are absent in the model. We will use ρ_n to denote the density consisting of fluctuations exclusively from the wavelength band $(\lambda_{n-1}, \lambda_n)$, while ρ_n^* will be its complement. As $\rho_0(\vec{r})$ has no meaning within the model, the mean den-

[1]Square brackets indicate that $g_{HS}[\rho,r]$ is a functional of $\rho(\vec{r})$ and a function of r.

sity and all the fluctuations are also expressed in $\rho_0^*(\vec{r})$, that is , $\rho(\vec{r}) = \rho_0^*(\vec{r})$. For convenience, we do not show explicitly temperature (T) in the expressions and formulae which follow. However it is assumed that the whole calculation is to be done at a specific temperature T. Also we do not show the explicit dependence of fluctuating density on $\vec{r}$ when the expression becomes cumbersome. Like mean field theory free energy density, the generalized free energy functional $f_0[\rho(\vec{r})]$ also contains a coarse graining length λ_0. However, it also contains contributions from fluctuations with wavelength greater than λ_0. In other words $f_0[\rho(\vec{r})] \equiv f_0[\rho_0^*(\vec{r})]$. Gradients in density arise from fluctuations of wavelength greater than λ_0. So we also have $f_G[\rho(\vec{r})] \equiv f_G[\rho_0^*(\vec{r})]$. Now the canonical partition function may be written as

$$e^{-\beta V f(\bar{\rho})} = \sum_{[\rho(\vec{r})]} e^{-\beta\ F[\rho(\vec{r})]} = \sum_{[\rho_0^*(\vec{r})]} e^{-\beta\ \int d\vec{r}\left(f_0[\rho_0^*(\vec{r})] + f_G[\rho_0^*(\vec{r})]|\nabla\rho_0^*|^{\ 2}\right)} \tag{2.4}$$

where the sum is over all density fluctuations of wavelengths greater than λ_0.

2.1.1 Partial summing of fluctuations

The renormalization group theory involves summing the above partition function over a band of fluctuations in (λ_0, λ_1) thereby obtaining the free energy density $\delta f_1[\rho_1^*]$ from density fluctuations in that band. Then, $\delta f_1[\bar{\rho}]$ is added, with appropriate volume factors, to the mean field theory free energy density $f_0(\bar{\rho})$ to obtain a new free energy $f_1(\bar{\rho})$. The $f_1(\bar{\rho})$ will contain contributions from density fluctuations up to wavelength λ_1. This process can then be continued in a recursive manner to include contributions from all wavelength bands. For implementing the first step in the scheme, the density $\rho_1(\vec{r})$ is written as

$$\rho_1(\vec{r}) = \rho_0^*(\vec{r}) - \rho_1^*(\vec{r}) \tag{2.5}$$

This separation is fully justified when we consider an expansion of Eq.(2.5) in terms of Fourier modes. We also separate the free energy density as

$$f_{01}[\rho_1(\vec{r})] = f_0[\rho_0^*(\vec{r})] - f_0[\rho_1^*(\vec{r})] \tag{2.6}$$

where $f_{01}[\rho_1(\vec{r})]$ is the part of $f_0[\rho_0^*(\vec{r})]$ containing fluctuations belonging only to the band (λ_0, λ_1). The second term on RHS contains density fluctuations with wavelengths greater than λ_1. Once the definition of $\rho_1(\vec{r})$ in Eq.(2.5) is justified, Eq.(2.6) follows as $f_0[\rho_1^*(\vec{r})]$ can be readily computed.
In a similar manner we rewrite the term containing $|\nabla\rho_0^*|^2$ as

$$f_{G1}[\rho_1, |\nabla\rho_1|] = f_G[\rho_0^*]|\nabla\rho_0^*|^2 - f_G[\rho_1^*]|\nabla\rho_1^*|^2 \tag{2.7}$$

The term $f_{G1}[\rho_1, |\nabla\rho_1|]$ is thus simply the difference between two functionals defined in terms of f_G.
Using Eqs.(2.5), (2.6) and (2.7), the partition function can be written as

$$e^{-\beta V f(\bar{\rho})} = \sum_{[\rho_1^*(\vec{r})]} e^{-\beta \int d\vec{r}\left(f_0[\rho_1^*(\vec{r})] + f_G[\rho_1^*]|\nabla\rho_1^*|^2\right)} \times e^{-\beta \int d\vec{r}\ \ \delta f_1[\rho_1^*, |\nabla\rho_1^*|]} \tag{2.8}$$

The second exponential term, which defines $\delta f_1[\rho_1^*, |\nabla\rho_1^*|]$, is

$$e^{-\beta \int d\vec{r}\ \delta f_1[\rho_1^*, |\nabla\rho_1^*|]} = \sum_{[\rho_1(\vec{r})]} e^{-\beta \int d\vec{r}(f_{01}[\rho_1] + f_{G1}[\rho_1, \nabla\rho_1])} \tag{2.9}$$

Eq.(2.9) shows that there are two contributions in $\delta f_1[\rho_1^*, |\nabla\rho_1^*|]$. One is from the coarse grained mean field theory free energy density and other is from the gradient term. All contribution to free energy density from fluctuations in the range (λ_0, λ_1) are contained in $\delta f_1[\rho_1^*, |\nabla\rho_1^*|]$.

2.1.2 Wilson's phase cell method

In order to evaluate the RHS of Eq.(2.9), we use Wilson's phase cell method for functional integration as explained in the intorduction(see Ref.[25]). The total volume of the system is divided into cells of volume V_1. Each cell volume V_1 is such that $\rho_1(\vec{r})$ varies significantly within it while $\rho_1^*(\vec{r})$ has only slow variation. Interaction between the cells is neglected. Thus fluctuations $\rho_1(\vec{r})$ within a cell is unaffected by variations in other cells. In order to represent a function like $\rho_1(\vec{r})$, Wilson introduced functions which are non-zero within a particular cell and zero elsewhere. These can be expressed, approximately, in

terms of Fourier modes in the interval (λ_0, λ_1). Properties of Wilson's functions are discussed in chapter 1. We give them here again for completeness. Wilson's function in the i^{th} cell is given by

$$\phi_i(\vec{r}) = \pm\frac{1}{\sqrt{V_1}} \tag{2.10}$$

where $+$ sign is for one half of the cell and $-$ sign is for the remaining half and zero elsewhere. These functions satisfy the following properties

$$\int_V d\vec{r} w_i(\vec{r}) = \int_{(V_1)_i} d\vec{r} w_i(\vec{r}) = 0 \tag{2.11}$$

$$\int_V d\vec{r} w_i(\vec{r}) w_j(\vec{r}) = \int_{(V_1)_i} d\vec{r} w_i(\vec{r}) w_j(\vec{r}) = \delta_{ij} \tag{2.12}$$

$$\int_V d\vec{r} \nabla\phi_i(\vec{r}) \nabla w_j(\vec{r}) = \int_{(V_1)_i} d\vec{r} \nabla w_i(\vec{r}) \nabla w_j(\vec{r}) \approx k_m^2 \delta_{ij} \tag{2.13}$$

where $(V_1)_i$ is the volume of the i^{th} cell, $k_m = \frac{2\pi}{\lambda_m}$ and λ_m is the mean wavelength in the band (λ_0, λ_1). Using Wilson's functions, $\rho_1(\vec{r})$ can be represented as

$$\rho_1(\vec{r}) = \sum_i \alpha_i \, w_i(\vec{r}) \tag{2.14}$$

With this representation for $\rho_1(\vec{r})$, the functional integral in Eq.(2.9) can be written as a multiple integral over the set of variables $\{\alpha_i\}$:

$$e^{-\beta \int d\vec{r} \, \delta f_1[\rho_1^*, |\nabla\rho_1^*|]} = \prod_i \int d(\alpha_i \times \sqrt{V_1}) \, e^{-\sum_i \beta \int_{V_1} d\vec{r} (f_{01}[\rho_1] + f_{G1}[\rho_1, \nabla\rho_1])} \tag{2.15}$$

The integration variable is taken as $(\alpha_i \times \sqrt{V_1})$ to make the integral dimensionless. Now, using Eq.(2.6), the integral of $f_{01}[\rho_1]$ over the cell volume V_1 can be written as

$$\int_{V_1} d\vec{r} f_{01}[\rho_1] = \frac{V_1}{2}\left(f_0[\rho_1^*(\vec{r}) + \frac{\alpha_i}{\sqrt{V_1}}] + f_0[\rho_1^*(\vec{r}) - \frac{\alpha_i}{\sqrt{V_1}}]) \right) - V_1 f_0[\rho_1^*(\vec{r})] \tag{2.16}$$

The simplest approximation in Wilson's phase cell method (see Ref. [25]) is to assume that $\rho_1^*(\vec{r})$ within the cell volume V_1 can be replaced by its value at the cell center. Generalization of the method to account for its variation has also been worked out [44]. Thus we obtain

$$\int_{V_1} d\vec{r} f_{01}[\rho_1] = \frac{V_1}{2}\left(f_0[\rho_1^*(\vec{r}_0) + \frac{\alpha_i}{\sqrt{V_1}}] + f_0[\rho_1^*(\vec{r}_0) - \frac{\alpha_i}{\sqrt{V_1}}]\right) - V_1 f_0[\rho_1^*(\vec{r}_0)] \tag{2.17}$$

Now $f_0[\rho_1^*(\vec{r}_0)]$ is a constant within V_1, and so its argument $\vec{r}_0$ will be omitted hereafter. The implications of this approximation in limiting the size of V_1 w.r.t. the the wavelength λ_1 will be discussed later. Using Eq.(2.7), the integral of $f_{G1}[\rho_1, |\nabla\rho_1|]$ over the cell volume V_1 can be written as

$$\int_{V_1} d\vec{r} f_{G1}[\rho_1, |\nabla\rho_1|] = \int_{V_1} d\vec{r}\{f_G[\rho_0^*](|\nabla\rho_1^*|^2 + |\nabla\rho_1|^2 + 2\nabla\rho_1^*.\nabla\rho_1) - f_G[\rho_1^*]|\nabla\rho_1^*|^2\} \tag{2.18}$$

Similar to the approximation for $\rho_1(\vec{r})$, we further replace $\nabla\rho_1(\vec{r})$ by its value $\nabla\rho_1(\vec{r}_0)$ at the cell centre. Then, the first term on the RHS of Eq.(2.18) becomes

$$\int_{V_1} d\vec{r} f_G[\rho_0^*]|\nabla\rho_1^*|^2 = \frac{V_1}{2}\left(f_G[\rho_1^* + \frac{\alpha_i}{\sqrt{V_1}}] + f_G[\rho_1^* - \frac{\alpha_i}{\sqrt{V_1}}]\right)|\nabla\rho_1^*|^2 \tag{2.19}$$

For obtaining the second term, which is proportional to $|\nabla\rho_1|^2$, first of all we note from the shape of Wilson's functions that $\nabla\rho_1$ is non-zero only when ρ_1 changes sign and hence becomes zero. Thus we get

$$\int_{V_1} d\vec{r}\, f_G[\rho_0^*(\vec{r})]|\nabla\rho_1|^2 = \int_{V_1} d\vec{r} f_G[\rho_1^*(\vec{r})]\alpha_i^2|\nabla\phi_i(\vec{r})|^2 = f_G[\rho_1(\vec{r}_0)^*]\alpha_i^2 k_m^2 \tag{2.20}$$

where we have replaced $f_G[\rho_1^*(\vec{r})]$ by its value at the center. The last equality follows from the orthogonality condition in Eq.(2.13). Within the same approximation, the third term on the RHS of Eq.(2.18) vanishes on integration over V_1 as there is no overlap of wave vectors in ρ_1^* and ρ_1. Thus Eq.(2.18) reduces to

$$\int_{V_1} d\vec{r} f_{G1}[\rho_1, |\nabla\rho_1|] = \frac{V_1}{2}\left(f_G[\rho_1^* + \frac{\alpha_i}{\sqrt{V_1}}] + f_G[\rho_1^* - \frac{\alpha_i}{\sqrt{V_1}}]\right)|\nabla\rho_1^*|^2 - V_1 f_G[\rho_1^*]|\nabla\rho_1^*|^2 + f_G[\rho_1^*]\alpha_i^2 k_m^2 \quad (2.21)$$

Using Eq.(2.17) and Eq.(2.21) in Eq.(2.15) and converting the total volume integral of $\delta f_1[\rho_1^*, |\nabla\rho_1^*|]$ to a sum over the cells, we obtain

$$e^{-\beta V_1\ \delta f_1(\rho_1^*, |\nabla\rho_1^*|)} = \int d\alpha \times \sqrt{V_1}\ e^{-\beta V_1 \delta f[\rho_1^*, |\nabla\rho_1^*|, V_1, k_m, \alpha]} \quad (2.22)$$

where the cell index i on α_i is omitted. The exponent in the integrand $\delta f[\rho_1^*, |\nabla\rho_1^*|, V_1, k_m, \alpha]$ is defined as

$$\delta f[\rho_1^*, |\nabla\rho_1^*|, V_1, k_m, \alpha] = \frac{1}{2}\left(f_0[\rho_1^* + \frac{\alpha}{\sqrt{V_1}}] + f_0[\rho_1^* - \frac{\alpha}{\sqrt{V_1}}] - 2f_0[\rho_1^*]\right) + \frac{1}{2}\left(f_G[\rho_1^* + \frac{\alpha}{\sqrt{V_1}}] + f_G[\rho_1^* - \frac{\alpha}{\sqrt{V_1}}] - 2f_G[\rho_1^*]\right)|\nabla\rho_1^*|^2 + f_G[\rho_1^*]\frac{\alpha^2}{V_1}k_m^2 \quad (2.23)$$

Changing the integration variable to $x = \alpha/\sqrt{V_1}$, Eq.(2.22) can be expressed as

$$-\beta V_1\ \delta f_1(\rho_1^*, |\nabla\rho_1^*|) = ln\left\{V_1 \int dx\ e^{-\beta V_1\ \delta f[\rho_1^*, |\nabla\rho_1^*|, k_m, x]}\right\} \quad (2.24)$$

where $\delta f[\rho_1^*, |\nabla\rho_1^*|, k_m, x]$ is given by

$$\delta f[\rho_1^*, |\nabla\rho_1^*|, k_m, x] = \frac{1}{2}\left(f_0[\rho_1^* + x] + f_0[\rho_1^* - x] - 2f_0[\rho_1^*]\right) + \frac{1}{2}\left(f_G[\rho_1^* + x] + f_G[\rho_1^* - x] - 2f_G[\rho_1^*]\right)|\nabla\rho_1^*|^2 + f_G[\rho_1^*]x^2 k_m^2 \quad (2.25)$$

In Eq.(2.24), the range of integration is [0, $min\{\rho, \rho_{max} - \rho\}$] where ρ_{max} corresponds to the fluid-solid transition density. As the integrand is an even function of x, we take $x \geq 0$. The upper limit arises from the requirement that the arguments of $f_0[\rho_1^* \pm x]$ and $f_G[\rho_1^* \pm x]$ are restricted to lie in the interval $(0, \rho_{max})$.

2.1.3 Redefining the correction term

The aim in calculating $\delta f_1[\rho_1^*, |\nabla\rho_1^*|]$ is to obtain the correction from density fluctuations of wavelength in the band (λ_0, λ_1). This can be added to the mean field theory free energy containing density fluctuations up to λ_0. The corrected free energy will then contain effects of fluctuations up to λ_1. Therefore, to avoid any spurious effects, it is necessary to renormalize $\delta f_1[\rho_1^*, |\nabla\rho_1^*|]$ to be zero when λ_1 is replaced by λ_0, which is the coarse graining length in the starting mean field theory . The term to be subtracted can be obtained simply by replacing k_m in Eq.(2.24) by $k_0 = 2\pi/\lambda_0$. Thus we redefine $\delta f_1(\rho_1^*, |\nabla\rho_1^*|)$ as

$$-\beta\, V_1 \delta f_1[\rho_1^*, |\nabla\rho_1^*|] = ln\left\{V_1 \int dx\; e^{-\beta V_1\ \delta f[\rho_1^*, |\nabla\rho_1^*|, k_m, x]}\right\} - ln\left\{V_1 \int dx\; e^{-\beta V_1\ \delta f[\rho_1^*, |\nabla\rho_1^*|, k_0, x]}\right\} \tag{2.26}$$

Thus the final expression for $\delta f_1[\rho_1^*, |\nabla\rho_1^*|]$ is given by

$$\delta f_1[\rho_1^*, |\nabla\rho_1^*|] = -\frac{1}{\beta V_1} ln\left\{\frac{\int dx\; e^{-\beta V_1\ \delta f[\rho_1^*, |\nabla\rho_1^*|, k_m, x]}}{\int dx\; e^{-\beta V_1\ \delta f[\rho_1^*, |\nabla\rho_1^*|, k_0, x]}}\right\} \tag{2.27}$$

Above expression is quite general in that all the features of the original Helmholtz free energy functional $F[\rho]$ are retained in it. That is, $f_0[\rho(\vec{r})]$ and $f_G[\rho(\vec{r})]$ are sufficiently general and do not refer to any specific liquid state theory. Also, the appearance of gradient term in the expression for $\delta f[\rho_1^*, |\nabla\rho_1^*|]$ is new. After evaluating Eq.(2.27) for small values of $|\nabla\rho_1^*|^2$, the LHS can be approximated as $\delta f_1[\rho_1^*, 0] + \delta f_1'[\rho_1^*, 0]|\nabla\rho_1^*|^2$ where $\delta f_1'$ denotes derivative with $|\nabla\rho_1^*|^2$. Addition of this result to $f_0[\rho_1^*] + f_G[\rho_1^*]|\nabla\rho_1^*|^2$ will generate the functional for next iteration. Thus $f_0[\rho_1^*]$ as well as $f_G[\rho_1^*]$ will be corrected after the first iteration. However, the contribution of derivative term would be small as the dependence of the direct correlation function $c[\rho(\vec{r}), r]$ on density is generally weak in the fluid phase.

2.1.4 GRGT iterations for Free energy density

The iterative scheme in GRGT for free energy density is as follows. For a given temperature T, the zeroth iterate is the mean field theory free energy density $f_0(\bar{\rho})$. The correction term δf_1 at first iteration is obtained by substituting $\bar{\rho}$ in place of ρ_1^* in Eq.(2.27). However, for obtaining the numerical results for this work, we shall restrict $f_G(\bar{\rho})$ to be a function of the mean density only. Then, terms multiplying $|\nabla\rho_1^*|$ will be absent even in Eq.(2.25). Results which will include the effects of these terms will be reported separately. For the remaining discussions, the correction δf_1 can be written explicitly as a function of mean density, and is given by

$$\delta f_1(\bar{\rho}) = -\frac{1}{\beta V_1} ln \left\{ \frac{\int dx\ e^{-\beta V_1\ \delta f(\bar{\rho},k_n,x)}}{\int dx\ e^{-\beta V_1\ \delta f(\bar{\rho},k_0,x)}} \right\} \tag{2.28}$$

where $\delta f(\bar{\rho}, k_n, x)$ can be written as

$$\delta f(\bar{\rho}, k_n, x) = \frac{1}{2}\left(f_0(\bar{\rho}+x) + f_0(\bar{\rho}-x) - 2f_0(\bar{\rho})\right) + f_G(\bar{\rho})x^2k_n^2 \tag{2.29}$$

We now have the first order corrected free energy density

$$f_1(\bar{\rho}) = f_0(\bar{\rho}) + \delta f_1(\bar{\rho}) \tag{2.30}$$

At this stage, $f_1(\bar{\rho})$ contains contribution of density fluctuations up to wave length λ_1. However, it is devoid of any contribution from higher wavelengths. But the process can be repeated to get $f_2(\bar{\rho})$ using Eq.(2.28) and Eq.(2.29) with V_2 and $f_1(\bar{\rho})$ replacing V_1 and $f_0(\bar{\rho})$ respectively. Thus the second order iterate will contain density fluctuations up to λ_2. Continuation of the process will yield a converged free energy density containing fluctuations up to any desired level.

The volume of the phase cell at the level of n^{th} iteration is

$$V_n = \left(\frac{z\lambda_n}{2}\right)^3;\ \lambda_n = 2^n\lambda_0;\ k_n = \frac{2\pi}{\lambda_n} \tag{2.31}$$

where z and λ_0 are two free parameters in the theory. These have been adjusted in earlier applications [34] to get good agreement with vapor-liquid phase diagram of model systems. However, we shall fix their values based on simple arguments, and look for the accuracy that can be achieved with the method described.

2.1.5 Determining free parameters

The parameter z may be inferred in the following way. If the density fluctuations in ρ_1 have wave numbers between $\Lambda_0/q < \Lambda < \Lambda_0$, then the volume occupied by them in k-space is $V_k = (2\Lambda_0)^3 - (2\Lambda_0/q)^3$. Then the minimum volume V_{min} occupied by the fluctuation wave-packet in real space is $(\frac{\lambda}{2})^3 \frac{q^3}{q^3-1}$, where $\lambda = 2\pi/\Lambda_0$. Comparing this volume V_{min} with the phase cell volume at n^{th} iteration, we get $z = q/(q^3-1)^{1/3}$. For $q = 2$, which is a compromise value for practical calculations, $V_{min} = (\frac{\lambda}{2} \times 1.0455)^3$ and hence $z = 1.0455$.

The second parameter may be inferred using an estimate of the correlation length in the mean field theory. The correlation length can be related to the RDF corresponding to the temperature and mean density under consideration. In the present method λ_0 is the typical wavelength up to which mean field theory accounts for fluctuations. The GRGT takes into account all density fluctuations starting from λ_0 including those present in the initial mean field theory free energy density f_0. Thus λ_0 can be taken as the shortest wavelength which is accounted for in the mean field theory. In a strict sense, it may not be possible to assign a precise value for λ_0. Here take it to be twice the position of the first peak (representing nearest neighbor correlations) of $4\pi r^2 h(r)$ where $h(r) = g(r) - 1$ corresponding to the highest density in the liquid phase(for a given temperature) i.e., the density near the melting line.

2.2 Relation to earlier GRGT's

Earliest developments of GRGT by White[34] assumed some specific forms of the free energy density functional. The Mean Spherical Approximation (MSA) was employed as the mean field theory by Tang and co-workers [36, 37]. Lue

and Prausnitz [38] developed a slightly more general approach somewhat similar to the development presented here. These approaches are briefly discussed below.

2.2.1 White's Theory

The expression derived by White[34] for $\delta f_1(\rho_1^*)$ can be recovered with some specific choices in our general approach. First of all, the mean field theory free energy density is taken as the first order perturbation theory result

$$f_{MFT}[\bar{\rho}] = f_{HS}[\bar{\rho}] + \frac{\bar{\rho}^2}{2}\int d\vec{r} u_{att}(\vec{r}) g_{HS}(\bar{\rho}, r) \tag{2.32}$$

The functional $f_0[\rho(\vec{r})]$ is explicitly defined by introducing the total density into hard sphere component as

$$f_0[\rho(\vec{r})] = f_{HS}[\rho(\vec{r})] \tag{2.33}$$

The fluctuating part corresponding to the term $f_G[\rho(\vec{r})]|\nabla\rho(\vec{r})|^2$ (see Eq.(2.3)) is taken as

$$\frac{\rho^2(\vec{r})}{2}\int d\vec{r}' \cos(\vec{k}.\vec{r}') u_{att}(r') g_{HS}[\rho(\vec{r}), r'] \tag{2.34}$$

The cosine term has been introduced in an ad-hoc way to bring in an explicit dependence of fluctuating part on wave vector. If the cosine term is expanded, one can easily see that the first term which is independent of k is the first order correction term to free energy density (second term in Eq.(2.32)). The second term depends on k^2 and can be seen to be exactly equal to the last term in Eq.(2.29) if one uses $-\beta u_{att}(r) g_{HS}(r)$ for direct correlation function. The normalization of δf_n is different in that the denominator in Eq.(2.27) is computed with $k_0 = 0$. The parameters λ_0 and z are adjusted for getting agreement with simulation data.

2.2.2 Tang's Theory

Tang and co-workers have developed a MSA solution for the Lennard-Jones fluid. The first order perturbation theory can be modified (after defining an equivalent hard sphere diameter) to incorporate the RDF from MSA in addition to the hard sphere function. Thus functional $f_0[\rho(\vec{r})]$ (see Eq.2.2) is defined as

$$f_0[\rho(\vec{r})] = f_{HS}[\rho(\vec{r})] + \frac{\rho^2(\vec{r})}{2} \int d\vec{r}' u_{att}(r') \left(g_{HS}[\rho(\vec{r}), r'] + \frac{g_{MSA}[\rho(\vec{r}), r']}{2} \right) \quad (2.35)$$

Tang and co-workers [36] consider the term corresponding to $f_G[\rho(\vec{r})]|\nabla\rho(\vec{r})|^2$ as follows. The attractive part of the potential introduces long wavelength fluctuations which they expressed as

$$\frac{1}{2} \int d\vec{r}_1 \int d\vec{r}_2 u_{att}(|\vec{r}_1 - \vec{r}_2|) \left(\rho^{(2)}(\vec{r}_1, \vec{r}_2) - \rho^2(\vec{r}_1) g[|\vec{r}_1 - \vec{r}_2|, \rho(\vec{r}_1)] \right) \quad (2.36)$$

Where $\rho^{(2)}(\vec{r}_1, \vec{r}_2)$ is two particle density and $\vec{r} = \vec{r}_1 - \vec{r}_2$. Here the assumption is that the above term, which cancels out in the mean field picture, gives the contribution of fluctuations. Corrections to mean field theory are then derived by assuming that the fluctuations in f_0 can be treated using Wilson's method and that in $f_G[\rho(\vec{r})]|\nabla\rho(\vec{r})|^2$ by introducing a cosine function explicitly dependent on wave vector. The normalization of δf_n is somewhat similar to that in White's theory. A slightly different formulation for f_G was also considered in [37].

2.2.3 Lue-Prausnitz Theory

Lue and Prausnitz pursued an approach somewhat similar to our method described in this work, though there are some important differences. Their starting free energy functional is

$$F[\rho(\vec{r})] = \int d\vec{r} \left\{ f_0[\rho(\vec{r})] - a\rho^2(\vec{r}) + \frac{a}{2}\xi^2 |\nabla\rho(\vec{r})|^2] \right\} \quad (2.37)$$

where $a\xi^2 = \frac{1}{6}\int d\vec{r} r^2 u_{att}(r)$ is a special case of f_G obtained by substituting $-\beta u_{att}(r)$ for $c[\rho(\vec{r}), r]$. The functional f_0 is taken as the MSA free energy density and White's method is followed.

Our formulation starting with the square gradient free energy functional is more general since the coefficient of square gradient in the above Eq.(2.37) is a special case of f_G in the present case. As discussed earlier, the general form of f_G leads to new terms in the iterative corrections. More specifically, δf_1 contains additional terms proportional to square gradient of density (see Eq.2.25), which is new to the theory. Thus our method has the advantage that it can be coupled with integral equation theories[5] through the direct correlation function $c[\rho(\vec{r}), r]$. Also, Wilson's phase cell method for functional integration is effected very much in line with his original ideas thereby bringing a close analogy between magnetic and fluid theories. We also find that the normalization of correction terms can be introduced for the sake of removing fluctuation contributions within the coarse graining length scale.

2.3 Square Well and Lennard-Jones fluids

We have applied the theory discussed above to square well fluids of ranges 3.0 and 1.5 and Lennard-Jones fluids with the following approximations. Reduced units ($\epsilon/k_B = \sigma = 1$ where ϵ is the well depth, k_B is the Boltzmann constant, σ is hard sphere diameter) are used throughout. Firstly, as mentioned in the discussion above Eq.(2.28), the square-gradient term in δf_1 has been neglected restricting f_G and thus $c[\rho, r]$ to be functions of average density $\bar{\rho}$. Secondly, we take for f_0, the free energy density obtained from first order perturbation theory (Eq.(2.2)). For the reference system free energy density, f_{HS}, we used the Carnahan-Starling [15] expression. We have chosen λ_0 to be the first peak of $4\pi r^2 h(r)$ of the hard sphere system at density corresponding to its fluid-solid transition ($\bar{\rho} = 1.02$). This choice is made because the structure of any fluid is mainly determined by the repulsive core. Further, the sensitivity of LVPD to λ_0 is assumed to be small. At this density, the λ_0 turned out to be 4.05. We have done calculations using two simple forms for the direct corre-

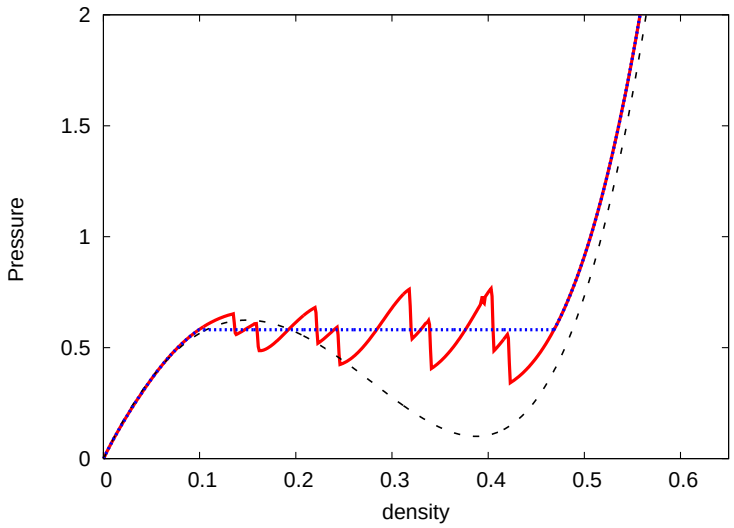

Figure 2.1: Subcritical isotherm of square well fluid of range = 3.0 at temperature T = 9.0. Temperature(T), Pressure(P) and density(ρ) are in reduced units . (dashed line: mean field theory with VanderWaals loop), (solid line : pressure after five iterations), (dotted line: fully converged pressure).

lation functions: First is given by $c_1(r) = -\beta u_{att}(r) g_{HS}(r)$ and the second is $c_2(r) = (1 - e^{\beta u_{att}(r)}) g_{HS}(r)$ (dependence of $c(r)$ and $g_{HS}(r)$ on average density is not shown explicitly for notational convenience). Our calculations used $g_{HS}(r)$ obtained for the hard sphere system from Percus Yevick(PY) closure. Even though the $g_{HS}(r)$ from PY closure is not consistent with the Carnahan-Starling expression for f_{HS}, the difference in final results would be negligible from those with a more accurate version of $g_{HS}(r)$. The numerical procedure used here is similar to that of White [33, 35] and hence is not discussed here. Similar approximations were used earlier [33–35, 38] but the parameters in the theory have been adjusted to in order to match the theoretical results with the simulation data for critical constants. Our aim in carrying out the numerical work is to see the accuracy in predictions based on the current method in its simplest form without adjusting the parameters.

A typical subcritical isotherm, for square well fluid of range 3.0, at different levels of iterations obtained from our theory is shown in fig.(2.1). The mean field theory pressure is a smooth curve with a Van der Waals loop. As the iter-

ations proceed, the region inside the binodal becomes oscillatory (as shown in fig.(2.1)). The amplitude of the oscillations decreases from iteration to iteration, making the isotherm flatter. Thus the current theory gives a flat isotherm in the binodal region. We found that, the number of iterations required to obtain a flat isotherm (or converged free energy density inside the binodal) depends on the temperature and the initial wavelength λ_0. This dependence is seen to be arising because of the normalization used in δf_1 (see Eq.(2.27)). Close to the critical region, typically few tens of iterations are required for obtaining a flat isotherm to single precision accuracy. But, far from the critical region, the number of iterations required increases to a few hundreds. However, in any case, the free energy density outside the binodal converges to single precision accuracy within ten iterations. We have also checked that the isotherm obtained using Maxwell's construction also converges (within five to ten iterations) to that obtained from the fully converged free energy density. Thus a prescription for obtaining the coexistence points could be that, close to the critical region (around 20% from T_c), iterations can be continued till the free energy density provides a flat isotherm in the binodal, while far from T_c, Maxwell's construction may be used.

Liquid Vapor coexistence curves for the square well fluids with ranges 3.0 and 1.5 are shown in fig.(2.2) and fig.(2.3), respectively. GRGT values for the critical constants (T_c, ρ_c, P_c) in the case of range 3.0 are $(9.83, 0.26, 0.91)$ while simulations [45] predict $(9.87, 0.26, 0.84)$, respectively. These results show that T_c and ρ_c obtained by GRGT are in excellent agreement with simulation data. However, the critical pressure P_c has a slightly larger deviation. In this case we find that the differences between results obtained by using the two forms of $c(r)$ described above are negligible. Fig.2.2 shows that GRGT results are significantly better than those of mean field theory as the critical region is approached. Both match well far from the critical region. There is also excellent agreement between the simulation data and the GRGT results throughout the phase diagram.

Critical parameters (T_c, ρ_c, P_c) for square well fluids with range 1.5 are $(1.30, 0.30, 0.14)$ using $c_1(r)$ and $(1.29, 0.32, 0.13)$ using $c_2(r)$. However, simulations [45] predict

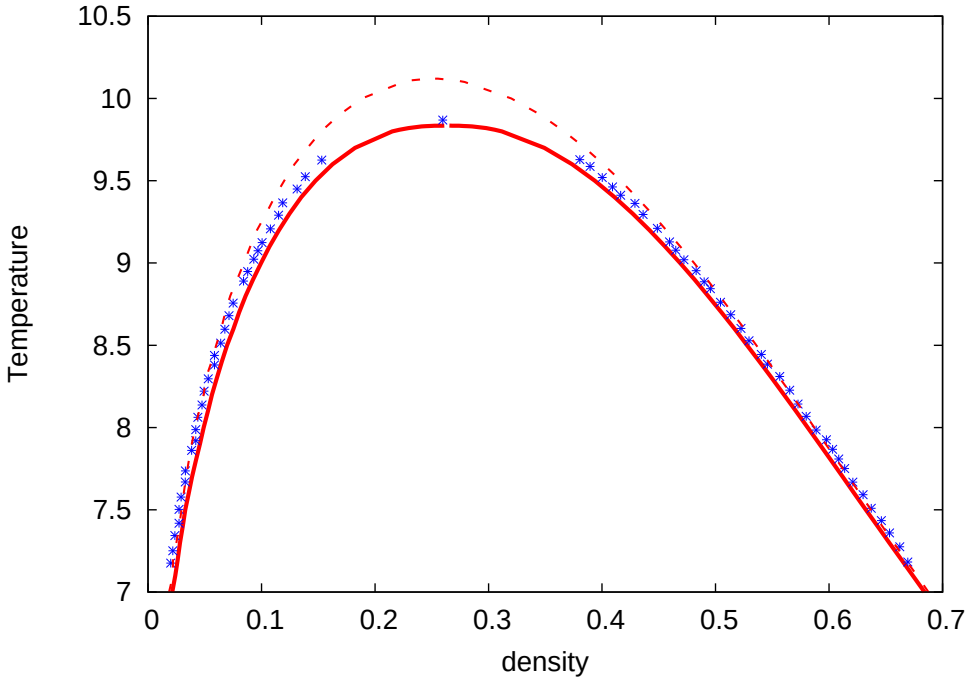

Figure 2.2: Liquid-vapour coexistence curve of square well fluid with range = 3.0. T and ρ are in reduced units. (dashed line : mean field theory), (solid line: GRGT), (squares : simulation data[45])

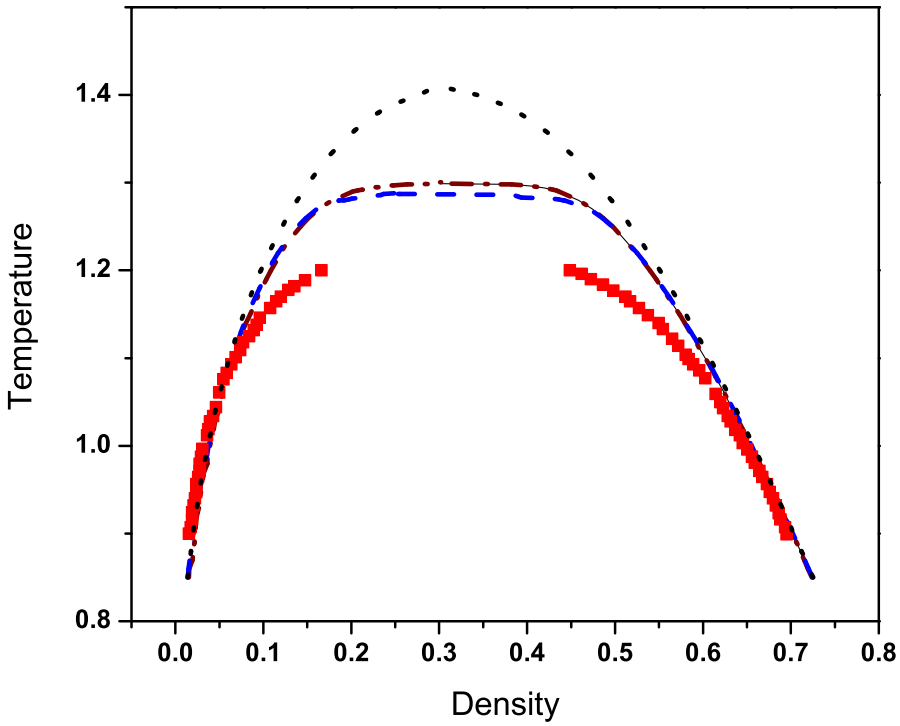

Figure 2.3: Liquid-vapour coexistence curve of square well fluid with width = 1.5. T and ρ are in reduced units. (Dotted line: mean field theory), (Dash-dot line: GRGT with $c_1(r)$), (Dashed line : GRGT with $c_2(r)$), (squares: simulation data[45])

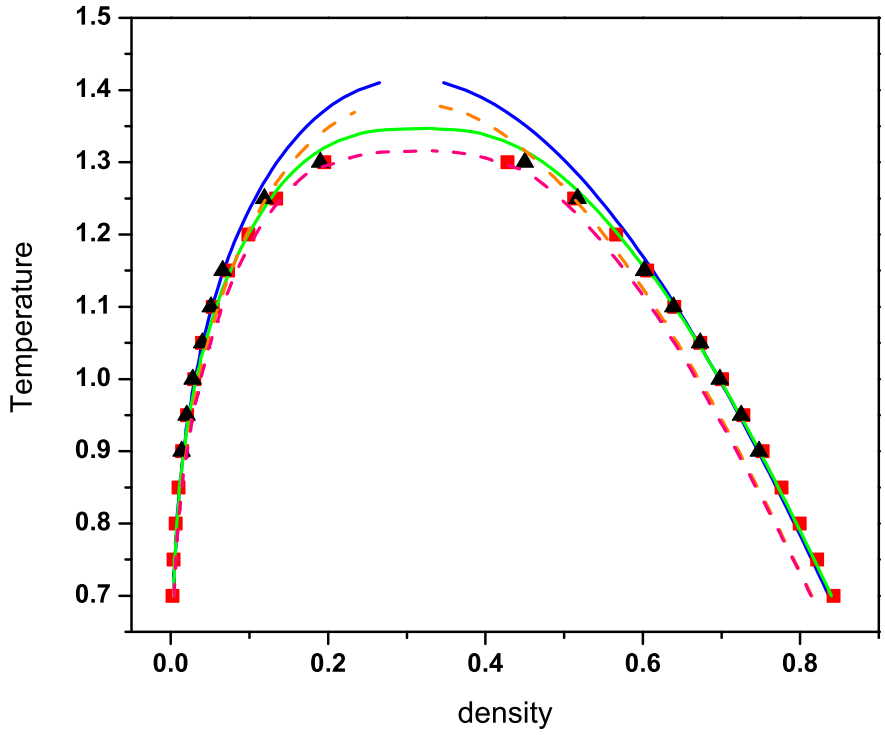

Figure 2.4: Liquid-vapour coexistence curve of Lennard-Jones fluid. T and ρ are in reduced units. (Upper solid line: HS-WCA), (lower solid line: HS-WCA + GRGT), (Upper dashed line : BH), (Lower dashed line: BH + GRGT), (squares [46] and triangles [47] simulation data)

$(1.218, 0.310, 0.095)$. Even though the GRGT improves the results with respect to mean field theory , there are still significant deviations from simulation data (see Fig.2.3). We also find that there are slight differences between the results obtained using the two forms of $c(r)$. Results using $c_2(r)$ are seen to provide slightly better T_c and P_c values in comparison to those of $c_1(r)$.

The phase diagram obtained using GRGT for Lennard-Jones fluid is shown in Fig.(2.4). We have done calculations using two mean field theory free energies. One is the first order Barker-Hendersen (BH)[10] theory and the other is the Hard-Sphere-Weeks-Chandler-Andersen (HS-WCA) theory of Amotz and Stell [19]. It can be seen from Fig.(2.4) that the BH theory is not very accurate along the liquid side of the phase diagram and its deficiency can be noticed in GRGT + BH theory results also. The HS-WCA is quite accurate in the region away from the critical point. The phase diagram of GRGT + HS-WCA also

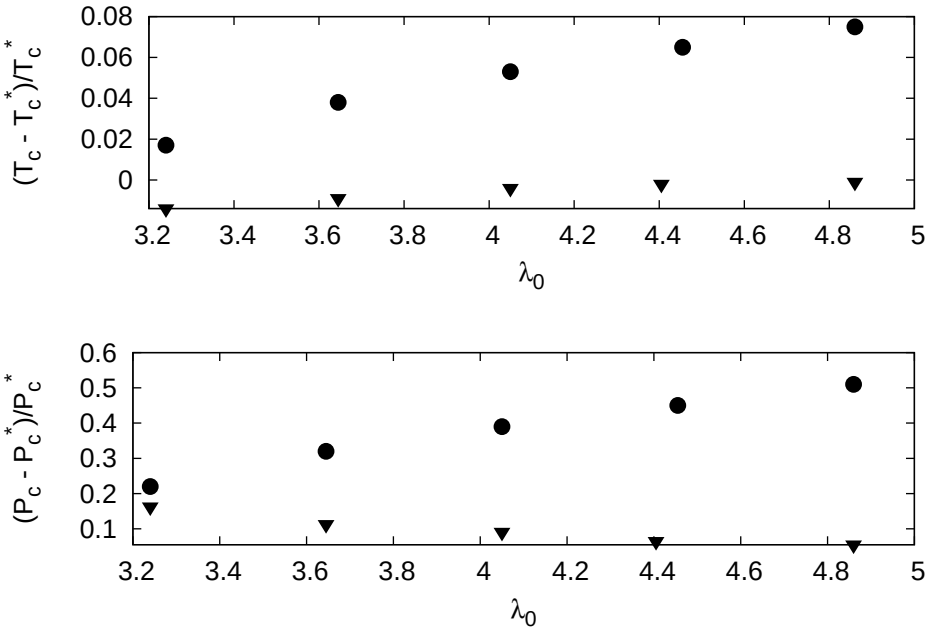

Figure 2.5: Relative deviation of calculated critical pressure P_c and critical Temperature T_c from the corresponding simulation values P_c^*, T_c^* against λ_0 in units of hard sphere diameter. Circles: square-well fluid of range = 1.5, Triangles: for square-well fluid of range = 3.0

matches with that of HS-WCA in this region and improves it close to the critical region. The whole phase diagram agrees well with simulation data. Differences in the results for the two different forms of $c(r)$ closures are negligible in this case also. The critical constants (T_c, ρ_c, P_c) obtained using GRGT + HS-WCA are $(1.34, 0.33, 0.15)$ while GRGT + BH provide $(1.32, 0.33, 0.14)$. These agree well with simulation data $(1.31, 0.31, 0.13)$ [46]. It can be noticed that the critical constants obtained using the GRGT + BH theory are more close to the simulation data than the GRGT + HS-WCA results. However, in view of its performance in the LVPD, we conclude that the high accuracy of GRGT + BH prediction of critical constants is fortuitous.

Also we have checked the sensitivity of LVPD $w.r.t.$ coarse graining length λ_0 in the case of square-well fluids. The variations of T_c and P_c when λ_0 is varied up to 20% around its original value (4.05) are shown in fig.(2.5). For the square-well fluid of range 3.0, relative deviation (for both T_c and P_c) is more

for small values of λ_0 and as λ_0 is increased, the results tend to simulation values. This shows that the effects of short range fluctuations will be slightly overestimated by choosing a smaller value of λ_0. In the case of square well fluid of range 1.5, the relative deviation decreases when λ_0 is decreased. Hence more fluctuation effects of shorter wavelengths than that obtained with $\lambda_0 = 4.05$ have to be added. In both the above cases, it can be seen that the results tend uniformly to simulation values as λ_0 is appropriately varied. Thus one of the reasons for the errors (see Fig.2.3) could be the approximate estimate of λ_0 chosen based on $g_{HS}(r)$ in the present calculation. A choice based on the $g(r)$ of the actual system would improve the accuracy of the results. The critical density ρ_c is seen to vary negligibly in both cases.

Also, it can be seen that in the case of square well fluid of range 3.0, the sensitivity of the results to λ_0 is quite small. This could be because of two reasons. First, the fluctuation effects are less owing to the larger range of the potential. Second, the mean field theory used is good enough far from the critical region and also in qualitative agreement with simulation results even in the critical region. Also, in the case of Lennard-Jones fluid, it can be seen that the liquid side of the LVPD obtained from GRGT + BH theory didn't improve over the BH theory far from the critical region where its agreement with simulation data is not good. Thus the current method of GRGT requires a mean field theory which is in good agreement with simulation/experimental values far from the critical region and a proper value of λ_0 chosen from the $g(r)$ of the actual system.

2.4 Summary and Conclusions

In this chapter, we have presented a general derivation of GRGT starting from the square-gradient approximation for the Helmholtz free energy functional. White's assumption of cosine variation of density is relaxed by using Wilson's functions to represent the density fluctuations. The generalization of GRGT to include a general functional (f_G) multiplying the gradient term is a new result and leads to additional terms in the iterative corrections to free energy den-

sity. We suggested a way to infer the parameters λ_0 and z in the theory, rather than adjusting them for agreement with simulation data. The theory has been applied to square well fluids of ranges 3.0 and 1.5 and Lennard-Jones fluids. We have shown that the present method gives a flat isotherm in the two phase region. We have not explicitly calculated the critical exponents. However, a flat sub-critical isotherm and a flatter phase diagram close to the critical region than the mean field theory phase diagram indicate the non-classical behavior of the critical exponents. Also earlier workers[48] have shown that the method reproduces non-classical critical exponents. Since our work is a generalization of the earlier methods, we expect the same to be valid here.

We observed that the present implementation of the GRGT has some shortcomings. The method is inaccurate for fluids with short range potentials even though there is some improvement over the mean field theory. The sensitivity of results to variation of λ_0 increases with decrease in the range of the potential. Also, as the range is decreased, the phase diagram close to the critical region becomes excessively flat. This problem has been reported by other workers also[49]. Apart from these, the convergence of the GRGT iteration scheme is slow away from the critical region .

One reason for inaccuracy of the present method for fluids with short range potentials is error in the mean-field Helmholtz free energy and the coefficient of the square-gradient term, termed as influence parameter in the literature[50], used in our calculations. Another possible reason could be the error in the Wilson's method of functional integration. However, it is apparent from the results that the error in the mean-field theory itself is significant throughout the phase diagram. Since the contribution of GRGT is supposed to be significant only close to the critical region, it is conjectured that the major error is from the mean-field terms.

In the next chapter, we develop an improved mean field theory for obtaining the Helmholtz free energy and structural properties of a homogeneous fluid so that the influence parameter may also be obtained.

CHAPTER 3

Coupling parameter expansion in perturbation theory of simple fluids

3.1 Introduction

In the previous chapter, we concluded that an accurate mean field Helmholtz free energy and an accurate DCF[1] would improve the results of the GRGT. Various mean field theories for obtaining the thermodynamic properties of simple fluids have been discussed in chapter 1 along with their limitations. The integral equation theory gives the correlation functions (i.e., the RDF and DCF) using which the thermodynamic properties may be obtained from various routes (i.e., the virial, the energy and the compressibility routes). However, the integral equation theory has no solution in the phase-coexistence region. Hence the method cannot be used in conjunction with GRGT. The perturbation theory as developed by Zhou[23, 24], called the coupling parameter expansion(CPE) method, seemed promising. However, the finite difference method used in obtaining the $\left.\frac{d^n g}{d\zeta^n}\right|_0$ is not accurate enough to obtain derivatives of order higher than three and requires smoothing procedures to remove unwanted fluctuations in the calculated derivatives. Apart from this the method is computationally much more expensive than the previously existing methods.

In this chapter, we present a new approach to evaluate the terms of the coupling parameter series expansion for Helmholtz free energy which is equivalent to that of Zhou but with added advantages. We assume that the RDF ($g(r)$) and the DCF ($c(r)$) of the perturbed system are functions of the coupling parameter ζ (introduced in Chapter 1) and that they can be expressed as a Taylor series in ζ around $\zeta = 0$. Then we derive a system of linear equations con-

[1]The influence parameter is second moment of the DCF.

necting the derivatives of $c(\zeta, r)$ in real space and $g(\zeta, r)$ in Fourier space, by using a general closure relation obtained from diagrammatic analysis and the OZE [1]. This coupled sets of equations is easily solved in a self-consistent way to obtain all the required derivatives. Thus the new method avoids using the finite difference method for obtaining the derivatives of $g(\zeta, r)$ and accurate derivatives up to any order can be easily obtained without requiring any smoothing procedures. Another important advantage of the present theory is that it gives both $g(r)$ and $c(r)$ of the actual system, apart from the Helmholtz free energy.

Initially, a simplified version of the theory[51] is derived which assumes that the derivatives of the bridge function do not depend on ζ. The assumption is equivalent to the reference hyper-netted chain(RHNC) approximation[52]. The simplified theory (hereafter referred as RHNC-CPE) is applied to square-well fluids of various ranges and correlation functions and liquid vapor coexistence curves are obtained. The results are compared with available simulation data. In the later part of the chapter, a generalized derivation of the method[53] which accounts for the dependence of bridge function on ζ is given. The generalized method is applied to square-well and Lennard-Jones fluids and its performance is analyzed.

The chapter is organized as follows. In section 3.2 first the general CPE method is derived and later the simplification using RHNC is discussed. In section 3.3 the RHNC-CPE method is applied to square well fluids. In section 3.4, a generalized version of the CPE method is presented. Application of generalized CPE to square-well and Lennard-Jones fluids is described in section 3.5. The chapter is concluded in section 3.6.

3.2 Coupling parameter expansion method

Consider a simple classical fluid of particles, at a temperature T, interacting with a spherically symmetric pair potential $u(r)$ where r is the inter-particle distance. The potential is split into $u_{ref}(r)$, the reference system potential, and $u_{per}(r)$ the perturbation part. It is assumed that the structural ($c(\zeta = 0, r)$ and

$g(\zeta = 0, r)$) and thermodynamic properties of the reference system are known. We will denote the radial distribution function , direct correlation function and the Helmholtz free energy density of the reference fluid as $g_0(r), c_0(r)$ and $f_0(\rho)$, where ρ is the macroscopic density of the homogeneous fluid. A fictitious system with interaction potential defined as

$$u(\zeta, r) = u_{ref}(r) + \zeta u_{per}(r) \tag{3.1}$$

is considered for the perturbation theory, where ζ is the coupling parameter. The effect of increasing ζ from zero to unity is to gradually switch on the perturbation. We postulate that the radial distribution function and direct correlation function of the system with potential $u(\zeta, r)$ can be written as a MacLaurin series in ζ, that is,

$$c(\zeta, r) = c_0(r) + \zeta \left(\frac{\partial c}{\partial \zeta}\right)_{\zeta=0} + \frac{\zeta^2}{2!}\left(\frac{\partial^2 c}{\partial \zeta^2}\right)_{\zeta=0} + ... \tag{3.2}$$

$$g(\zeta, r) = g_0(r) + \zeta \left(\frac{\partial g}{\partial \zeta}\right)_{\zeta=0} + \frac{\zeta^2}{2!}\left(\frac{\partial^2 g}{\partial \zeta^2}\right)_{\zeta=0} + ... \tag{3.3}$$

It is assumed that the series converge for all ζ in $[0, 1]$ and the direct correlation function and radial distribution function of the actual system can be obtained by putting $\zeta = 1$. Hereafter we shall denote n^{th} partial derivative of any function $X(\zeta, r)\ w.r.t\ \zeta$ as $X^{(n)}(\zeta, r)$.

A general closure relation for the direct correlation function $c(\zeta, r)$ provided by liquid state theory is [1, 5]

$$c(\zeta, r) = \exp(-\beta u(\zeta, r) + y(\zeta, r) + B(\zeta, r)) - y(\zeta, r) - 1 \tag{3.4}$$

where $y(\zeta, r)$ is the indirect correlation function defined as $h(\zeta, r) - c(\zeta, r)$ and $h(\zeta, r) = g(\zeta, r) - 1$ is the total correlation function of the fictitious fluid. The bridge function $B(\zeta, r)$ is a sum of an infinite series of the "bridge diagrams" [5]. Since $g(\zeta, r)$, and hence $h(\zeta, r)$, as well as $c(\zeta, r)$ are expanded in a series in ζ, the correlation function $y(\zeta, r)$ is also a series in ζ. The n^{th} order coefficient in its series is given by $y^{(n)}(\zeta, r) = h^{(n)}(\zeta, r) - c^{(n)}(\zeta, r)$.

In a similar manner, the bridge function $B(\zeta, r)$ also should be considered as a series in ζ. Several approximations to $B(\zeta, r)$ in terms of $y(\zeta, r)$ and certain empirical parameters are available [5]. However to simplify the present formulation, we assume that $B(\zeta, r)$ is independent of ζ which is nothing but the RHNC approximation. Thus the bridge function of the perturbed system, close to $\zeta = 0$, is assumed to be the same as that of the reference system. This approximation has been used by Zhou [23] as all the derivatives of $g(\zeta, r)$, needed in the theory, are to be computed only at $\zeta = 0$. Adequacy of this assumption, except for short range potentials, has also been established by Zhou by comparing its results with simulation data [24].

3.2.1 Third Order Theory

First of all we shall elaborate the method for third order RHNC-CPE, wherein the series in Eq.(3.2) and Eq.(3.3) are truncated after the first three terms. As $B(r)$ is assumed to be independent of ζ, differentiating Eq.(3.4) $w.r.t.\ \zeta$ we get

$$c^{(1)}(\zeta, r) = (-\beta u_{per}(r) + y^{(1)}(\zeta, r))g(\zeta, r) - y^{(1)}(\zeta, r) \tag{3.5}$$

where we have used the definition of the $g(\zeta, r)$ given by [1, 5]:

$$g(\zeta, r) = \exp(-\beta u(\zeta, r) + y(\zeta, r) + B(r)) \tag{3.6}$$

In a similar manner the second derivative is obtained as,

$$c^{(2)}(\zeta, r) = (-\beta u_{per}(r) + y^{(1)}(\zeta, r))^2 g(\zeta, r) + y^{(2)}(\zeta, r)(g(\zeta, r) - 1) \tag{3.7}$$

To get another set of relations between $c^{(n)}(\zeta, r)$ and $y^{(n)}(\zeta, r)$, we consider the OZE in Fourier space:

$$h(\zeta, k) = \frac{c(\zeta, k)}{1 - \rho c(\zeta, k)} \tag{3.8}$$

where $h(\zeta, k)$ and $c(\zeta, k)$ are the Fourier transforms of $h(\zeta, r)$ and $c(\zeta, r)$, respectively. For instance, the transform of $h(\zeta, r)$ and its inverse are defined

as

$$h(\zeta,k) = 4\pi \int_0^\infty \frac{sin(kr)}{kr} h(\zeta,r)dr \tag{3.9}$$

$$h(\zeta,r) = \frac{1}{2\pi^2} \int_0^\infty \frac{sin(kr)}{kr} h(\zeta,k)dk \tag{3.10}$$

Differentiating Eq.(3.8) $w.r.t.\ \zeta$ we obtain

$$h^{(1)}(\zeta,k) = c^{(1)}(\zeta,k)s^2(\zeta,k) \tag{3.11}$$

where the structure factor $s(\zeta,k)$ is defined as

$$s(\zeta,k) = \frac{1}{1-\rho c(\zeta,k)} \tag{3.12}$$

In a similar way, the second derivative $h^{(2)}(\zeta,k)$ is obtained as

$$h^{(2)}(\zeta,k) = c^{(2)}(\zeta,k)s^2(\zeta,k) + 2\rho(c^{(1)}(\zeta,k))^2 s^3(\zeta,k) \tag{3.13}$$

Eq.(3.11) and Eq.(3.13) now provide $y^{(1)}(\zeta,k)$ and $y^{(2)}(\zeta,k)$. As the $g(0,r)$ and the structure factor $s(0,k)$ of the reference system are known, Eq.(3.5) and Eq.(3.7) can be evaluated at $\zeta = 0$. Thus the closed set of four linear equations, defining the third order theory, are given by

$$c^{(1)}(0,r) = (-\beta u_{per}(r) + y^{(1)}(0,r))g(0,r) - y^{(1)}(0,r) \tag{3.14}$$

$$c^{(2)}(0,r) = (-\beta u_{per}(r) + y^{(1)}(0,r))^2 g(0,r) + y^{(2)}(0,r)(g(0,r)-1) \tag{3.15}$$

$$y^{(1)}(0,k) = c^{(1)}(0,k)(s^2(0,k)-1) \tag{3.16}$$

$$y^{(2)}(0,k) = c^{(2)}(0,k)(s^2(0,k)-1) + 2\rho(c^{(1)}(0,k))^2 s^3(0,k) \tag{3.17}$$

We solve this system of equations using a simple iterative method. Starting with guess solutions for $y^{(1)}(0,r)$ and $y^{(2)}(0,r)$, which are usually taken as zero, we determine $c^{(1)}(0,r)$ and $c^{(2)}(0,r)$. Then their Fourier transforms are obtained using an fast Fourier transform algorithm, thereby obtaining $y^{(1)}(0,k)$

and $y^{(2)}(0,k)$. Inverse Fourier transforms of these functions provide $y^{(1)}(0,r)$ and $y^{(2)}(0,r)$ for the next iteration, and the procedure is continued till convergence is obtained. More details of the numerical procedure are discussed in the next section.

The correlation functions $c(1,r)$ and $g(1,r)$ of the actual system are obtained from Eq.(3.2) and Eq.(3.3), respectively, by putting $\zeta = 1$. The CPE for Helmholtz free energy density $f(\rho)$ of a homogeneous fluid is given by [1]

$$f(\rho) = f_{ref}(\rho) + \frac{\rho^2}{2}\int_0^1 d\zeta \int d\vec{r}\, u_{per}(r) g(\zeta, r) \tag{3.18}$$

where $f_{ref}(\rho)$ is the free energy density of the reference system. Substituting Eq.(3.3) in Eq.(3.18) and integrating over ζ, we get

$$f(\rho) = f_{ref}(\rho) + \frac{\rho^2}{2}\int d\vec{r}\, u_{per}(r)\left(g_0(r) + \frac{1}{2!}\, g^{(1)}(0,r) + \frac{1}{3!}\, g^{(2)}(0,r)\right) \tag{3.19}$$

Here we have used the shortened notation for the derivatives $(\partial^n g(r)/\partial\zeta^n)_{\zeta=0}$ which is readily obtained as $y^{(n)}(0,r) + c^{(n)}(0,r)$. Thus the method provides the direct correlation function , radial distribution function as well as the free energy density.

3.2.2 General Order Theory

The RHNC-CPE method outlined above can be generalized to any arbitrary order. Writing $g(\zeta, r)$ in the short form

$$g(\zeta, r) = \exp(f(\zeta, r)) \tag{3.20}$$

$$f(\zeta, r) = -\beta\left(u_{ref}(r) + \zeta u_{per}(r)\right) + y(\zeta, r) + B(r) \tag{3.21}$$

the general expression for its n^{th} order derivative is found to be

$$g^{(n)}(\zeta, r) = \sum_{m=0}^{(n-1)} [C_m^{(n-1)}]\; f^{(n-m)}(\zeta, r)\; g^{(m)}(\zeta, r),\; n \geq 1 \tag{3.22}$$

where $[C_m^{(n-1)}]$ is the binomial coefficient. The derivatives $f^{(n)}(\zeta, r)$ are given by

$$f^{(n)}(\zeta, r) = -\beta u_{per}(r)\ \delta_{n,1} + y^{(n)}(\zeta, r),\ n \geq 1 \tag{3.23}$$

where $\delta_{n,1}$ is the Kronecker delta. The derivatives $g^{(n)}(\zeta, r)$ can be computed using Eq.(3.22) in a recursive manner, using $f^{(n)}(\zeta, r)$ either from an initial guess or from the previous iteration. Now, using Eq.(3.6), we rewrite the closure in Eq.(3.4) as

$$c(\zeta, r) = g(\zeta, r) - y(\zeta, r) - 1 \tag{3.24}$$

which readily provides its n^{th} order derivative

$$c^{(n)}(\zeta, r) = g^{(n)}(\zeta, r) - y^{(n)}(\zeta, r),\ n \geq 1. \tag{3.25}$$

The structure factor introduced in Eq.(3.12) is rewritten as

$$s(\zeta, k) = 1 + \rho c(\zeta, k)\ s(\zeta, k) \tag{3.26}$$

This equation can be differentiated using the Leibniz rule to obtain

$$s^{(n)}(\zeta, k) = \rho \sum_{m=0}^{n} [C_m^n]\ c^{(n-m)}(\zeta, k)\ s^{(m)}(\zeta, k),\ n \geq 1. \tag{3.27}$$

Transferring the last term in the sum to the $l.h.s$ and using Eq.(3.12) we get

$$s^{(n)}(\zeta, k) = [s^{(0)}(\zeta, k)]\ \rho \sum_{m=0}^{(n-1)} [C_m^n]\ c^{(n-m)}(\zeta, k)\ s^{(m)}(\zeta, k),\ n \geq 1 \tag{3.28}$$

Using the values of $c^{(m)}(\zeta, k)$ from the current iteration, Eq.(3.28) can be evaluated recursively. Finally, using $s(\zeta, k) = 1 + \rho h(\zeta, k)$, the derivatives of $y(\zeta, k) = h(\zeta, k) - c(\zeta, k)$ are expressed as

$$y^{(n)}(\zeta, k) = \rho^{-1}\ s^{(n)}(\zeta, k) - c^{(n)}(\zeta, k),\ n \geq 1 \tag{3.29}$$

Eq.(3.25) and Eq.(3.29) provide the general equations for the derivatives. These can be readily solved using the same iteration method outlined for third order

theory.

3.3 Application to Square Well Fluids

We applied the RHNC-CPE theory described above to square-well fluids as ample amount of simulation data for different square-well widths are available for comparison. Radial distribution functions for ranges 1.3 and 1.5 and phase diagrams for ranges 1.25 to 2.3 are considered to test the accuracy of the present theory. First order theory is known to be highly inaccurate for these cases. Results of calculations using third, fifth and seventh order versions of the present theory are compared with those of first order theory and simulations. Reduced units ($\epsilon/k_B = \sigma = 1$, where ϵ is the well depth and σ is hard sphere diameter) are used throughout.

3.3.1 Numerical Procedure

The numerical procedure used to solve the coupled set of linear equations for the derivatives $c^{(n)}(0,r)$ and $g^{(n)}(0,r)$ is as follows. It is assumed that $c^{(0)}(0,r) = c_0(r)$ and $g^{(0)}(0,r) = g_0(r)$ are known. If only $g_0(r)$ is known, $c_0(r)$ can be calculated using the Ornstein Zernike equation and a proper numerical procedure [54, 55]. To compute the derivatives, say, in n^{th} order theory, Eq.(3.25) in real space and Eq.(3.29) in Fourier space are solved employing an iterative procedure. First of all, we choose guess solutions for $y^{(m)}(0,r)$, for all m in the range $1 \leq m \leq n$, and compute $g^{(m)}(0,r)$, recursively, using Eq.(3.22). In practice, we take null solutions as the starting guesses. Then, $c^{(m)}(0,r)$ are obtained using Eq.(3.25). Next, their Fourier transforms $c^{(m)}(0,k)$ are computed using an FFT algorithm. Mesh widths in the range 0.01 to 0.001 are found to be adequate. These are employed in Eq.(3.28) to obtain $s^{(m)}(0,k)$ recursively. These functions, when used in Eq.(3.29), provide $y^{(m)}(0,k)$. Inverse Fourier transformation gives $y^{(m)}(0,r)$. This completes the first iteration. However, before starting the next iteration, we employ a linear mixing of the previous and new solutions: $\alpha y^{(m)}(0,r)+(1-\alpha)y^{(m)}(0,r) \rightarrow y^{(m)}(0,r)$. They are then used in Eq.(3.25) for the second iteration. The procedure is repeated until

the root mean square differences between successive iterates of $y^{(m)}(0,r)$, for all m, are less than a prescribed tolerance. We find that $\alpha = 0.5$ and tolerance of 10^{-8} are adequate to get accurate solutions.

3.3.2 Structural Properties

For application to square-well fluids, the hard sphere fluid is the natural reference system. Even though any bridge function can be used in Eq.(3.4), to determine the properties of the hard sphere system, we have used $B(r)$ provided by Malijevsky and Labik [56], as used by Zhou[24]. The Ornstein Zernike equation is then solved for the hard sphere system using the standard iterative method [57]. With the properties of hard sphere fluid so determined, the derivatives up to fourth order ($g^{(n)}(0,r),\ n = 1,4$) from the present theory can be directly compared with those of Zhou. Fig.3.1 shows this comparison and we find that the derivatives obtained from the present method and the finite difference method used by Zhou match with negligible deviations. However, our numerical scheme is much simpler and even higher order derivatives can be easily calculated without resorting to any smoothing procedures. Radial distribution function of square-well fluids obtained using fifth order and seventh order versions of the present theory are plotted in Fig.3.2, Fig.3.3 and Fig.3.4. For the case of range 1.5 (see Fig.3.2), $g(r)$ obtained using our theory is in excellent agreement with simulation results [58] except for a very small deviation in the square-well region for $\rho = 0.2$. Similar convergence of the RHNC-CPE series is found for range 1.3 (see Fig.3.3) even though some differences with simulation data are noticeable at $\rho = 0.4$ also. In Fig.3.4 we show $g(r)$ obtained using third, fifth and seventh order versions of the theory for square-well fluid of range 1.25 at temperature $T = 0.56$, density $\rho = 0.2$ and for square-well fluid of range 1.2 at temperature $T = 0.45$, density $\rho = 0.4$. These cases clearly show that the convergence of the series is slow for short-ranged potentials at very low temperatures and densities. Thus for extremely short ranged potentials, contribution from terms higher than sixth order in Taylor series expansion of $g(r)$ become important. In Fig.3.5, $c(r)$ obtained using seventh order version of our theory is compared with the simulation re-

sults of [59] for two cases: square-well fluid of range 1.25 at $T = 2.0$, $\rho = 0.75$ and square-well fluid of range 1.2 at $T = 2.0$, $\rho = 0.75$. The agreement with experiment is good in the former case whereas slight deviation is found in the latter case. Comparison for smaller widths was not possible because of lack of simulation data for $c(r)$.

We have also observed that the present approach doesn't have any numerical convergence problems neither in the two-phase region nor close to the critical region. In contrast, the integral equation theories generally fail to have a solution in the two phase region and the numerical algorithms have slow convergence in the critical region. This is an interesting feature of the present theory and requires a further detailed investigation with different bridge functions and interatomic potentials. Further, the DCF $c(r) = c(1, r)$ obtained using the present method can find applications in density functional theories of inhomogeneous fluids. For example, in the square-gradient functional for inhomogeneous systems, the coefficient of the gradient term, called influence parameter, depends explicitly on $c(r)$ of the homogeneous system. As the integral equation theories generally do not have solutions in the spinodal region, interpolation techniques are required to obtain the influence parameter[50]. The DCF ($c(1, r)$) of the actual system obtained from our method can be directly used to obtain the influence parameter which is required for the GRGT calculations. The present theory also has the advantage of accommodating any bridge function for computing the derivatives, though we have used only the simple hard sphere version for this work.

3.3.3 Liquid-Vapor Phase Diagrams

We compare the liquid-vapor phase diagrams (LVPD) for square-well fluids of ranges $1.25,\ 1.375,\ 1.5$ and 2.3 using first order, third order, fifth order and seventh order versions of the present RHNC-CPE method. These are shown in Fig.(3.6) together with simulation data for the different ranges. It is clear that there is an enormous improvement in the results over first order perturbation theory, which is quite apparent for smaller ranges i.e., 1.5 and smaller. For range 2.3, the difference between fifth order and seventh order RHNC-CPE

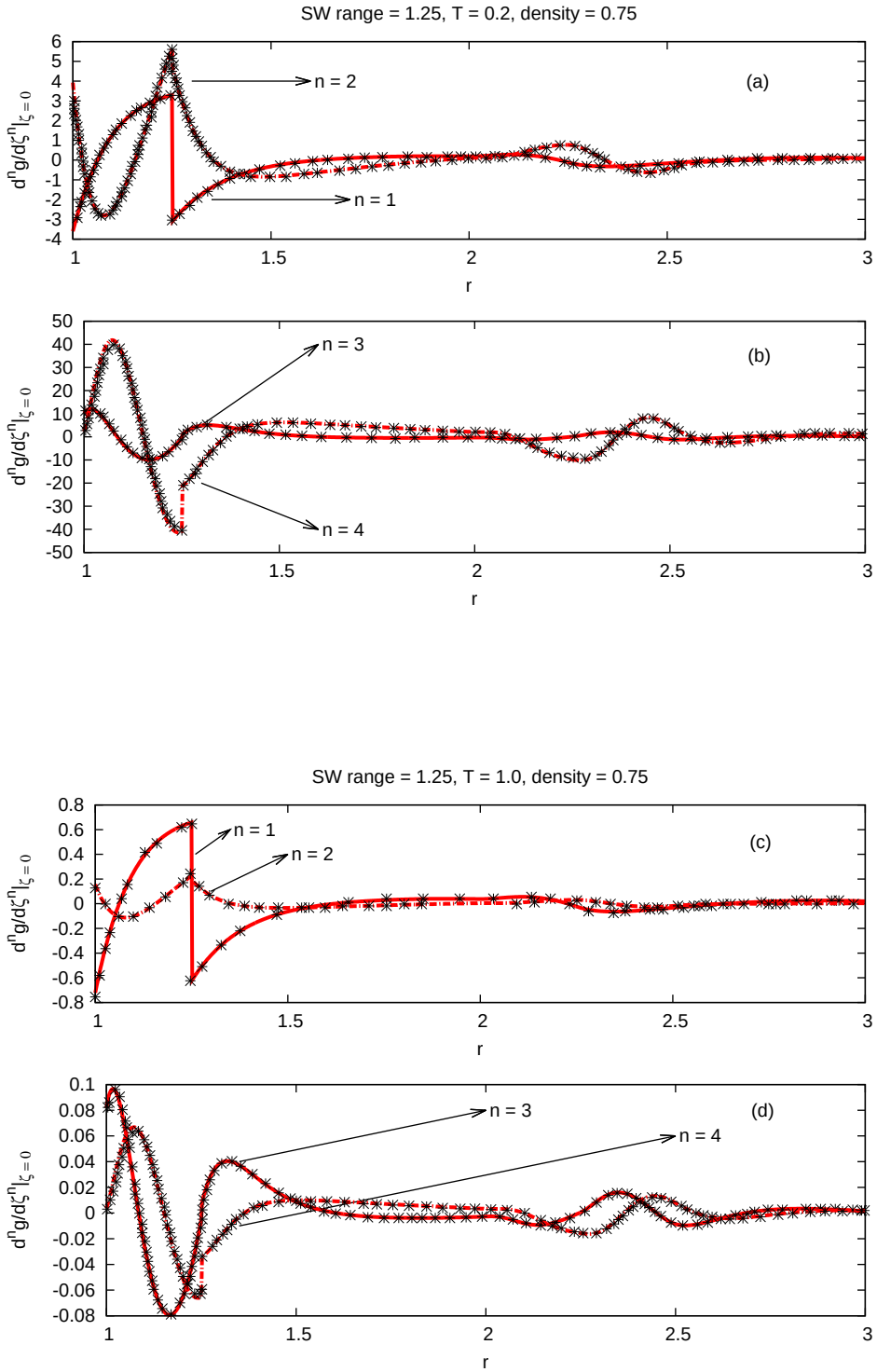

Figure 3.1: (From top to bottom) First and second figure are derivatives of $g(r)$ up to fourth order for square-well fluid of range 1.25 at reduced temperature $T = 0.2$ and reduced density $\rho = 0.75$. Third and fourth figure are derivatives of $g(r)$ up to fourth order for square-well fluid of range 1.25 at reduced temperature $T = 1.0$ and reduced density $\rho = 0.75$. (solid line and dash-dot: present theory), (stars: Zhou's results [24])

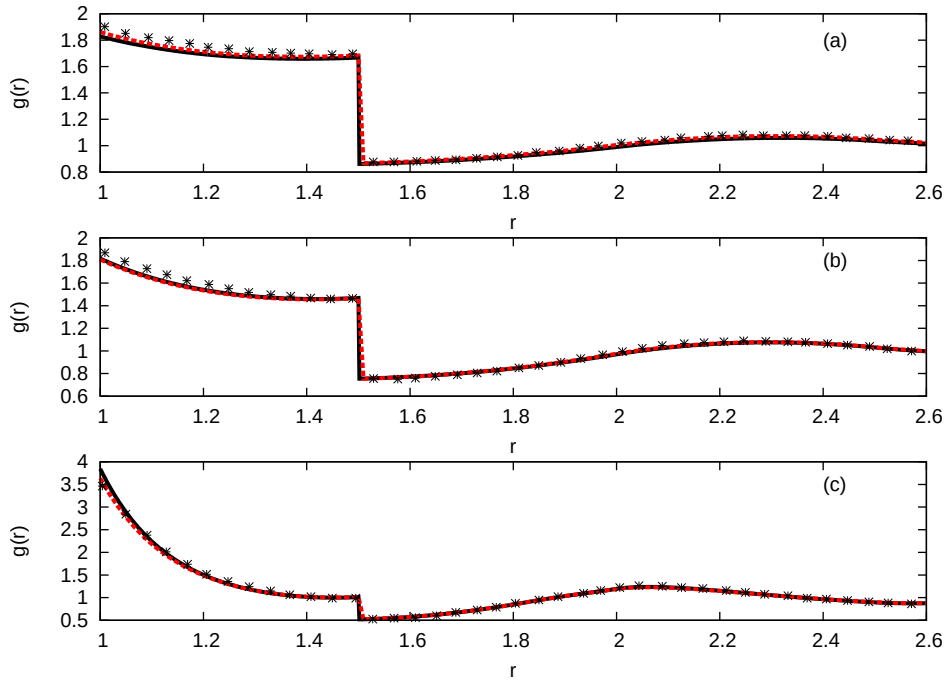

Figure 3.2: $g(r)$ for square-well fluid of range 1.5 at reduced temperature $T = 1.5$. Plots from top to bottom are for reduced density $\rho = 0.2$, 0.4 and 0.8 respectively. (Solid line: fifth order RHNC-CPE), (Dashed line : seventh order RHNC-CPE), (stars: simulation results [58])

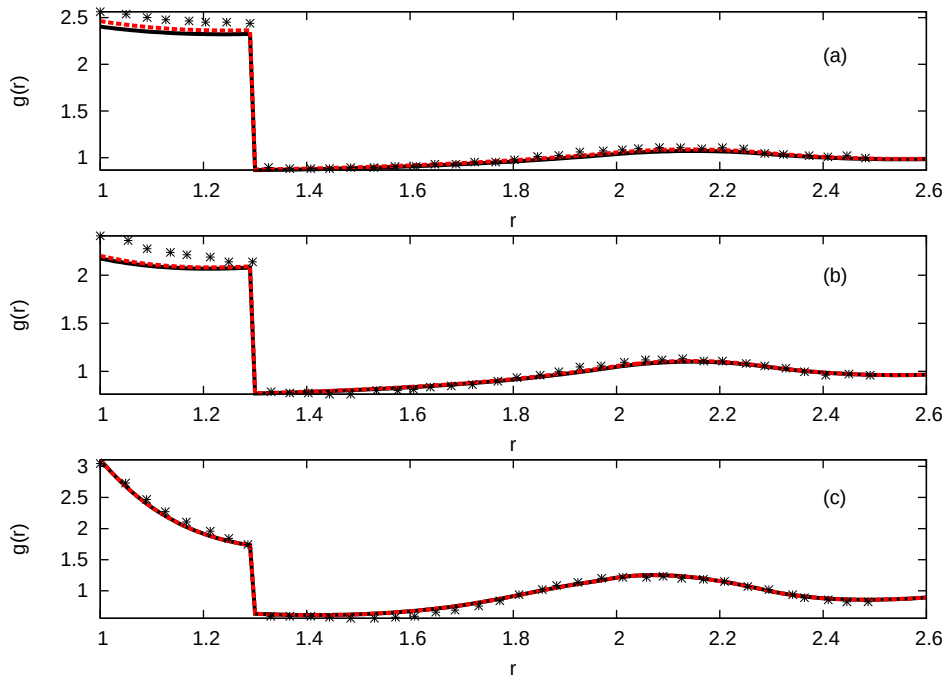

Figure 3.3: $g(r)$ for square-well fluid of range 1.3 at reduced temperature $T = 1.0$. Plots from top to bottom are for reduced density $\rho = 0.2$, 0.4 and 0.8 respectively. (Solid line: fifth order RHNC-CPE), (Dashed line : seventh order RHNC-CPE), (stars: simulation results [58])

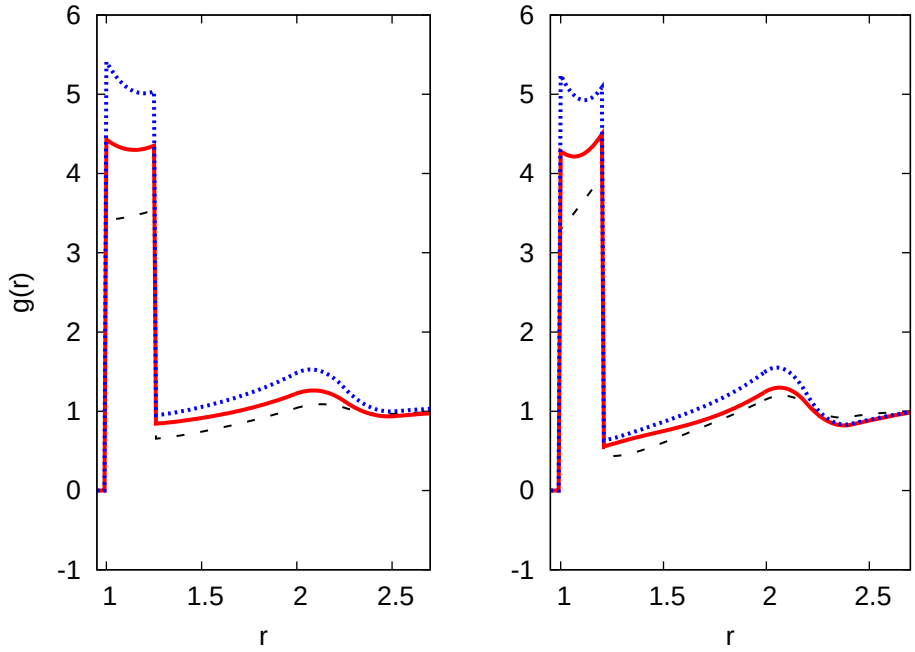

Figure 3.4: (Left figure) $g(r)$ for square-well fluid of range 1.25 at temperature $T = 0.56$ and density $\rho = 0.2$ in reduced units. (Right figure) $g(r)$ for square-well fluid of range 1.2 at temperature $T = 0.45$ and density $\rho = 0.4$ in reduced units. (Dashed line: third order RHNC-CPE), (Soild line: fifth order RHNC-CPE), (Dotted line : seventh order RHNC-CPE)

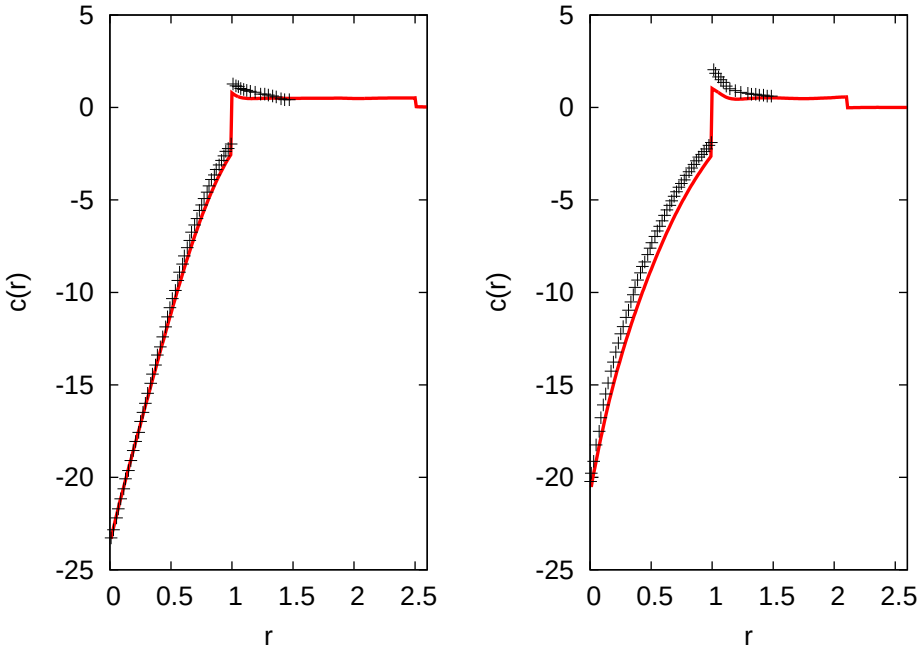

Figure 3.5: (Left) $c(r)$ for square-well fluid of range 2.5, Temperature $T = 2.0$, density $\rho = 0.75$ in reduced units. (Right) $c(r)$ for square-well fluid of range 2.1, Temperature $T = 2.0$, density $\rho = 0.75$ in reduced units.(solid line: seventh order RHNC-CPE results), (pluses: Simulations[59])

is small even in the critical region and we can conclude that the perturbation series of Helmholtz free energy has practically converged. However, they differ from the first order RHNC-CPE and simulation data in the critical region. Similar results are noted even for the cases of range 1.5 even though the error in first order RHNC-CPE is much larger. For ranges 1.375 and 1.25, the differences between the fifth and seventh order RHNC-CPE are quite small, but noticeable in certain parts of the phase plane. Thus for the cases presented, convergence of the perturbation series of Helmholtz free energy is satisfactory and faster than that of the series of $g(r)$ which is expected. However, there is still significant deviation from the simulation results for the three cases i.e., for square-well fluids of ranges $1.25,\ 1.375,\ 1.5$. We also note that neglecting the ζ dependence of bridge function $B(\zeta, r)$ has brought in more asymmetry than expected in the phase diagram resulting in a shift of the critical point towards the liquid side. Now that the perturbation series has converged, we can clearly conclude that the deviation is caused because of the following reasons: first is the bridge function used in the calculation and the RHNC approximation and secondly because of long range fluctuations. Improving the results using a better bridge function is within the scope of the theory. Whereas methods of renormalization group theory need to be used to bring in better agreement in the critical region[42].

3.4 Generalized coupling parameter expansion method

As explained above,there has been significant deviation of the obtained liquid vapor phase diagrams using the RHNC version of coupling parameter expansion from simulation data for narrow square-well fluids. It was concluded that the deviation and slow convergence could be because of neglected derivatives of bridge function $w.r.t.\ \zeta$ in our calculations and the error in the bridge function we have chosen for calculation.

In this section we describe a generalized version of CPE method[53] with application to square-well and Lennard-Jones fluids. We use the bridge func-

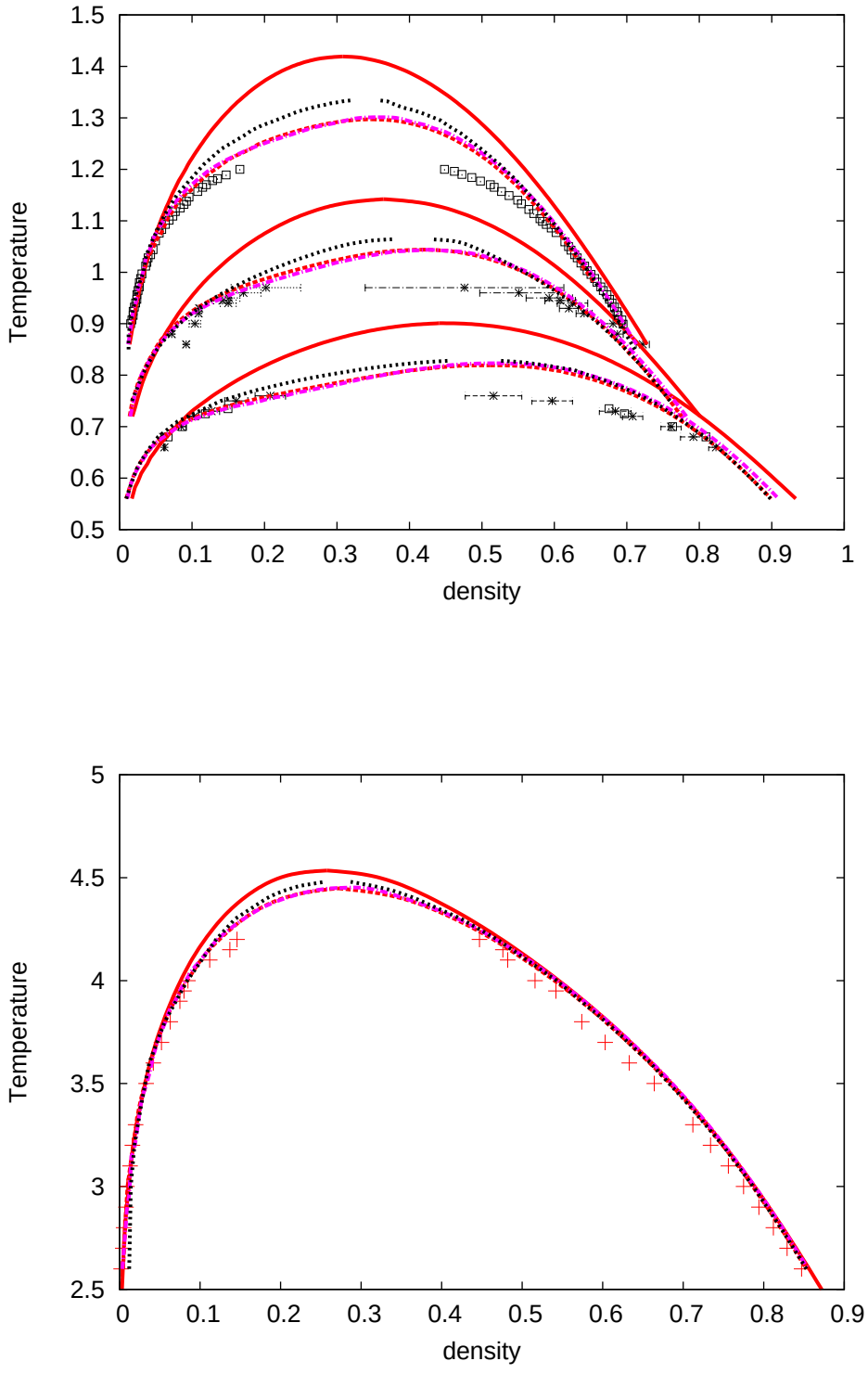

Figure 3.6: (Top figure) Liquid-vapour coexistence curves in reduced temperature and density of square-well fluids of widths 1.5, 1.375 and 1.25 in reduced units (from top to bottom). (Bottom figure) liquid-vapour coexistence curve in reduced temperature and density of square-well fluid of width 2.3 in reduced units. (Solid line: First order RHNC-CPE), (Dotted line: Third order RHNC-CPE), (Dashed line: Fifth order RHNC-CPE), (Dash-Dot line : seventh order RHNC-CPE), (stars,squares,pluses: simulation results [45, 60–62])

tion proposed by Sarkisov[63] with slight modification for square-well fluids[64] and include its derivatives $w.r.t.\ \zeta$ in the calculation. Thus we refer to the method as S-CPE hereafter. We obtain RDFs, isotherms and LVPDs for square-well fluids of various ranges and compare with those obtained from solving the OZE with the modified Sarkisov bridge function and available simulation data. We also compare our results with available results of other existing theories.

Also, using the RHNC-CPE, we were able to obtain the $g(r)$ and $c(r)$ inside the spinodal and close to the critical region without any problems of convergence of the iteration scheme even though our numerical scheme was very simple. This could be an indication of the existence of the solution to OZE inside the spinodal region. The $g(r)$ and $c(r)$ in the two-phase region find applications in the density functional theory of fluids [43]. One example is the calculation of surface tension. This calculation requires the $c(r)$ in the two phase region. As the integral equation theories do not have solution in some part of the liquid vapor coexistence region, earlier calculations of surface tension were done using an interpolation formula given by Ebner $et.al.$ [65] to obtain $c(r)$ inside the two-phase region. Using the generalized coupling parameter expansion we calculate the surface tension for square-well fluids of ranges 1.25, 1.375 and 1.75 using the expression obtained from the square gradient functional for Helmholtz free energy and compare with simulation results.

As an application of CPE to non-hard sphere reference systems, we apply it to Lennard-Jones fluid. We use the Sarkisov bridge function[63] for both reference system and perturbation part. The radial distribution functions, isotherms and the liquid vapor coexistence curves for the Lennard-Jones fluid are obtained and compared with those obtained from integral equation theory and simulations wherever available.

Basic theory is the same as explained in the section 3.2 except for a generalization to include derivatives of bridge function in the calculation. Thus, in the Eq.(3.21), $B(r)$ is replaced by $B(\zeta, r)$. The general expression for n^{th} order

derivative of $g(\zeta, r)$ from Eq.(3.21) now becomes

$$g^{(n)}(\zeta, r) = \sum_{m=0}^{(n-1)} [C_m^{(n-1)}]\ \phi^{(n-m)}(\zeta, r)\ g^{(m)}(\zeta, r),\ n \geq\ 1 \tag{3.30}$$

where $[C_m^{(n-1)}]$ is the binomial coefficient. The derivatives $\phi^{(n)}(\zeta, r)$ are given by

$$\phi^{(n)}(\zeta, r) = -\beta u_{per}(r)\ \delta_{n,1} + y^{(n)}(\zeta, r) + B^{(n)}(\zeta, r),\ n \geq 1 \tag{3.31}$$

where $\delta_{n,1}$ is the Kronecker delta. The derivatives $g^{(n)}(\zeta, r)$ can be computed using Eq.(3.30) in a recursive manner, using $\phi^{(n)}(\zeta, r)$ either from initial guess or from previous iteration. Remaining part of the derivation is exactly same as earlier.

For example, to obtain Taylor series expansion up to second term, the set of four equations given by

$$\begin{aligned}
c^{(1)}(0,r) &= (-\beta u_{per}(r) + y^{(1)}(0,r) + B^{(1)}(0,r))g(0,r) - y^{(1)}(0,r) && (3.32)\\
c^{(2)}(0,r) &= (-\beta u_{per}(r) + y^{(1)}(0,r) + B^{(1)}(0,r))^2 g(0,r) && (3.33)\\
&\quad + B^{(2)}(0,r)g(0,r) + y^{(2)}(0,r)(g(0,r) - 1) &&\\
y^{(1)}(0,k) &= c^{(1)}(0,k)(s^2(0,k) - 1) && (3.34)\\
y^{(2)}(0,k) &= c^{(2)}(0,k)(s^2(0,k) - 1) + 2\rho(c^{(1)}(0,k))^2 s^3(0,k) && (3.35)
\end{aligned}$$

have to be solved (where $g(0,r)$ is $y(0,r) + c(0,r) + 1$).

3.5 Applications

3.5.1 Square-Well Fluids: correlation functions and liquid vapor coexistence curves

Seventh order version of the generalized CPE method is applied to square-well fluids. (Hereafter in the thesis, by X-CPE we mean seventh order X-CPE unless specified. X can be RHNC or S etc. While mentioning other orders of CPE, the order number is specified.) The closure proposed by Sarkisov with a slight

modification by Mendoub[64]

$$B(\zeta, r) = (1 + 2y^*(\zeta, r))^{1/2} - 1 - y^*(\zeta, r) \tag{3.36}$$

where

$$\begin{aligned} y^*(\zeta, r) &= y(\zeta, r) + \rho f_M(\sigma^+)/2,\ r < \sigma \\ &= y(\zeta, r) + \rho f_M(r)/2,\ r \geq \sigma \end{aligned} \tag{3.37}$$

and σ is the Hard sphere diameter is used. We obtained the RDF and DCF of the reference system using the same bridge function by solving the OZE using a similar procedure as explained above to maintain consistency. In the above equation, f_M is the Mayer function.

Reduced units ($\epsilon/k_B = \sigma = 1$, where ϵ is the well depth and σ is hard sphere diameter) are used throughout the chapter. For convenience, we denote $c(0, r)$, $g(0, r)$ by $c_0(r)$, $g_0(r)$ respectively and $c(1, r)$, $g(1, r)$ by $c(r)$, $g(r)$ respectively. In Fig.(5.9) we compare $g(r)$ obtained using the S-CPE and that obtained through Integral equation theory [64] for square-well fluid of range 1.3 for densities 0.2 and 0.8 and temperature $T = 1.0$. Clearly, there is negligible difference between results obtained using present method and those obtained from Integral equation theory . Also, the agreement with simulation results is good. We observed that except for very low temperatures and low densities, results of fifth order and seventh order S-CPE methods have negligible deviation showing that the Taylor series has converged. Convergence of the iteration scheme has been good in the whole phase diagram. $g(r)$ obtained by S-CPE method for square-well fluid of range 1.25 in the spinodal region at $\rho = 0.4$ and $T = 0.65$ is shown in Fig.(3.7). Above observations show that the present method may be viewed as an alternative way of solving the Ornstein Zernike equation.

In Fig.(3.8) we give plots of LVPDs for square-well fluids of ranges 1.25 and 1.375 respectively obtained using S-CPE with and without including the derivatives of bridge function in the calculations. We used the Carnahan-Starling expression for Helmholtz free energy density of the hard sphere reference system. Our results are compared with simulations, those obtained

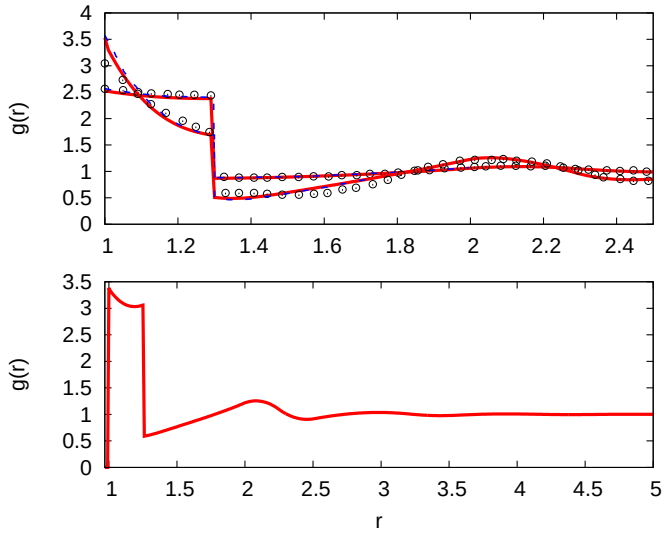

Figure 3.7: Top: $g(r)$ for square-well fluid of range 1.3 for densities 0.2, 0.8. (Circles: simulation results[58]); (Dashes: Integral equation theory results [64]); (Solid lines: results from S-CPE). Bottom: $g(r)$ for square-well fluid of width 1.25, temperature $T = 0.65$ and density 0.4.

from Integral equation theory [64] and our previous RHNC-CPE results using Malijevsky-Labik brdige function. We also depict the results of SCOZA[66] and those of Intermediate Range Square Well Equation Of State (IRSWEOS) developed by Gil-Villegas et al.[68]. The IRSWEOS is an analytical EOS for square well fluids based on perturbation theory which includes the macroscopic compressibility approximation for second order term and higher order terms.

It can be seen that the LVPDs obtained from the S-CPE are very much improved in the liquid part of the LVPD over those of integral equation theory [64]. A reason for this improvement is the use of the Carnahan Starling expression for hard sphere free energy density. A comparison of the LVPDs obtained by RHNC-CPE with Sarkisov closure and S-CPE shows that the correction due to the derivatives becomes important close to the critical region and along the liquid side of the phase diagram. Neglecting them leads to shifting of the critical point to high density region. Also,it can be seen from the plots that our results are in close agreement with simulation data than those of SCOZA and

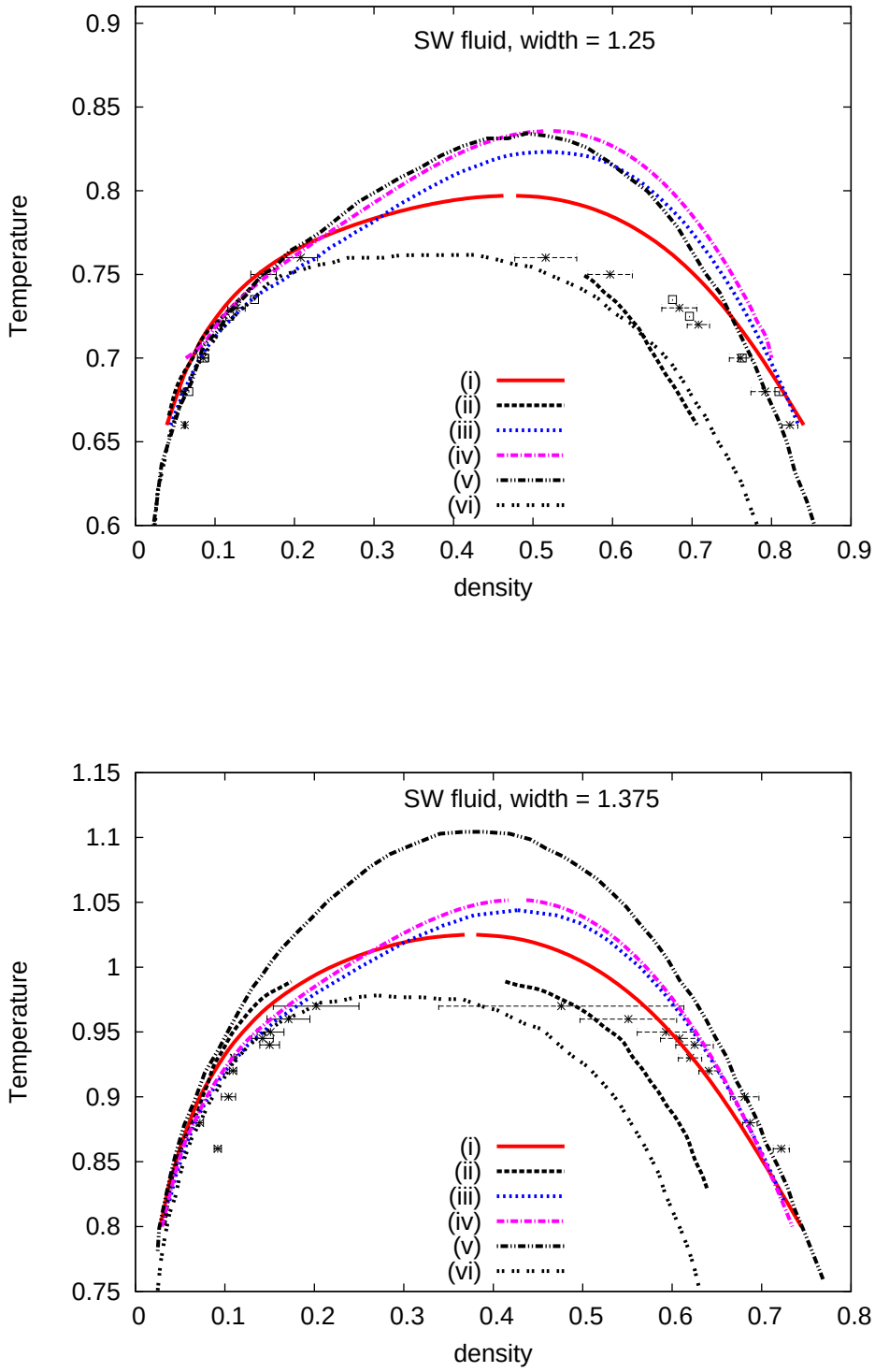

Figure 3.8: Top: LVPD of square-well fluid of range 1.25. Bottom: LVPD of square-well fluid of range 1.375. (i) S-CPE, (ii) Integral equation theory results with Sarkisov B(r) obtained from Mendoub et. al.[64], (iii) RHNC-CPE with Malijevsky Labik B(r)[51]), (iv) RHNC-CPE with Sarkisov B(r), (v) IRSWEOS[66], (vi) SCOZA[66]. Squares and stars are simulation results[60, 61]

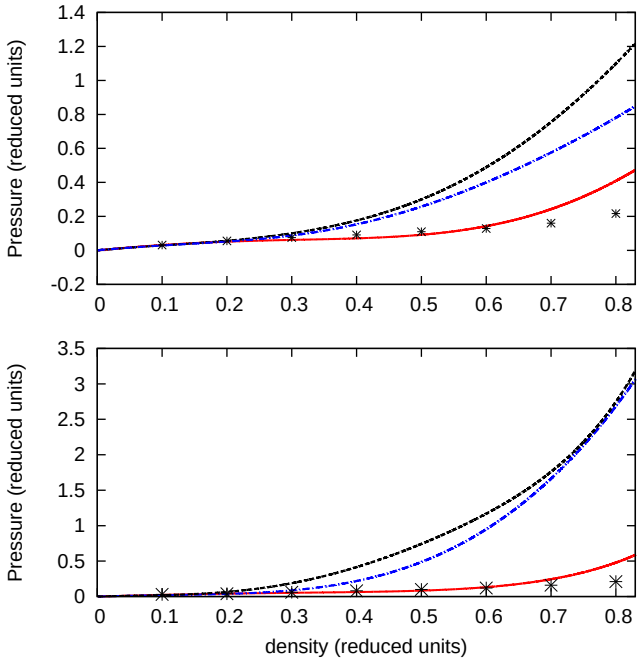

Figure 3.9: (a) Pressure(P) of square-well fluid of range 1.04 at $T = 0.37$.(b) P of square-well fluid of range 1.01 at $T = 0.255$. P and T are in reduced units. Stars: Simualtion results [67]. (Solid Line: 3^{rd} order S-CPE), (Dash-dot: 5^{th} order S-CPE), (Dash: 7^{th} order S-CPE)

IRSWEOS.

In Fig.(3.9), pressure isotherms obtained using 3^{rd}, 5^{th} and 7^{th} order S-CPE method for square-well fluids of extremely short ranges 1.01 and 1.04 are plotted for temperatures 0.255 and 0.37 respectively. The figures depict that the 3^{rd} order results are much closer to the simulation results. A comparison of the three versions shows that the series is indeed convergent at each density point. But it is converging to a point away from the simulation results. This is because of the inaccuracy of the bridge function for very short ranged fluids. Thus the apparent closeness of the third order perturbation theory results to the simulation results is fortuitous. However, the results may be improved using a different choice of bridge function which is accurate for extremely short range potentials.

3.5.2 Square-well fluids: surface tension

Possibility of obtaining $c(r)$ in two phase region allows for calculation of surface tension of liquids. We use the $c(r)$ obtained from S-CPE to obtain surface tension for square-well fluids. Formula for surface tension is obtained by Yang et. al. [69] from square-gradient functional for Helmholtz free energy of inhomogeneous fluids. A brief derivation is as follows: The square-gradient approximation for Helmholtz free energy functional of an inhomogeneous liquid occupying volume Ω at temperature T is given by

$$F[\rho(\vec{r})] = \int d\vec{r}\,\{f(\rho(\vec{r})) + f_g(\rho(\vec{r}))|\nabla\rho(\vec{r})|^2\} \tag{3.38}$$

where $f(\rho)$ is Helmholtz free energy density of homogeneous liquid. The second term is the effect of in-homogeneity. $\rho(\vec{r})$ is the number density in an infinitesimal volume around $\vec{r}$.$F[\rho(\vec{r})]$, $f(\rho(\vec{r}))$ and $f_g(\rho(\vec{r}))$ are all functions of T even though the dependence is not shown explicitly.

The coefficient f_g of gradient term also referred as influence parameter is

$$f_g[\rho(\vec{r})] = \frac{1}{12\beta}\int d\vec{r}' r'^2 c[\rho(\vec{r}), r'] \tag{3.39}$$

We assume that the liquid-vapor interface is flat and that z-axis is normal to the

interface pointing out into the vapor from the liquid. In such a case, Eq.(3.38) becomes

$$F[\rho(z)] = A \int dz \, \{f(\rho(z)) + f_g(\rho(z)) \left| \frac{d\rho(\vec{r})}{dz} \right|^2 \} \tag{3.40}$$

where A is the surface area. Grand free energy of the system is given as

$$\Gamma[\rho(z)] = F[\rho(z)] - \mu N \tag{3.41}$$

where μ is the chemical potential of the system and N is the total number of particles

Minimizing Γ $w.r.t.$ ρ we get

$$\frac{d}{dz} \left[f_g(\rho) \left(\frac{d\rho}{dz} \right)^2 \right] = \frac{d\gamma(\rho)}{dz} \tag{3.42}$$

where $\gamma(\rho)$ is the grand free energy density.

Integrating above Eq.(3.42) with boundary conditions

$$\rho(z \to \infty) = \rho_g; \rho(z \to -\infty) = \rho_l \tag{3.43}$$

gives

$$\frac{d\rho}{dz} = \left[\frac{\gamma(\rho) - \gamma(\rho_l)}{f_g(\rho)} \right]^{1/2} \tag{3.44}$$

where ρ_l and ρ_g are coexisting liquid and vapor densities for temperature T under consideration. Surface tension S can be calculated using the formula[50]

$$S = 2 \int_{-\infty}^{\infty} f_g(\rho) \left(\frac{d\rho}{dz} \right)^2 dz \tag{3.45}$$

Using Eq.(3.44) in above equation gives

$$S = 2 \int_{\rho_g}^{\rho_l} [f_g(\rho)(\gamma(\rho) - \gamma(\rho_l))]^2 \tag{3.46}$$

In the above equations $\gamma(\rho_l)$ may be replaced by $\gamma(\rho_g)$ also as both have same value.

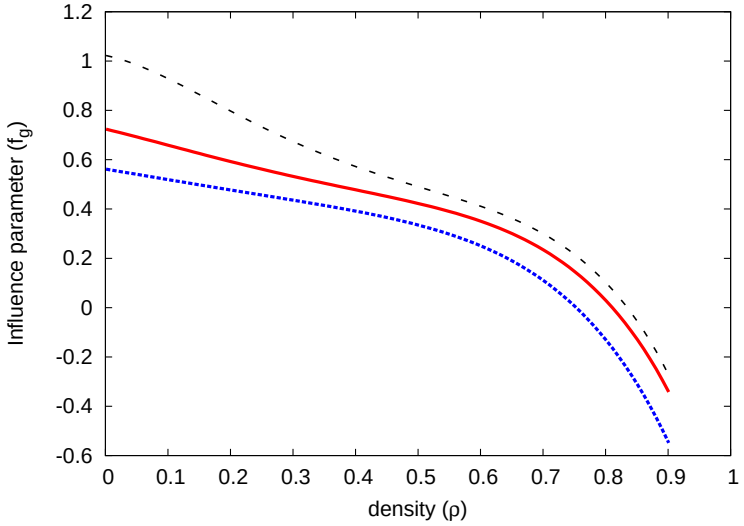

Figure 3.10: Coefficient of square gradient functional for square-well fluid of range 1.25. Curves from top to bottom are for temperatures T = 0.6, 0.8 and 1.0.

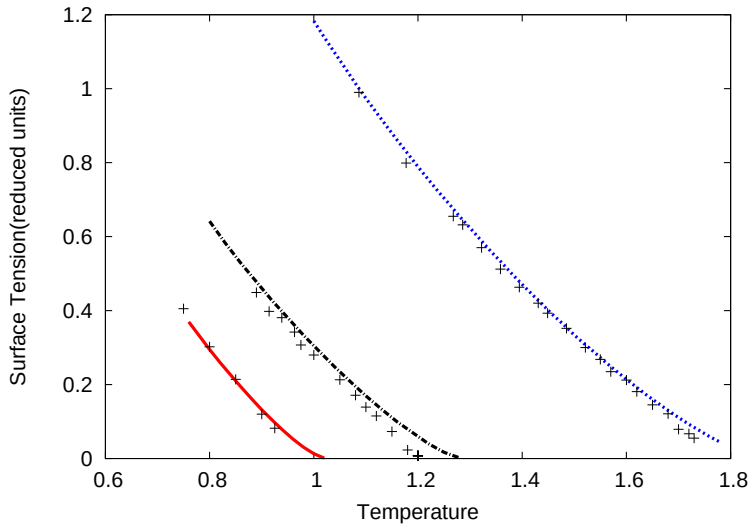

Figure 3.11: Surface tension for square-well fluids in reduced units. From left to right are for ranges 1.375, 1.5 and 1.75. stars, pluses, crosses are simulation results[70, 71]. Lines: S-CPE.

Above explained formalism is applied to square-well fluids of ranges 1.375, 1.5 and 1.75 with $c(r)$ obtained from S-CPE as explained above. Fig.(3.10) shows $f_g(\rho)$ as a function of ρ for different temperatures for square-well fluid of range 1.25. From Fig.(3.10) it can be seen that $f_g(\rho)$ becomes negative at high densities which is unphysical. This might be an artifact of the approximate bridge function used. However, within the binodal, where f_g is required for the calculation of surface tension(S), it is positive. Surface tensions obtained from our calculation are plotted as a function of T in Fig.(3.11). Our results compare well with simulations except close to the critical temperatures.

3.5.3 Lennard Jones Fluid

The theoretical formalism explained in section 3.4 is general and can be applied to non-hard sphere reference systems also. As an example, we applied the theory to Lennard Jones fluid. The Lennard Jones potential was split into reference and perturbation parts according to the Weeks Chandler and Anderson (WCA)[17] method. In this case, we used for $B(\zeta, r)$, the expression proposed by Sarkisov [63] which is same as Eq.(3.36) with

$$\begin{aligned} y^*(\zeta, r) &= y(\zeta, r) - \rho\beta u(r_m),\ r < r_m \\ &= y(\zeta, r) - \rho\beta u(r),\ r \geq r_m \end{aligned} \tag{3.47}$$

where r_m is the minimum energy point of the Lennard-Jones potential. The $c_0(r)$ and $g_0(r)$ of the reference system are obtained by solving the OZE with the same bridge function. Thus, in effect, we solved the OZE Lennard-Jones fluid with the above bridge function using the perturbation method. In Fig.(3.12), we compare the $g(r)$ of Lennard-Jones fluid obtained from S-CPE method with simulation results. There is excellent agreement between the theory and simulation results for the cases shown except for a slight deviation in the case of lowest temperature. In Fig.(3.13), Equation of State(EOS) of Lennard-Jones fluid for various temperatures calculated using S-CPE method is compared with those obtained by solving OZE by Sarkisov[63]. Pressure(P) is calculated

using the virial formula given by

$$P = \rho k_B T - \frac{1}{6}\rho^2 \int_0^\infty \frac{du(r)}{dr} g(r) 4\pi r^3 dr \tag{3.48}$$

Values obtained by our method matched well with those given by Sarkisov. In this case also, we could obtain the pressure at all density points in the phase diagram as $g(r)$ at any point in the phase diagram including critical point could be calculated which was not possible with integral equation theory. In Fig.(3.14), LVPD of Lennard-Jones fluid is shown and compared with simulation results. We plotted the LVPD obtained in two ways. One is obtained by Maxwell construction of pressure isotherm obtained using Eq.(3.48) which is the so called virial route. Alternatively, LVPD is also obtained from the free-energy route. It is obtained as follows: Pressure isotherm of the reference fluid is calculated using Eq.(3.48) with $u_{ref}(r)$. From this, Helmholtz free energy density of the reference fluid is obtained from the formula below

$$f_{ref}(\rho) = \rho k_B T \int_0^\rho (\frac{P_{ref}(\rho')}{\rho'^2} - 1) d\rho + \rho k_B T ln(\rho) \tag{3.49}$$

Once the reference free energy is known, method described in section 3.4 can be applied to get the free energy density of the required system. The pressure isotherm is calculated by differentiating the Helmholtz free energy $w.r.t.$ volume of the system. Maxwell construction is done to get the coexistence points. From the figure, it can be seen that the LVPD obtained from the two routes differ slightly along the liquid part of the coexistence curve. Also, there is some deviation of both LVPDs from the simulation results. This is due to the bridge function used. Even though Sarkisov bridge function is supposed to be quiet accurate, there is some inconsistency between various thermodynamic routes. Imposition of the thermodynamic consistency between various routes as a constraint would solve the problem and may improve the accuracy of the results.

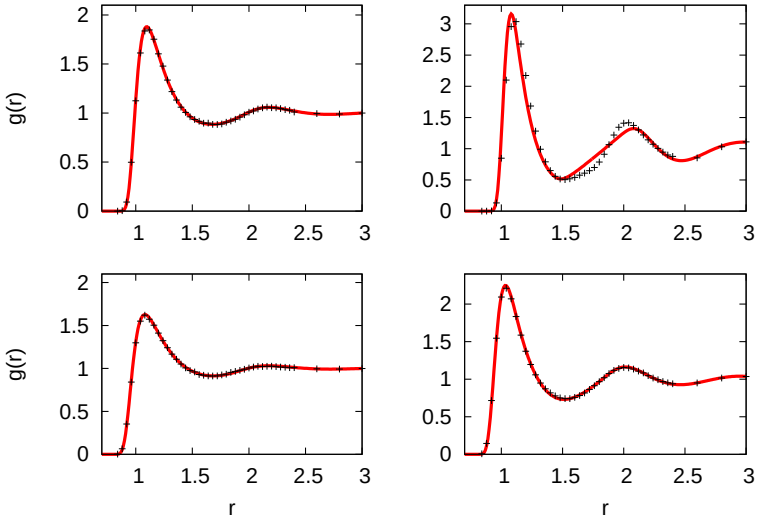

Figure 3.12: Lennard-Jones RDFs for different temperatures and densities obtained using S-CPE. (pluses: Simulation results[72]),(Top left: $T = 1.552, \rho = 0.45$),(Bottom left: $T = 2.934, \rho = 0.45$),(Top right: $T = 0.658, \rho = 0.85$),(Bottom right: $T = 2.888, \rho = 0.85$). T and ρ are in reduced units

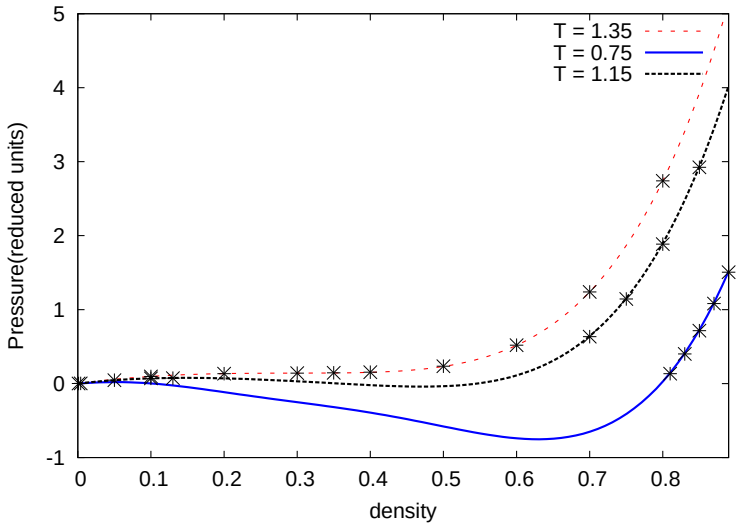

Figure 3.13: : Pressure (reduced units) of Lennard-Jones fluid for different temperatures. Stars: Values obtained using Integral equation theory by Sarkisov[63]. Lines: S-CPE results with Sarkisov bridge function. (Solid line: T = 0.75),(Dotted line: T = 1.15),(Dashes: T = 1.35)

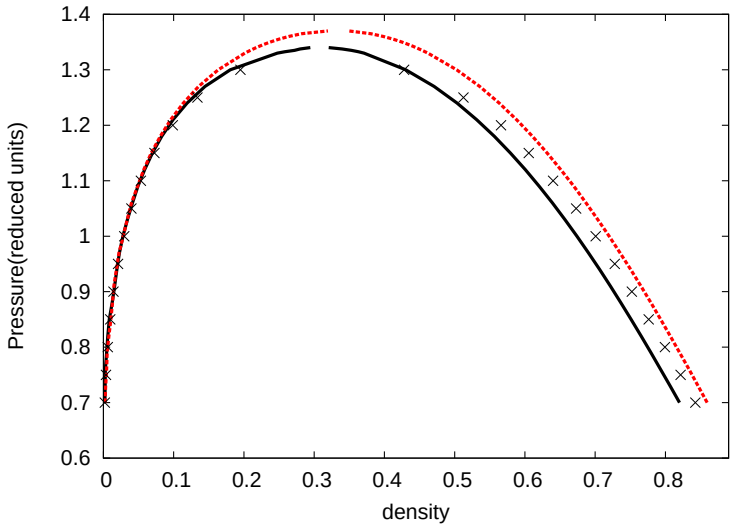

Figure 3.14: LVPD of Lennard-Jones fluid. (Dashed line: EOS calculated using energy route). (Solid line:EOS obtained using virial route). In both cases S-CPE is used. Crosses are simulation results[46].

3.6 Summary

In this chapter we have presented a new approach to the coupling parameter expansion in liquid state theory of simple fluids. The method combines ideas of thermodynamic perturbation theory and integral equation theories. This hybrid scheme avoids the problems of integral equation theories in the two phase region. A simple way to calculate the terms in the perturbation series expansion to any arbitrary order is illustrated. Apart from the Helmholtz free energy, the present approach also gives the RDF and DCF of the actual perturbed system.

Initially, using the RHNC-CPE method, we have obtained thermodynamic and structural properties of the square-well fluids of various ranges. We have seen that the Helmholtz free energy series has practically converged by seventh order for the cases considered. However we found that the convergence of $g(r)$ and $c(r)$ is slower at low temperatures and low densities for short ranged square well fluids. We also found that the liquid vapor phase diagrams of fluids of short ranged potentials obtained using the RHNC-CPE still

disagree with simulation data. Apart from this, the simplified method works only for fluids with hard sphere reference system.

An improvement in the accuracy and applicability to non-hard sphere fluids was expected with the generalized version of the CPE method which takes into account the derivatives of the bridge function in calculating the derivatives of the RDF[1]. Accordingly, we generalized the method and applied the S-CPE to square-well fluids to see the improvement in results over the simplified version and to Lennard-Jones fluids to show the applicability of the method with non-hard sphere reference systems. We also obtained the surface tension in square-well fluids of various ranges which requires the direct correlation function in the coexistence region and compared with simulation data from literature. The results showed that the correlation functions obtained using our method in the coexistence region are accurate.

The applications lead to the following conclusions about generalized CPE.(i) Inclusion of derivatives of the bridge function in the perturbation theory has a significant effect on structural and thermodynamic properties of liquids. (ii) If accurate reference system data is available, it can be used in the perturbation theory to improve the accuracy of the results over those of integral equation theory. (iii) The present method may be viewed as an alternative way of solving the OZE with the advantage that a solution can be obtained in the whole phase diagram. (iv) The accuracy of the method is limited by the bridge function used in the calculation.

Thus we now have an improved mean field Helmholtz free energy and influence parameter calculated from a single theory which can be used in the GRGT method to obtain the accurate thermodynamic properties globally.

[1]The derivatives are with respect to coupling parameter

CHAPTER 4

Equivalence of coupling parameter expansion and Zwanzig's expansion

4.1 Introduction

In this chapter, we show that the CPE is equivalent to the HTSE in the case of pairwise additive interaction potentials.

The series expansions for Helmholtz free energy as given by Eq.(1.20) (called as HTSE) and Eq.(1.28) (called as CPE) apparently look different. In a few recent papers[24, 67, 73–77], it has been argued that the HTSE and CPE are actually different beyond the first order term. It also has been stated that, only for the special case of the hard sphere reference system and only for reduced temperature equal to 1, the two series are equal. However, the conclusions were not based on any rigorous results and the arguments were heuristic. Apart from this, a function having two different series expansions contradicts the uniqueness of power series expansion. This raises questions about the validity of the conclusions made in the papers[24, 67, 73–77]. In view of this, we re-examine the equivalence of CPE and HTSE and prove rigorously that both the expansions are equivalent in the case of pair potentials[78]. This result is not very surprising and can be guessed easily based on the uniqueness theorem. However, the equivalence of CPE and HTSE leads to interesting scaling relations in the case of fluids with interaction potential having a hardcore repulsion(for example, the square well fluid) if the hardcore repulsive part is taken as reference. Apart from the scaling of terms of Helmholtz free energy series with temperature, the terms of series of RDF and the DCF also scale with temperature. As a consequence, once the terms of CPE are calculated along a particular isotherm for such fluids, the structure and thermodynamic prop-

erties of those fluids at other temperatures can be obtained using the scaling relations.

In section 4.2, we prove the equivalence of CPE and HTSE and in section 4.3 we describe the consequences of the equivalence of HTSE and CPE. The chapter is concluded in section 4.4.

4.2 The HTSE and the CPE

Consider a fluid of N interacting particles in a volume V at reduced temperature T. Reduced units ($\epsilon/k_B = \sigma = 1$, where ϵ is the well depth and σ is hard sphere diameter) are used throughout. The Zwanzig's expansion or HTSE for Helmholtz free energy F of the system is given by

$$F = F_{ref} + \sum_{n=1}^{\infty} \frac{\omega_n}{n!}(-\beta)^{n-1} \tag{4.1}$$

where

$$\omega_1 = \langle U_{per} \rangle_0 \tag{4.2}$$

$$\omega_2 = \langle U_{per}^2 \rangle_0 - \langle U_{per} \rangle_0^2 \tag{4.3}$$

$$\omega_3 = \langle U_{per}^3 \rangle_0 - 3\langle U_{per}^2 \rangle_0 \langle U_{per} \rangle_0 + 2\langle U_{per} \rangle_0^3 \tag{4.4}$$

$$\cdots\cdots\cdots$$

$$\omega_s = s! \sum_{\{n_j\}} (-1)^{\Sigma n_j - 1} (\Sigma n_j - 1)! \prod_{j=1}^{\infty} \frac{1}{n_j!} \left(\frac{\langle U_{per} \rangle_0^j}{j!} \right)^{n_j} \tag{4.5}$$

The subscript 0 implies that the averages are with respect to the reference system ensemble. In the Eq.(4.5), the $\{n_j\}$ implies that the summation is a multiple sum over all possible n_j's such that the constraint $\sum_0^\infty j n_j = s$ is satisfied. Here n_j's are positive integers. It can be seen that for all $j > s$, n_j's are zero. Above series for F doesn't require a pairwise additive interaction potential. However, in the case of a spherically symmetric pairwise additive potential $u(r)$, the ω_1 simplifies to

$$\omega_1 = \frac{2\pi N^2}{V}\int_0^\infty u_{per}(r)g_0(r)r^2dr \tag{4.6}$$

where $u_{per}(r)$ is the perturbation part of $u(r)$ when separated as $u(r) = u_{ref}(r)+u_{per}(r)$. $g_0(r)$ is the radial distribution function of the reference system. r is the radial distance from the origin. ω_2 has been shown to depend on correlation functions up to fourth order. An approximation to ω_2, has been derived by Barker and Henderson[12] as described in section 1.3 of chapter 1.

In the CPE, as mentioned in the introduction, a hypothetical fluid is considered with total potential energy given by $U_\zeta = U_{ref} + \zeta U_{per}$. Differentiating $F(\zeta)\ w.r.t.\ \zeta$ and integrating between limits $\zeta = 0$ to $\zeta = 1$ gives

$$F = F_{ref} + \int_0^1 \langle U_{per}\rangle_\zeta d\zeta \tag{4.7}$$

The subscript ζ in the above equation implies that the average is $w.r.t.$ the ensemble with potential energy U_ζ. Expanding $\langle U_{per}\rangle_\zeta$ around $\zeta = 0$ in a Taylor series and substituting $\zeta = 1$, we get the HTSE. In the case of pairwise additive potentials, above Eq.(4.7) can be re-written in terms of pair correlation function ($\rho_\zeta^{(2)}(1,2)$) of the hypothetical system i.e.,

$$F = F_{ref} + \frac{1}{2}\int_0^1 d\zeta \int_V d1d2u_{per}(1,2)\rho_\zeta^{(2)}(1,2) \tag{4.8}$$

Following Hansen[1], we denote the position vector $\vec{r}_i$ of i^{th} particle by i to simplify notation. $d1$ denotes the volume element $d\vec{r}_1$ around $\vec{r}_1$. Expanding $\rho_\zeta^{(2)}(1,2)$ in a Taylor series around $\zeta = 0$ and substituting in above Eq.(4.8), we get the CPE for F given by

$$F = F_{ref}+\frac{1}{2}\int_0^1 d\zeta \int_V d1d2u_{per}(1,2)\left(\rho_0^{(2)}(1,2) + \zeta\left.\frac{d\rho^{(2)}}{d\zeta}(1,2)\right|_0 + \left.\frac{\zeta^2}{2!}\frac{d^2\rho^{(2)}}{d\zeta^2}(1,2)\right|_0 + ...\right) \tag{4.9}$$

If the system is homogeneous and isotropic, $\rho_\zeta^{(2)}(1,2)$ becomes equal to $\rho^2 g_\zeta(|1-2|)$ and the integral in Eq.(4.9) simplifies. Here ρ is the density of the system and $g_\zeta(r)$ is the RDF of the hypothetical system.

4.2.1 Equivalence of HTSE and CPE

It can be easily seen that first order terms in both the series are same; as mentioned above, in a homogeneous system, $\rho_\zeta^{(2)}(1,2)$ becomes equal to $\rho^2 g_\zeta(|1-2|)$ and

$$\frac{1}{2}\int_0^1 d\zeta \int_V d1d2 u_{per}(1,2)\rho_0^{(2)}(1,2) = \omega_1 \tag{4.10}$$

In order to see the equivalence of second term of CPE with that of HTSE, consider the definition of $\rho_\zeta^{(2)}(1,2)$ i.e.,

$$\rho_\zeta^{(2)}(1,2) = N(N-1)\frac{1}{Z_N(\zeta)}\int_V d\vec{r}^{(N-2)} exp(-\beta U_\zeta) \tag{4.11}$$

where

$$Z_N(\zeta) = \int_V d\vec{r}^{(N)} exp(-\beta U_\zeta) \tag{4.12}$$

Here $\int_V d\vec{r}^{(N)}$ implies $\int_V ... \int_V d1d2...dN$

Now,

$$\begin{aligned}\frac{d\rho_\zeta^{(2)}}{d\zeta} &= \frac{N(N-1)}{Z_N(\zeta)}\int_V d\vec{r}^{(N-2)}(-\beta U_{per})exp(-\beta U_\zeta) \\ &\quad -\frac{N(N-1)}{Z_N^2(\zeta)}\int_V d\vec{r}^{(N-2)} exp(-\beta U_\zeta)\int_V d\vec{r}^{N}(-\beta U_{per})exp(-\beta U_\zeta)\end{aligned} \tag{4.13}$$

Substituting the above equation in second order term of CPE we get,

$$\begin{aligned}\frac{1}{2}\int_0^1 d\zeta \int_V d1d2 u_{per}(1,2)\zeta \left.\frac{d\rho^{(2)}}{d\zeta}(1,2)\right|_0 &= \frac{N(N-1)}{2Z_N(0)}\int_V d\vec{r}^{N}(-\beta U_{per})exp(-\beta U_{ref})u_{per}(1,2) \\ &- \frac{N(N-1)}{2Z_N^2(0)}\int_V d\vec{r}^{N} u_{per}(1,2)exp(-\beta U_{ref}) \\ &\times \int_V d\vec{r}^{N}(-\beta U_{per})exp(-\beta U_{ref})\end{aligned} \tag{4.14}$$

Consider the first term in the RHS of the above equation. It can be seen that the integral remains invariant if $(1,2)$ is replaced by any other possible pair and there are exactly $N(N-1)/2$ possible pairs. The same argument holds for the second term on the RHS of above Eq.(4.14). Thus the above equation becomes,

$$\begin{aligned}
\frac{1}{2}\int_0^1 d\zeta \int_V d1d2u_{per}(1,2)\zeta \left.\frac{d\rho^{(2)}}{d\zeta}(1,2)\right|_0 &= \frac{1}{Z_N(0)}\int_V d\vec{r}^N(-\beta U_{per})exp(-\beta U_{ref})U_{per} \\
&\quad -\frac{1}{Z_N^2(0)}\int_V d\vec{r}^N U_{per}exp(-\beta U_{ref}) \\
&\quad \times \int_V d\vec{r}^N(-\beta U_{per})exp(-\beta U_{ref}) \\
&= -\beta\langle U_{per}^2\rangle_0 + \beta\langle U_{per}\rangle_0^2 \\
&= -\beta\omega_2/2 \qquad (4.15)
\end{aligned}$$

Now to prove the equivalence of a general term of CPE to that of HTSE, we first define the following:

$$\begin{aligned}
P_0 &= P = \int_V d3..dNexp(-\beta U_\zeta) \\
P_1 &= \frac{dP}{d\zeta} = \int_V d3..dN(-\beta U_{per})exp(-\beta U_\zeta) \\
P_2 &= \frac{d^2P}{d\zeta^2} = \int_V d3..dN(-\beta U_{per})^2exp(-\beta U_\zeta) \\
&\ldots\ldots\ldots\ldots\ldots\ldots\ldots\ldots\ldots\ldots \\
P_s &= \frac{d^sP}{d\zeta^s} = \int_V d3..dN(-\beta U_{per})^sexp(-\beta U_\zeta) \qquad (4.16)
\end{aligned}$$

and

$$\begin{aligned}
Z_0 &= Z_N(\zeta) = \int_V d1..dNexp(-\beta U_\zeta) \\
Z_1 &= \frac{dZ_N(\zeta)}{d\zeta} = \int_V d1..dN(-\beta U_{per})exp(-\beta U_\zeta) \\
Z_2 &= \frac{d^2Z_N(\zeta)}{d\zeta^2} = \int_V d1..dN(-\beta U_{per})^2exp(-\beta U_\zeta) \\
&\ldots\ldots\ldots\ldots\ldots\ldots\ldots\ldots\ldots\ldots \\
Z_s &= \frac{d^sZ_N(\zeta)}{d\zeta^s} = \int_V d1..dN(-\beta U_{per})^sexp(-\beta U_\zeta) \qquad (4.17)
\end{aligned}$$

Here $d1$ implies $d\vec{r}_1$ and so on. It can be easily seen that

$$\begin{aligned}
\frac{1}{N(N-1)}\rho_{\zeta}^{(2)}(1,2) &= \frac{P_0}{Z_0} \\
\frac{1}{N(N-1)}\frac{d\rho_{\zeta}^{(2)}(1,2)}{d\zeta} &= \frac{P_1}{Z_0} - \frac{P_0}{Z_0^2}Z_1 \\
\frac{1}{N(N-1)}\frac{d^2\rho_{\zeta}^{(2)}(1,2)}{d\zeta^2} &= \frac{P_2}{Z_0} - 2\frac{P_1}{Z_0^2}Z_1 + 2\frac{P_0}{Z_0^3}Z_1^2 - \frac{P_0}{Z_0^2}Z_1^2
\end{aligned} \tag{4.18}$$

To get the s^{th} ($s \geq 1$) derivative of $\rho_{\zeta}^{(2)}(r_1, r_2)$, the s^{th} derivative of $\frac{P_0}{Z_0}$ is required which in turn requires the the s^{th} derivative of $\frac{1}{Z_0}$. Since Z_0 is a well behaved function, it can be expected that s^{th} derivative of $\frac{1}{Z_0}$ w.r.t. ζ exits. The s^{th} derivative of $\frac{1}{Z_0}$ is [79]

$$\begin{aligned}
\frac{d^s}{d\zeta^s}\left(\frac{1}{Z_0}\right) &= s!\sum_{\{n_j\}}(-1)^{\alpha}\frac{\alpha!}{Z_0^{\alpha+1}}\prod_{j=1}^{\infty}\frac{1}{n_j!}\left(\frac{Z_j}{j!}\right)^{n_j} \\
\alpha &= \sum_{j=1}^{\infty} n_j
\end{aligned} \tag{4.19}$$

where $\sum_{\{n_j\}}$ is again a multiple sum over n_j's such that the constraint $\sum_{j=1}^{\infty} jn_j = s$ is satisfied. Using Leibnitz formula for calculating the s^{th} derivative of a product of two functions we get

$$\frac{1}{N(N-1)}\frac{d^s\rho_{\zeta}^{(2)}(1,2)}{d\zeta^s} = \sum_{r=0}^{s}\frac{s!}{(s-r)!r!}P_{s-r}\frac{d^r}{d\zeta^r}\left(\frac{1}{Z_0}\right) \tag{4.20}$$

The $(s+1)^{th}$ term in CPE(Eq.(4.9)) is,

$$\Gamma_{s+1} = \frac{1}{(s+1)!}\frac{1}{2}\int_V d1d2u_{per}(1,2)\left.\frac{d^s\rho_{\zeta}^{(2)}(1,2)}{d\zeta^s}\right|_0 \tag{4.21}$$

Substituting Eq.(4.20) in Eq.(4.21) and after some algebra, the $(s+1)^{th}$ term in

CPE becomes

$$\Gamma_{s+1} = \frac{1}{(s+1)!}\sum_{r=0}^{s}\frac{s!}{(s-r)!}\frac{\langle(-\beta U_{per})^{s-r+1}\rangle_0}{-\beta}\sum_{\{n_j\}}(-1)^{\alpha}\alpha!\prod_{j=1}^{\infty}\frac{1}{n_j!}\left[\frac{\langle(-\beta U_{per})^{j}\rangle_0}{j!}\right]^{n_j} \quad (4.22)$$

$$= \frac{1}{(s+1)!}\frac{-1}{\beta}\sum_{r=0}^{s}s!\sum_{\{n_j\}}(-1)^{\alpha}\alpha! \times \prod_{\substack{j=1\\ j\neq s-r+1}}^{\infty}\frac{1}{n_j!}\left[\frac{\langle(-\beta U_{per})^{j}\rangle_0}{j!}\right]^{n_j}\frac{(n_{s-r+1}+1)(s-r+1)}{(n_{s-r+1}+1)!}\left[\frac{\langle(-\beta U_{per})^{s-r+1}\rangle_0}{(s-r+1)!}\right]^{n_{s-r+1}+1} \quad (4.23)$$

Now consider a set of $\{n'_j\}$s such that, for all $j \neq s-r+1$, $n'_j = n_j$ and for $j = s-r+1$, $n'_j = n_j + 1$. Then,

$$\sum_{j=1}^{\infty} jn'_j = \sum_{j=1}^{\infty} jn_j + (s-r+1) = s+1 \quad (4.24)$$

and

$$\alpha' = \sum_{j=1}^{\infty} n'_j = \sum_{j=1}^{\infty} n_j + 1 = \alpha + 1 \quad (4.25)$$

Using Eq.(4.24) and Eq.(4.25) in Eq.(4.23), we get,

$$\Gamma_{s+1} = \frac{1}{(s+1)!}\frac{-1}{\beta}\sum_{r=0}^{s}(n'_{s-r+1})(s-r+1)s!\sum_{\{n'_j\}}(-1)^{(\alpha'-1)}(\alpha'-1)!\prod_{j=1}^{\infty}\frac{1}{n'_j!}\left[\frac{\langle(-\beta U_{per})^{j}\rangle_0}{j!}\right]^{n'_j} \quad (4.26)$$

where n'_js satisfy the constraint of Eq.(4.24). It can be seen easily that $\sum_{r=0}^{s}(n'_{s-r+1})(s-r+1) = s+1$, as all n_js for $j > s+1$ must be zero for the constraint of Eq.(4.24) to be satisfied. Thus Eq.(4.26) becomes

$$\Gamma_{s+1} = (-\beta)^s\sum_{\{n'_j\}}(-1)^{(\alpha'-1)}(\alpha'-1)!\prod_{j=1}^{\infty}\frac{1}{n'_j!}\left[\frac{\langle(U_{per})^{j}\rangle_0}{j!}\right]^{n'_j} \quad (4.27)$$

$$= (-\beta)^s\frac{\omega_{s+1}}{(s+1)!} \quad (4.28)$$

which is nothing but $(s+1)^{th}$ order term in HTSE.

4.3 Fluids with Hardcore Repulsion

Consider a homogeneous fluid with particles interacting via a pairwise additive spherically symmetric potential. Let the potential $u(r)$ have a hardcore repulsion($u_{ref}(r)$) and a slowly varying attractive part($u_{per}(r)$) whose value is small compared to k_bT so that it can be treated as a perturbation. i.e.,

$$\begin{aligned} u(r) &= \infty \; r \leq r_0 \\ &= u_{per}(r) \; r > r_0 \end{aligned} \tag{4.29}$$

If the hardcore part is taken as the potential of the reference system, the ensemble averages $w.r.t.$ the hard-sphere reference system become independent of temperature. As a result, the ω_is in Equations(4.3- 4.5) become independent of temperature. Hence the HTSE becomes a power series in $\beta = 1/k_bT$[1]. Since it has now been shown that the terms of CPE are equivalent to those of HTSE, the terms of CPE also scale with powers of β. s^{th} term of the series is proportional to β^{s-1} as can be seen from Eq.(4.28).

It can also be seen that the derivatives of RDF and the direct correlation function(DCF) also scale with powers of β. Consider s^{th} derivative of $\rho_\zeta(1,2)$. It can be seen from Eq.(4.20) that each term in the summation in the R.H.S. depends upon the following term:

$$\frac{P_{s-r}}{Z_0^{\alpha+1}} \prod_{j=1}^{\infty} Z_j^{n_j} \tag{4.30}$$

which can be re-written as follows

$$\begin{aligned} \frac{P_{s-r}}{Z_0^{\alpha+1}} \prod_{j=1}^{\infty} Z_j^{n_j} &= \frac{P_{s-r}}{Z_0} \prod_{j=1}^{\infty} \left[\frac{Z_j}{Z_0}\right]^{n_j} \\ &= \frac{P_{s-r}}{Z_0} \beta^r (\langle(-U_{per})\rangle_0^{n_1} \langle(-U_{per})^2\rangle_0^{n_2} \langle(-U_{per})^3\rangle_0^{n_3} .....) \end{aligned} \tag{4.31}$$

When evaluated at $\zeta = 0$ with $u_{ref}(r)$ as that of hard-sphere, it can be seen from the Eq.(4.16) that P_{s-r} depends on β^{s-r}. Since the averages in above Eq.(4.31) become independent of temperature, the total dependence on β of each term

in the R.H.S. of Eq.(4.20) would be β^s. Thus,

$$\left.\frac{d^s\rho_\zeta^{(2)}(1,2)}{d\zeta^s}\right|_{\zeta=0} = \rho^2 \left.\frac{d^s g_\zeta(r)}{d\zeta^s}\right|_{\zeta=0} \propto \beta^s \tag{4.32}$$

Also, since $\left.\frac{d^s g_\zeta(r)}{d\zeta^s}\right|_{\zeta=0} \propto \beta^s$, its Fourier transform also would be proportional to β^s i.e.,

$$\left.\frac{d^s \hat{g}_\zeta(k)}{d\zeta^s}\right|_{\zeta=0} = \left.\frac{d^s \hat{h_\zeta}(k)}{d\zeta^s}\right|_{\zeta=0} \propto \beta^s \tag{4.33}$$

where $h_\zeta(r) = g_\zeta(r) - 1$ is the total correlation function and $\hat{h}_\zeta(k)$ is its Fourier transform. The Ornstein-Zernike equation for the hypothetical fluid in Fourier space is given by[1],

$$h_\zeta(k) = \frac{c_\zeta(k)}{1 - \rho c_\zeta(k)} \tag{4.34}$$

Using similar arguments given in the case of $\left.\frac{d^s g_\zeta(r)}{d\zeta^s}\right|_{\zeta=0}$, it can be seen that

$$\left.\frac{d^s c_\zeta(r)}{d\zeta^s}\right|_{\zeta=0} \propto \beta^s \tag{4.35}$$

Thus from the above discussion, it can be seen that, for the class of fluids with hardcore repulsion, apart from the Helmholtz free energy series, the Taylor series for $c(r)$ and $g(r)$ obtained by expanding around $\zeta = 0$ also becomes power series in β. As a result, if the coefficients of the series are obtained along one isotherm, then the whole phase diagram can be obtained provided the series converges. To obtain the coefficients of the series which are related to the derivatives of $g_\zeta(r)$ and $c_\zeta(r)$ at $\zeta = 0$, few recently developed methods are available as discussed in the introduction[23, 51, 53].

To test the scaling relations derived above, we applied the method discussed in Ref.[53] to square well(SW) fluids. The calculation method used is exactly the same as in Ref.[53] and hence is not repeated here. We obtained the derivatives of $g(r)$ of SW fluid of width 0.25 at various reduced temperatures(T) and plotted $T^n \frac{d^n g_\zeta(r)}{d\zeta^n}|_0$ for $n = 1, 2, 3$ and 6 in Fig.(4.1). It can be seen

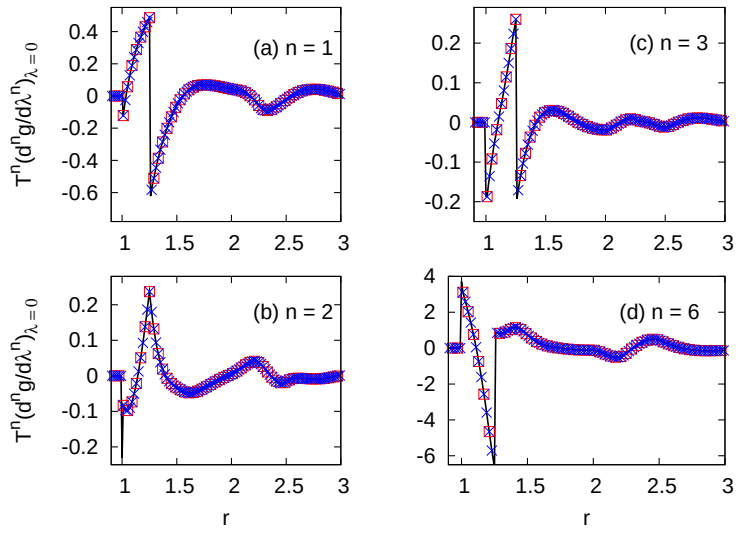

Figure 4.1: Scaled derivatives of g(r) of square-well fluid of width 0.25 at reduced density $\rho = 0.8$ at various reduced temperatures. Solid line: T = 0.9, hollow squares: T = 0.6, crosses: T =1.5

from Fig.(4.1) that the curves corresponding to each derivative at different temperatures coincide after scaling. Also we obtained the first three coefficients of the HTSE for SW fluids of width 1.2 and 2.0 using the same method of Ref.[53]. In the case of square-well fluid of width 1.2, the coefficients of HTSE are obtained by calculating the terms of CPE at $T = 0.7$ and scaling with temperature according to $T^n\Gamma_{n+1}$ where Γ_n is n^{th} order term in the CPE for Helmholtz free energy per particle. In the same way, the coefficients of HTSE for SW fluid of width 2.0 are obtained by calculating the terms of CPE at $T = 2.0$ followed by scaling. The results are compared with simulation data[75] in Fig(4.2) and Fig(4.3). It can be seen that there is an excellent match between simulation data and present calculations which confirms the scaling relations.

4.4 Conclusion

We have shown rigorously that the CPE and HTSE are equivalent when the interaction potential is pairwise additive. As a result, we have shown that for fluids with interaction potential having a hardcore repulsion, if the hard-sphere

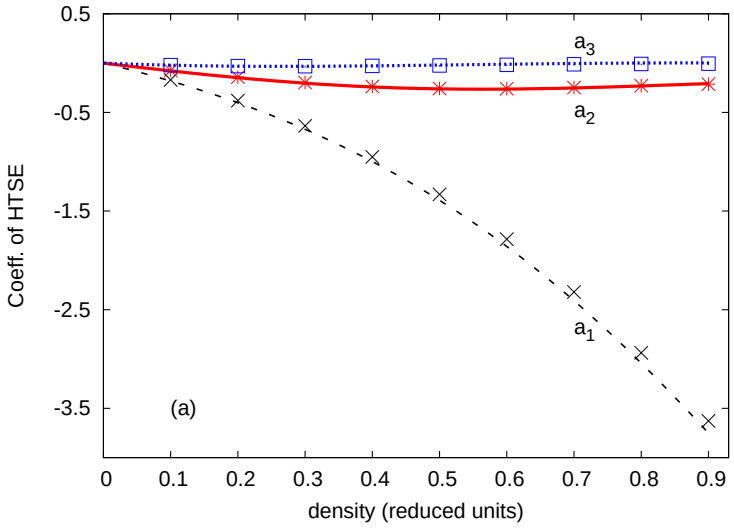

Figure 4.2: First three coefficients of HTSE for square-well fluid of width 1.2. Lines are present results, symbols are simulation data[75]. a_1, a_2 and a_3 are first three coefficients of HTSE for Helmholtz free energy per particle respectively.

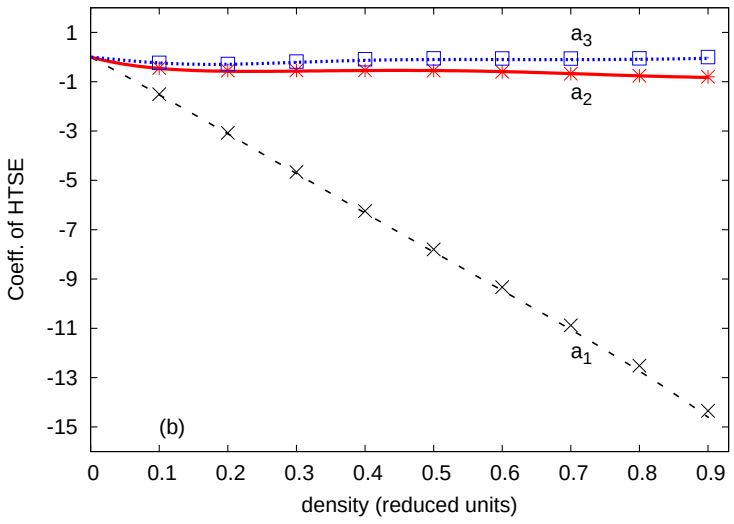

Figure 4.3: First three coefficients of HTSE for square-well fluid of width 2.0. Lines are present results, symbols are simulation data[75].a_1, a_2 and a_3 are first three coefficients of HTSE for Helmholtz free energy per particle respectively.

fluid is taken as the reference system, the terms of CPE and the derivatives of RDF and DCF w.r.t. the coupling parameter follow a scaling relation with temperature. We have also confirmed the scaling relations through applications of our theory to square well fluids. Thus, for such fluids, if the derivatives of RDF are known along an isotherm, the structural and thermodynamic properties can be obtained at any other temperature provided the series is convergent at that temperature.

CHAPTER 5

Combination of Global Renormalization Group Theory with Coupling Parameter expansion method: Application to square-well fluids

5.1 Introduction

In chapter 2 we formulated a generalized GRGT and applied it to obtain the equation of state of square-well and Lennard-Jones fluids. We noted that the method, as implemented in chapter 2, is not accurate for fluids with short range interaction potentials because the mean-field Helmholtz free energy and the influence parameter used in implementing the GRGT in chapter 2 were inaccurate for short range potentials. We conjectured that the results of GRGT would improve if an improved mean-field Helmholtz free energy and an improved influence parameter are used.

In that regard we developed a method to obtain the terms of CPE for Helmholtz free energy, RDF and DCF of a homogeneous fluid in chapter 3. We applied the seventh order version of CPE method to square-well fluids of various ranges and showed that there is enormous improvement in the obtained EOS and the LVPD . We also have seen that the Helmholtz free energy, the RDF and the DCF converged by seventh order for square-well potentials with range above 1.25 and were in excellent agreement with simulation results. Using the DCF obtained from S-CPE, we obtained the influence parameter. To assess the accuracy of our obtained influence parameter, we calculated the surface tension of square-well fluids which requires the influence parameter as an input. The calculated surface tensions matched well with simulation results.

Eventhough there were improvements in describing the thermodynamic properties, the obtained Helmholtz free energy from this procedure is of mean

field type and doesn't correctly describe the critical behavior. In this chapter, we use the improved Helmholtz free energy and influence parameter obtained from S-CPE in the GRGT and apply it to square-well fluids and study the improvement in liquid-vapor coexistence curves in the critical region. We also obtain the critical exponents using the present method. Apart from these, we also study the Yang-Yang anomaly[80].

The Yang-Yang anomaly is basically the divergence of the second derivatives of both the chemical potential and pressure at the critical point as opposed to the divergence of the second derivative of only pressure in the exactly solvable models like lattice gas. The Yang-Yang anomaly was observed in propane and CO_2 for the first time by Fisher and Orkoulaus[81] in the year 2000. Because of the anomaly, the assumption that the description of fluid criticality can be done using two scaling fields, viz. the thermal field (T/T_c-1) and the ordering field (μ/μ_c-1) become inadequate. Fisher and Orkoulaus showed that in addition to these fields, the pressure deviation $(P-P_c)$ also should be taken into account in order to explain the anomaly. The consequence is an additional term in the scaling relation for the coexistence diameter proportional to $(T/T_c-1)^{2\beta}$ with $\beta(=0.326)$ being the standard exponent for order parameter. Later Fisher and co-workers[82] investigated the anomaly in square-well fluids using Monte-Carlo simulations.

The chapter is organized as follows. In section 5.2, we give the basic recipe of the theories used in the calculations. In section 5.3,we apply the method to square-well fluids of widths $1.375, 1.5, 1.75$ and 2.0 and carry out the studies mentioned above. The results are analyzed and the paper is concluded in section 5.4.

5.2 Theory

In this section, we give a recipe of the S-CPE and the GRGT that we use in the applications. The system under consideration contains N classical particles in a volume V at an average density $\rho = N/V$ and temperature T. The S-CPE method used here is same as the generalized version discussed in Chapter 3.

Hence the details are not repeated here.

The GRGT method implemented is almost same as that explained in chapter 2 except for inclusion of the fluctuation contribution due to gradient term neglected in Eq.(2.27) of Chapter 2. We recollect that the contribution of fluctuations within the wavelength band (λ_0, λ_1) with mean wavelength λ_1^m is

$$\Delta f_1[\rho_1^*, |\nabla\rho_1^*|] = -\frac{1}{\beta V_1} ln \left\{ \frac{\int dx\ e^{-\beta V_1\ \delta f[\rho_1^*, |\nabla\rho_1^*|, k_1, x]}}{\int dx\ e^{-\beta V_1\ \delta f[\rho_1^*, |\nabla\rho_1^*|, k_0, x]}} \right\} \tag{5.1}$$

where V_1 is the volume of the phase cell such that $\rho_1(\vec{r})$ varies significantly within it while $\rho_1^*(\vec{r})$ has only a slow variation. The volume V_1 is related to the mean wavelength λ_1^m . k_1 is the wavenumber corresponding to the mean wavelength λ_1^m. k_0 is the wavenumber corresponding to the mean wavelength(λ_0^m) in the band $(0, \lambda_0)$ and

$$\delta f[\rho_1^*, |\nabla\rho_1^*|, k, x] = \frac{1}{2}\left(f_0[\rho_1^* + x] + f_0[\rho_1^* - x] - 2f_0[\rho_1^*]\right)$$
$$+\frac{1}{2}\left(f_{G_0}[\rho_1^* + x] + f_{G_0}[\rho_1^* - x] - 2f_{G_0}[\rho_1^*]\right)|\nabla\rho_1^*|^2 + f_{G_0}[\rho_1^*]x^2k^2. \tag{5.2}$$

λ_0^m is a parameter in the method which may be chosen based on intuition. λ_0^m has to be chosen to be large enough so that the density picture holds and small enough so that the fluctuations not included in the mean field theory get accounted in the RG iterations. We chose a compromise value which is "4" in the reduced units of the problem. Once λ_0^m is chosen, λ_1^m is taken to be $2\lambda_0^m$. The volumeV_1 of the phase cell is taken to be $\left(\frac{z\lambda_1^m}{2}\right)^3$. In our previous chapter 2, we showed that the use of Wilson's method requires z to be close to $1(1.0455)$.

In chapter 2, we neglected the second term in the RHS of the above equation assuming it to be small. However, contribution to Δf_1 from the neglected term may be calculated simply by expanding the exponential corresponding to that

term assuming it to be small. After some manipulation, we get

$$\Delta f_1[\rho_1^*, |\nabla\rho_1^*|] = -\frac{1}{\beta V_1} ln \left\{ \frac{\int dx\ e^{-\beta V_1\ \delta' f(k_1,x)}}{\int dx\ e^{-\beta V_1\ \delta' f(k_0,x)}} \right\} + \left\{ \frac{\int dx\ e^{-\beta V_1\ \delta' f(k_1,x)} f_{Gd}(x)}{\int dx\ e^{-\beta V_1\ \delta' f(k_1,x)}} - \frac{\int dx\ e^{-\beta V_1\ \delta' f(k_0,x)} f_{Gd}(x)}{\int dx\ e^{-\beta V_1\ \delta' f(k_0,x)}} \right\} |\nabla\rho_1^*|^2 \quad (5.3)$$

In the above Eq.(5.3),

$$\delta' f(k,x) = \frac{1}{2}\left(f_0[\rho_1^* + x] + f_0[\rho_1^* - x] - 2f_0[\rho_1^*]\right) + f_{G_0}[\rho_1^*]x^2k^2 \quad (5.4)$$

and

$$f_{Gd}(x) = \frac{1}{2}\left(f_{G_0}[\rho_1^* + x] + f_{G_0}[\rho_1^* - x] - 2f_{G_0}[\rho_1^*]\right). \quad (5.5)$$

Thus Δf_1 contains two terms. The first term(hereafter denoted as $\Delta' f_1$) is a correction to the free energy$f_0(\rho_1^*)$ which when added gives the first iterate of Helmholtz free energy i.e., $f_1(\rho_1^*) = f_0(\rho_1^*) + \Delta' f_1(\rho_1^*)$. The coefficient of the square-gradient in the second term ($\Delta'' f_1$) is a correction to the Influence Parameter $f_{G_0}(\rho_1^*)$ in Eq.(2.3) which when added gives the first iterate of influence parameter i.e., $f_{G_1}(\rho_1^*) = f_{G_0}(\rho_1^*) + \Delta'' f_1(\rho_1^*)$. This completes the first iteration of the scheme. The free energy thus obtained contains effects of fluctuations up to a mean wavelength λ_1^m. In calculating Δf_1 using Eq.(5.3), Eq.(5.4) and Eq.(5.5), it is assumed that $\rho_1^* \approx \rho$.

The second iteration includes the effects of fluctuations with a mean wavelength $\lambda_2^m = 2\lambda_1^m$. The corresponding phase cell volumeV_2 is $\left(\frac{z\lambda_2^m}{2}\right)^3 = 2^3 V_1$. The above procedure is repeated with the V_2, λ_2^m, $f_1(\rho_1^*)$ and $f_{G_1}(\rho_1^*)$ replacing their older counterparts and assuming $\rho_2^* \approx \rho$. When this is done, we get Δf_2, the first part of which is added to Helmholtz free energy ($f_1(\rho_2^*)$) and second part to influence parameter ($f_{G_1}(\rho_2^*)$) to obtain $f_2(\rho_2^*)$ and $f_{G_2}(\rho_2^*)$.

In the above described method, the mean wavelength of density fluctuations at each iteration is incremented by twice to value in the previous iteration. Thus, $\lambda_n^m = 2^n\lambda_0^m$ at the n^{th} iteration and $k_n = \frac{2\pi}{\lambda_n^m}$. The corresponding phase cell volume is $V_n = \left(\frac{z\lambda_n^m}{2}\right)^3$. In evaluating $\Delta f_n[\rho_n^*, |\nabla\rho_n^*|]$, it is assumed

that $\rho_n^* \approx \rho$.The procedure is continued until the HFE converges to the required tolerance.

5.3 Application to square-well fluids

In this section, we apply the S-CPE+GRGT method to square-well fluids of ranges $1.375, 1.5, 1.75$ and 2.0. Reduced units ($\epsilon/k_B = \sigma = 1$, where ϵ is the well depth and σ is hard sphere diameter) are used throughout the paper.

First we obtain the the Helmholtz free energy density $f_0(\rho, T)$ and the influence parameter $f_2(\rho, T)$ using the S-CPE. For each isotherm, the S-CPE calculations are done to obtain $f_0(\rho, T)$ and $f_2(\rho, T)$ for densities between 0 and 0.9 with grid spacing 0.01. Then Newton's interpolation formula is used and the $f_0(\rho, T)$ and $f_2(\rho, T)$ are obtained with required grid spacing by interpolation. Typically we used grid spacing between 0.0005 to 0.0001 for the interpolated Helmholtz free energy density and influence parameter. The Helmholtz free energy density so obtained is used in GRGT iteration scheme. In all the calculations, Eq.(5.3) containing the additional correction term to $f_2(\rho, T)$ is used to obtain GRGT correction. However, we found that the effect of the correction term is negligible.

5.3.1 Convergence of GRGT iterations

We first studied the convergence of the GRGT iteration scheme. The Root Mean Square Deviation (RMSD) given by

$$RMSD = \sqrt{\frac{\sum_{i=1}^{N_{mft}} \left(f_n(\rho_i) - f_{n-1}(\rho_i)\right)^2}{N_{mft}}} \tag{5.6}$$

is found to be good and quite fast throughout the phase diagram. The RMSD reduced to 10^{-10} within 10 iterations. Regarding the point-wise convergence, we have seen that for an isotherm below the critical temperature, the rate of convergence inside the phase coexistence region is different from that outside the region (see Fig.(5.1)). Outside the phase coexistence region the point-wise

convergence is quite fast for all densities and was similar to RMSD. Whereas for densities inside the coexistence region, the convergence is good initially but became slower after certain iterations at some densities. In Fig.(5.1), we plot the deviation of Helmholtz free energy density after 100 iterations from that after 99 iterations for square-well fluid of range 1.5 at temperatures 0.9, 1.1 and 1.15. The deviation is higher for $T = 0.9$ and also number of such density points are more for that temperature. The rate of convergence picked up as the temperature is increased and close (roughly about 10%) to the critical temperature, the convergence became similar to that of regions outside the phase diagram. For $T = 1.1$, the deviation decreased further and for $T = 1.15$ there is uniform convergence for all the densities.

The slow point-wise convergence inside the liquid-vapor phase diagram shows up when thermodynamic quantities related to derivatives of Helmholtz free energy are calculated. In Fig.(5.2), the isotherms of square-well fluid of range 1.5 are plotted for $T = 1.0$ and $T = 1.2$. It can be seen that the isotherm has become flat inside the liquid vapor coexistence region after the GRGT correction. However, because of non-uniform and slow-convergence at some densities, some spikes have appeared in the coexistence region for the $T = 1.0$ isotherm. The liquid-vapor coexistence points can still be obtained using the Maxwell's construction or searching for points of equal chemical potential and pressure. A similar situation was encountered by Ghobadi and Elliott[83] in their application of GRGT (in combination with discontinuous molecular dynamics and perturbation theory) to fluids of chain molecules. Ghobadi and Elliott used a stability constraint introduced by Tang[84] and Gross to improve the shape of the isotherm in the unstable region. However, it was observed that the flatness of the isotherm in the coexistence region is lost with the introduction of the constraint.[83]. The problem of non-uniform point-wise convergence did not appear in the case of $T = 1.2$ isotherm where the temperature is very close to the critical temperature. At this temperature, the rate of point-wise convergence is similar to the rate of root-mean-square convergence. Thus the present method may be used to study the critical behavior of fluids without any smoothing procedures.

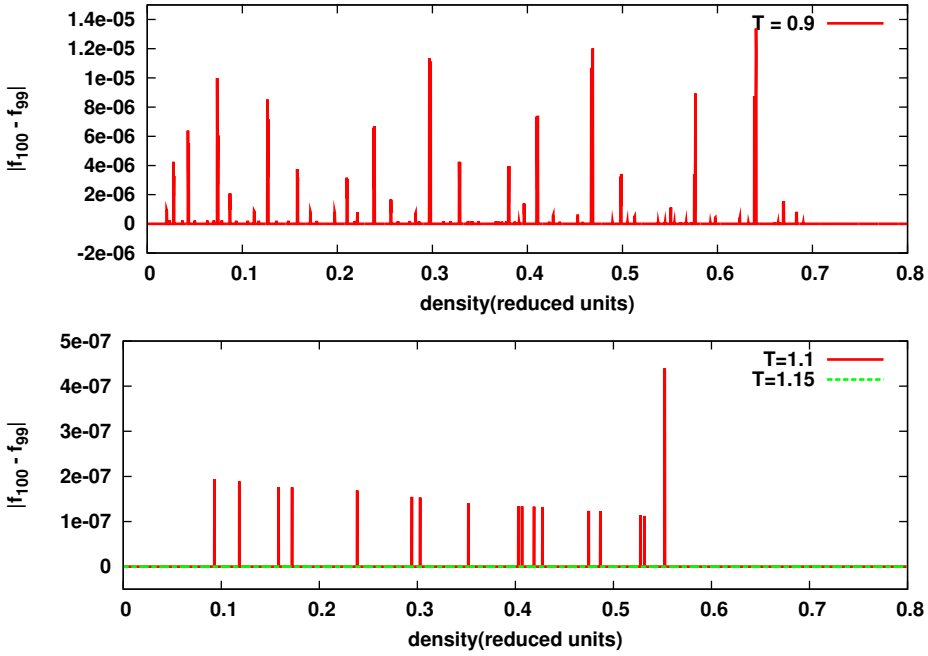

Figure 5.1: Deviation of 100^{th} iterate of Helmholtz free energy density(f_{100}) from 99^{th} iterate (f_{99}) for square-well fluid of range 1.5 at temperatures $T = 0.9$, 1.1 and 1.15. The deviation at $T = 1.15$ is practically zero.

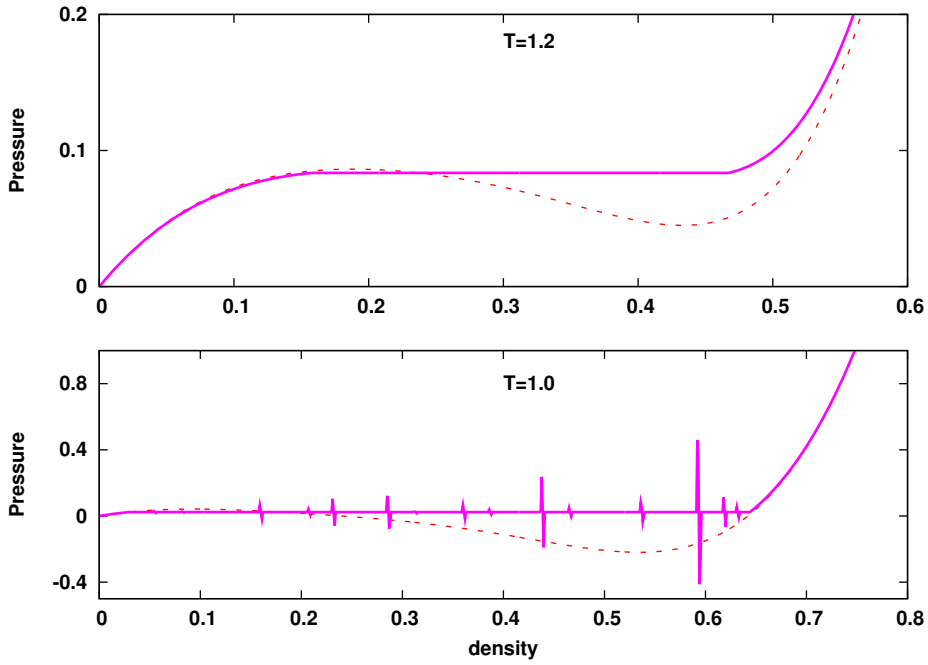

Figure 5.2: Isotherms of square-well fluid of range 1.5 at temperatures $T = 1.0$ and $T = 1.2$. Dashes: seventh order CPE, solid line: GRGT. For $T = 1.0$, the number of GRGT iterations done were 100. For $T = 1.2$, the number of GRGT iterations done were 20.

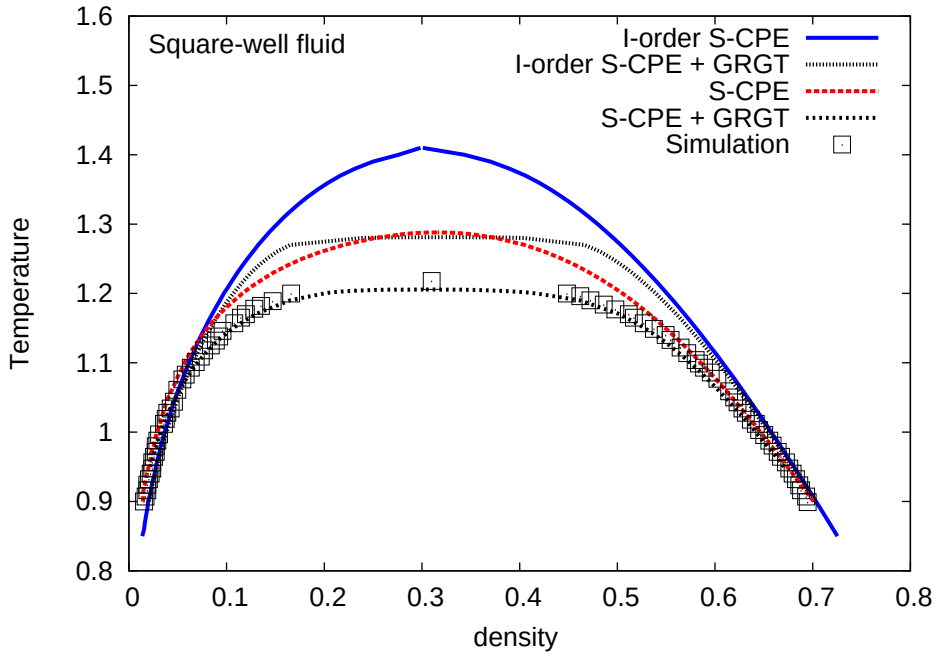

Figure 5.3: LVPD of square-well fluid of range 1.5 in reduced units in (temperature)T Vs (density) ρ plane. Squares are simulation results[45]. Figure shows LVPDs obtained using I-order S-CPE, I-order S-CPE+GRGT, S-CPE and S-CPE+GRGT respectively.

5.3.2 Liquid vapor phase diagrams

Using the CPE+GRGT method, we obtained the LVPDs of square-well fluids of ranges 1.375, 1.5, 1.75 and 2.0. In Fig.(5.3) and Fig.(5.4), the LVPD of square-well fluid of range 1.5 is plotted in $T\ Vs\ \rho$ and $P\ Vs\ \rho$ planes respectively. The figures depict the LVPD obtained using I-order S-CPE , I-order S-CPE+GRGT, S-CPE and S-CPE+GRGT respectively. It can be seen from the figures that the GRGT correction when applied over I-order S-CPE could not bring satisfactory improvement. Whereas, the S-CPE itself improved the LVPD enormously over that of I-order S-CPE. Adding the GRGT correction to the S-CPE brought the LVPD quite close to the simulation results. Also, the LVPD of I-order S-CPE + GRGT is excessively flat close to the critical point. Excessive flatness of the phase diagram close to the critical region has been reported earlier by Esther et al.[49] and Ghobadi et al.[83]. In both these works, the authors attempted

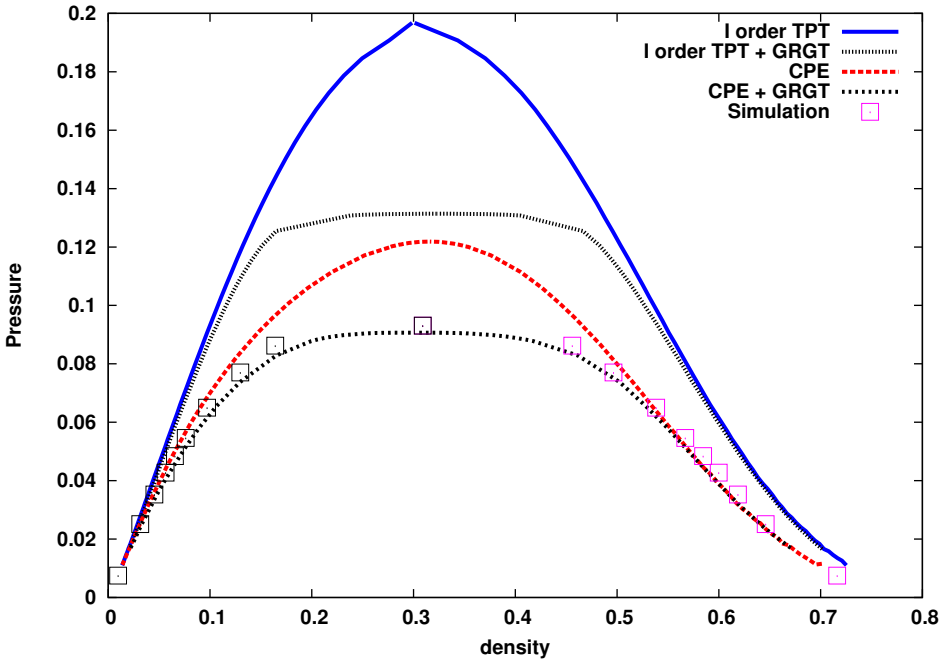

Figure 5.4: LVPD of square-well fluid of range 1.5 in reduced units in pressure(P) Vs density(ρ) plane.

to address the problem by changing the rate of increase of fluctuation wavelength. But it was observed that changing the rate of increase of fluctuations deteriorates the values of critical exponents[49]. We observed that the problem didn't arise when the S-CPE + GRGT has been used to obtain the LVPD. Also we show below that the critical exponents obtained using our method compare well with non-classical Ising model exponents.

The LVPDs obtained using S-CPE+ GRGT for square-well fluids of other ranges are depicted in Fig.(5.5) and Fig.(5.6). Overall it can be seen that the addition of GRGT correction improved the LVPD close to the critical region.

The following points have been noted regarding application of CPE+GRGT in general to obtain the vapor-liquid phase equilibria. It is known that the mean field theories become exact in the limit of infinitely long ranged potential[86]. This trend was observed in our earlier work[51] in which LVPDs of square-well fluids of various ranges have been obtained using various orders of CPE. We observed that the CPE practically converged by third order for fluids with long-range potentials (e.g., square- well fluid of range 2.3) and was qualitatively accurate in predicting the critical constants. Elliott and coworkers[87] and Jackson and coworkers[88] also found that the third order perturbation theory is accurate enough for obtaining the vapor-liquid equilibria of various fluids of chain molecules. However, we observed[51] that the convergence of CPE slowed down in the coexistence region as the range of the potential is reduced and a qualitative convergence has been observed only by seventh order of CPE. Even with the seventh order version of CPE, a clear deviation from the simulation data was observed indicating the need for GRGT correction. This is the reason we used the seventh order CPE+GRGT in the present calculations. Thus it may be concluded that for long range potentials, the CPE alone may be sufficient if only the LVPDs are to be obtained. The use of CPE + GRGT is required for short ranged potentials. In practice one may check the deviation of converged CPE results from those of simulation or experiment and then decide on addition of the GRGT correction. In the case of square-well fluids, we observed that the GRGT correction may not be important for the potentials with ranges greater than 2.0.

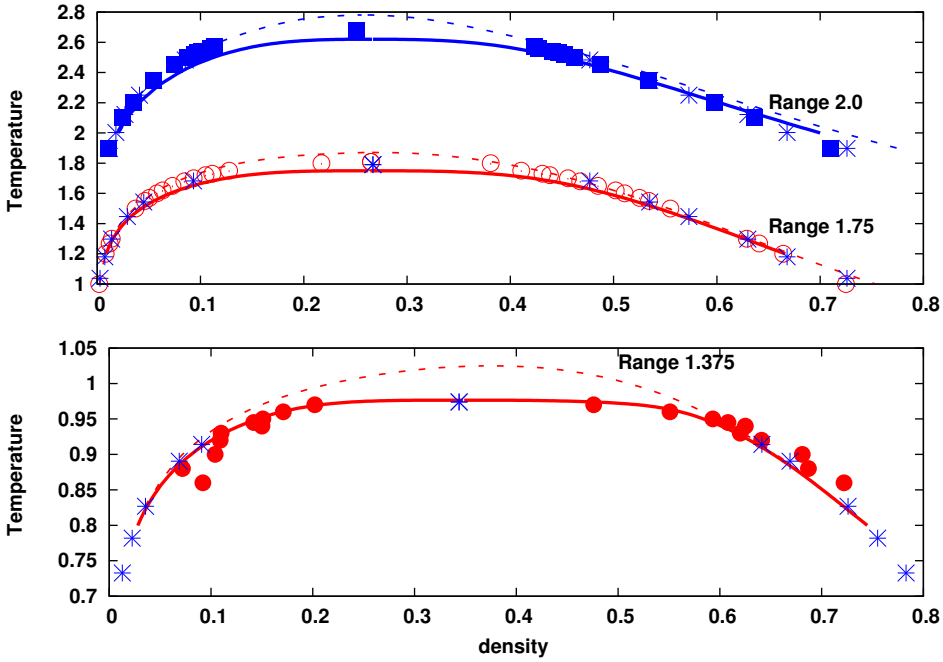

Figure 5.5: LVPD of square-well fluids of ranges 1.375, 1.75 and 2.0 in reduced units in temperature(T) Vs density(ρ) plane.Squares, hollow circles[70], solid circles[60] and stars[85] are simulation results. Solid line: S-CPE + GRGT, dashes: S-CPE.

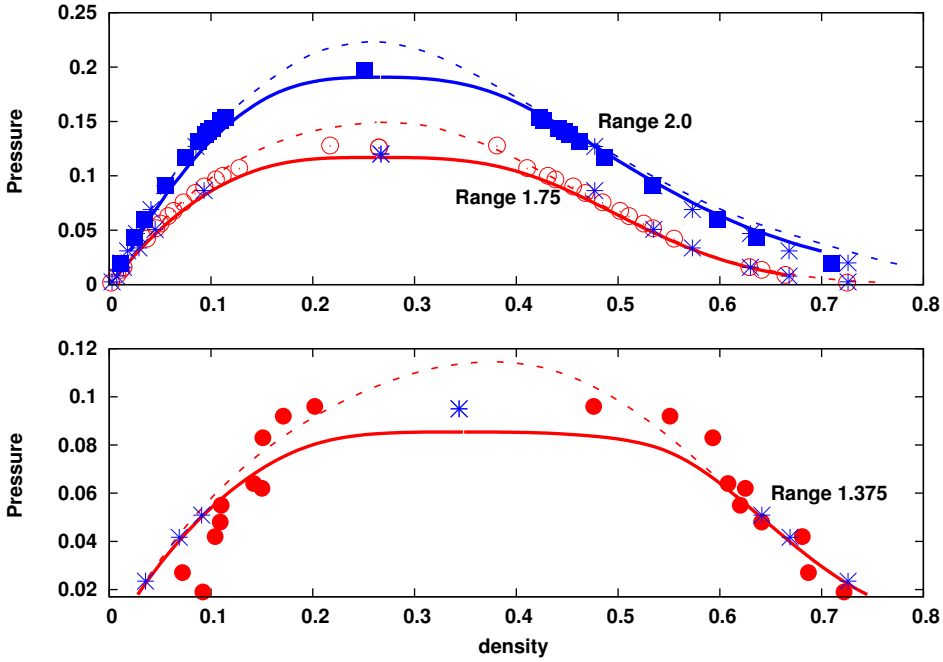

Figure 5.6: LVPD of square-well fluids of ranges 1.375, 1.75 and 2.0 in reduced units in pressure(P) Vs density (ρ) plane. Solid circles[60], hollow circles, squares[70] and stars[85] are simulation results. Solid line: S-CPE + GRGT, dashes: S-CPE.

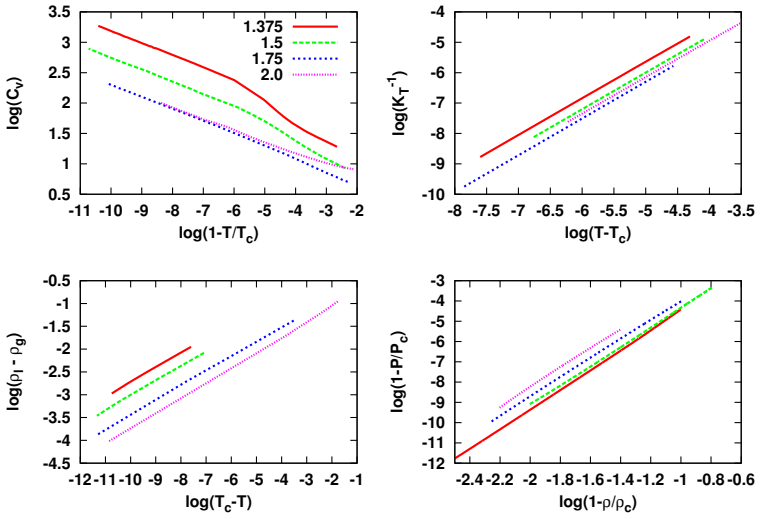

Figure 5.7: Plots of curves from which the critical exponents are obtained. Top left: $log(C_v)$ Vs $log(1 - T/T_c)$ along the critical isochore. Top right: $log(K_T^{-1})$ Vs $log(T - T_c)$ along the critical isochore for $T \to T_c^+$. Bottom left: $log(\rho_l - \rho_g)$ Vs $log(T_c - T)$ along the LVPD. Bottom right: $log(1 - P/P_c)$ Vs $log(1 - \rho/\rho_c)$ along the critical isotherm.

5.3.3 Critical Exponents and Yang-Yang Anomaly

As explained above, the GRGT iteration scheme converges fast close to the critical point thus permitting a study of the critical behavior predicted by the method. We obtained the critical exponents α, β, γ and δ for square-well fluids of ranges 1.375, 1.5, 1.75 and 2.0 using the S-CPE+ GRGT.

We could locate the T_c within a deviation of 0.1% and ρ_c within a deviation of 1%. The necessary quantities C_v, K_T^{-1}, LVPD and critical isotherm are obtained in the critical region and the exponents are obtained by fitting the data to the scaling law of each exponent. Log-log plots of the quantities we obtained using S-CPE+GRGT close to the critical region are shown in Fig.(5.7). The exponents we obtained for square-well fluids of various ranges are given in Table.5.1 along with the exact exponents of three dimensional Ising universality class[89]. It can be seen that our method predicts non-classical exponents close to the three dimensional Ising universality class and the Rushbrooke's[90] and the Griffiths'[91] equalities are qualitatively satisfied.

Having obtained non-classical critical exponents we proceeded further to

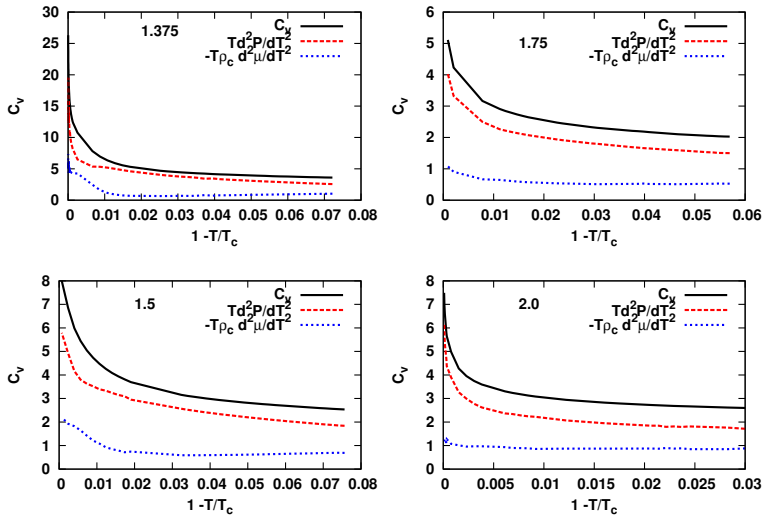

Figure 5.8: (Color Online) Specific heat(C_v), Second derivatives $C_v^p = T\frac{d^2P}{dT^2}$ and $C_v^\mu = -T\rho_c\frac{d^2\mu}{dT^2}$ for square-well fluids of ranges 1.375, 1.5, 1.75 and 2.0 along the critical isochore. (ρ_c is the critical density.)

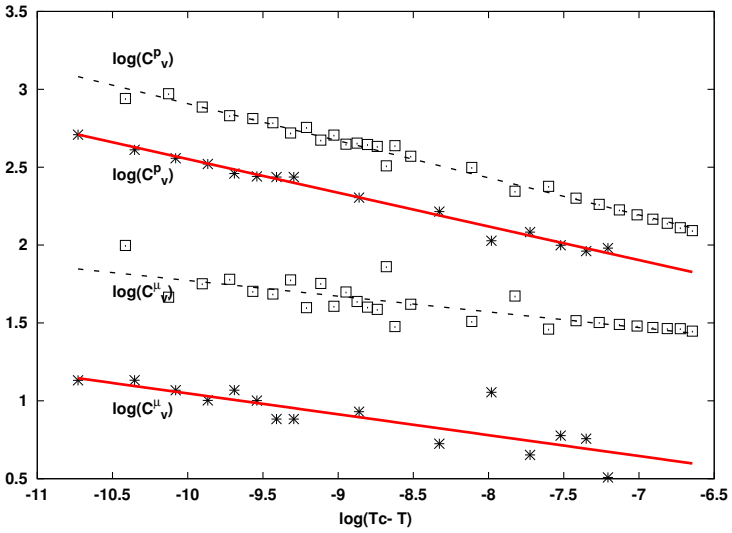

Figure 5.9: Plot of $log(C_v^p)$ and $log(C_v^\mu)$ Vs $log(T_c - T)$ for square-well fluids of ranges 1.375 and 1.5 along the critical isochore. Lines are linear fits to data. Hollow squares: square-well fluid of range 1.375, stars: square-well fluid of range 1.5.

study the Yang-Yang anomaly as explained in the introduction. The Yang-Yang anomaly is as follows: The specific heat capacity at constant volume C_v of a substance can be written as

$$C_v = T\frac{d^2P}{dT^2} - \rho T\frac{d^2\mu}{dT^2} \tag{5.7}$$

where μ is the chemical potential. Yang and Yang predicted that both the second derivatives in the above Eq.(5.7) would diverge at the critical point for real systems. However, in lattice gas and related models, only the pressure derivative was found to diverge. Thus it is termed as an anomaly by Fisher[81] who first figured out such an anomaly in CO_2 and propane by carefully analyzing the experimental data. Later simulations have been done for square-well fluid[92] of width 1.5 and it was found that the strength of Yang-Yang anomaly determined by the

$$R_\mu = (-\rho_c T\frac{d^2\mu}{dT^2}/(T\frac{d^2P}{dT^2} - \rho_c T\frac{d^2\mu}{dT^2})) \tag{5.8}$$

parameter(introduced by Fisher) is -0.042.

We obtained the first(C_v^p) and second (C_v^μ) terms of above Eq.(5.7) for the square-well fluids of ranges 1.375, 1.5, 1.75 and 2.0 along the critical isochore. The plots of the C_v and each term of the R.H.S. of the Eq.(5.7) are shown in Fig.(5.8). The figure shows that both the terms diverge. But the divergence of C_v^p is faster than that of C_v^μ.

To quantify the observation we did the following study. Close to the critical point we fitted the C_v^p and C_v^μ using a scaling law similar to Eq.(1.32). The exponents we obtained are listed in table.(5.2). The exponent pertaining to divergence of C_v^p is denoted as α_p and that corresponding to C_v^μ as α_μ. We also plot in Fig.(5.9) the variation of logarithms of C_v^p and C_v^μ with $log(T_c - T)$ for square-well fluids of ranges 1.375 and 1.5. From the table.(5.2) it can be seen that the divergence of C_v^μ is slower than C_v^p. This implies that the R_μ parameter as predicted by GRGT tends to 0 at T_c for all the square-well fluids considered. Thus the Yang-Yang anomaly as predicted by GRGT is differing from what has been obtained by simulations[92].

5.4 Summary and Discussion

In this chapter, we applied the S-CPE + GRGT method to square-well fluids of various ranges and carried out the following studies to assess the performance of the method. We first studied the convergence of the GRGT iteration scheme. The root mean square convergence is satisfactory for all the temperatures. The point-wise convergence of GRGT iterations is quite fast outside the co-existence region but is slow and non-uniform in the coexistence region away from the critical point. However, as the critical point is approached, the point-wise convergence becomes faster and uniform. The LVPDs obtained using S-CPE+GRGT showed significant improvement over those obtained using I-order S-CPE + GRGT method. The critical exponents obtained using S-CPE + GRGT turned out to be non-classical and of Ising universality class. Finally we studied the Yang-Yang anomaly using the method. It is observed that the method predicts the existence of Yang-Yang anomaly but the strength of the anomaly differs from what was obtained in simulations. A possible reason for the difference may be the Wilson's approach used for functional integration which is too simplified. As can be seen from table.5.1, the method predicted a higher value for exponent α implying that the method doesn't capture the correct divergence behavior of C_v. Hence the GRGT, even though being able to predict the existence of the Yang-Yang anomaly, may be predicting the rates of divergences incorrectly. A similar problem was observed with the HRT also[93]. In fact, the sharp cut-off version HRT doesn't even yield the divergence of specific heat at the critical point [39].

We conclude the following: The recent developments implementing renormalization group ideas in liquid state theories are succesful in predicting accurate vapor-liquid phase equilibria of simple fluids, producing flat isotherms in coexistence region and predict non-classical critical exponents. However, the prediction of Yang- Yang anomaly is still a challenge to be achieved. Replacing the Wilson's method in GRGT with a more accurate way of functional integration may provide a solution.

Table 5.1: Critical Exponents for square-well fluids of various ranges obtained using GRGT

Range	α	β	γ	δ	$\alpha+\beta(1+\delta)$	$\alpha+2\beta+\gamma$
1.375	0.198	0.321	1.2031	4.808	2.062	2.0431
1.5	0.198	0.3203	1.2041	4.7516	2.040	2.0427
1.75	0.196	0.319	1.208	4.704	2.014	2.042
2.0	0.191	0.335	1.197	4.779	2.126	2.058
Exact	0.110	0.327	1.237	4.789	2.0	2.0

Table 5.2: critical exponents related to second derivatives of pressure and chemical potential

Range	α_p	α_μ
1.375	0.238	0.101
1.5	0.216	0.134
1.75	0.241	0.134
2.0	0.222	0.082

CHAPTER 6

Vapor-liquid equilibria of metals

6.1 Introduction

Equation of state of metals in fluid regime is required in various simulations of high energy density physics [94]. For example, during the unloading of shocked compressed materials and in exploding wire experiments etc., the materials (which are metals in most cases) pass through the liquid-vapor coexistence region and become plasma. To perform hydrodynamic simulations of those experiments, an equation of state of the metals which includes the liquid vapor phase transition is required. Errors in the LVPDs predicted by equation of state can lead to serious discrepencies in the simulation results.

In the preceding chapter, we applied the CPE+GRGT to study the square-well fluids. In this chapter, we apply the method to study liquid metals modeled using empirical pair potentials. We propose a modified form of pair potential and obtain its parameters using the zero Kelvin isotherm of the concerned metal. We also perform classical molecular dynamics simulations using the potentials and obtain vapor-liquid phase coexistence points which shall be used for comparison with the results of CPE+GRGT using the same potential. Details are outlined below.

Calculation of thermodynamic properties of materials invariably requires the interactions between the particles of the material to be known. Two forms of empirical pair potentials are widely used to model the inter-particle interactions in metals. They are the generalized Lennard-Jones (GLJ)[95] and the Morse potentials[96]. The forms of these potentials are given below.

Recently, Sun Jiuxun[97] obtained the parameters of a modified GLJ potential for various materials and showed that the zero Kelvin pressure isotherm obtained from this potential is quite accurate when compared with ab-initio

data. However, we observed that the zero Kelvin energy isotherm obtained from the potential is erroneous. Also we noticed that the modified GLJ potential with parameters as obtained by Sun cannot be used in simulations and in theoretical methods for most of the materials[98].

The parameters of Morse potential for various cubic metals have been obtained by Lincoln et. al. [99] using equilibrium lattice parameter, bulk modulus and cohesive energy data. J.K. Singh et. al. [100] obtained the liquid-vapor phase diagrams of various metals modeled using the Morse potential as parametrized by Lincoln et. al. through grand-canonical Monte Carlo simulations. The results of J.K. Singh et. al. show that there is enormous deviation between the simulation and experimental values in the case of alkali metals. In the case of other metals like Aluminum, Copper there was no experimental liquid vapor coexistence data for comparison and an inference could not be drawn. The deviations would have arisen because of obtaining the potential parameters using only few physical quantities like cohesive energy, bulk modulus and lattice parameter which are just equilibrium properties.

Our hunch is that, a potential whose cold curve (zero Kelvin isotherm) matches with the experimental cold curve or the one obtained from well-trusted ab-initio calculations, would predict thermodynamic properties accurately over a wide range of thermodynamic conditions. On the other hand, accurate and fast ab-initio calculations of the cold curve are possible with the present day available codes. So in the present work, we use the cold curve obtained from ab-initio calculations based on density functional theory to obtain parameters of the potential for various metals. We fit the cold curve obtained from a given form of potential to that obtained from ab-initio calculation for the concerned metal. This, in-addition to the potential parameters, gives a clear idea of the accuracy of the cold curve corresponding to a potential away from equilibrium.

We applied the above mentioned method to obtain the parameters of Sodium, Potassium, Aluminum and Copper. In the case of Morse and GLJ potentials, we observed that the cold curves obtained from those potential forms do not accurately fit the ab-initio data away from the equilibrium, particularly in the case of Sodium and Potassium. Hence we propose a modified form of em-

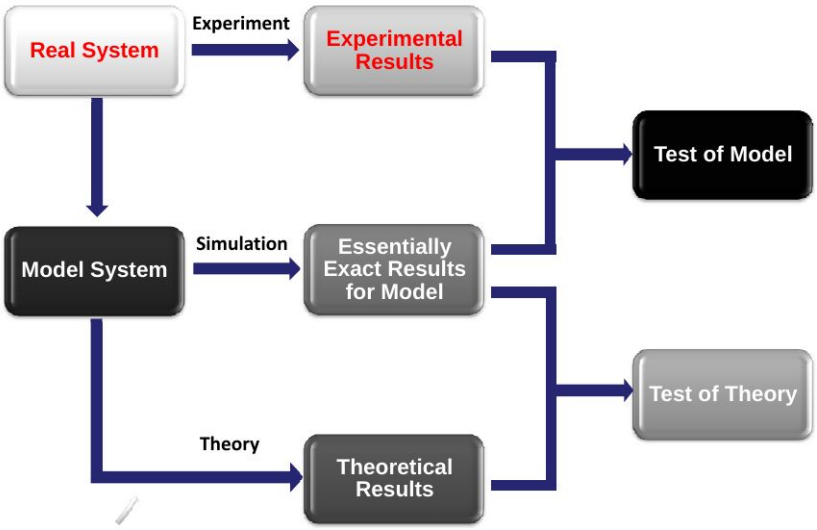

Figure 6.1

pirical pair potential for metals; the cold curve of which is expected to fit the ab-initio data accurately. Parameters of the modified potential have been obtained for Aluminum, Copper, Sodium and Potassium.

With the new potentials in hand, the calculations of equations of state for the metals could be readily performed. However, in the case of materials being modeled using empirical inter-particle potentials, the accuracy of the calculations is decided by two major factors. First is the accuracy of the empirical potential in representing the inter-particle interactions. Second is the accuracy of the calculation method (which in our case is CPE+GRGT). In order to get a correct picture of the distinct roles played by the inter-particle potential and the CPE+GRGT method in determining the accuracy of the calculated properties, the essentially exact results predicted by the inter-particle potential model have to be obtained using simulations. The simulation results when compared with experimental data give an idea about the accuracy of the potential. The results of calculations of the theoretical model(CPE+GRGT) when compared with those of simulations give an idea about the accuracy of the theoretical method. The basic idea is illustrated in the Fig.6.1.

Thus, with the new potentials, we perform the CPE+GRGT calculations

and obtain the vapor-liquid coexistence curves. Also, for the purpose of comparison with CPE+GRGT results, we perform particle transfer molecular dynamics (PTMD)[101–103] simulations with the new potentials and obtain the vapor-liquid coexistence points[104]. The PTMD is a method to simulate the liquid vapor coexistence conditions which has been developed taking inspiration from Gibbs Ensemble Monte Carlo method originated by Panagiotopoulos [47]. A detailed description of the PTMD method is given below. Also we have done NPT ensemble simulations to obtain isobars of Aluminum and Copper at 0.3GPa to test the accuracy of the present potentials at lower temperatures. Finally, the CPE+GRGT results are compared with experimental data and simulation data.

The chapter is organized as follows. In section 6.2, various forms of pair potentials are given along with the modified form that we propose. Our method of obtaining the parameters of the pair potentials is also described. In section 6.3, we describe the classical molecular dynamics simulations we performed to obtain the vapor liquid coexistence curves and the results are analyzed in comparison with available experimental/simulation data. . In section 6.4, the results of CPE+GRGT calculations are compared with obtained simulation data and experimental data and are analyzed. The chapter is concluded in section 6.5.

6.2 Pair Potential Models for Metals

The GLJ potential is given by

$$u_{LJ}(r) = \frac{\epsilon}{m_1 - n_1}\left[n_1\left(\frac{r_0}{r}\right)^{m_1} - m_1\left(\frac{r_0}{r}\right)^{n_1}\right] \tag{6.1}$$

Jiuxun[97] proposed a relation between m_1 and n_1 so that only one is independent. The relations are $m_1 = 6n - 3$ and $n_1 = 3n - 3$. Taking his modification into account, the potential becomes,

$$u_{LJ}(r) = \frac{\epsilon}{3n}\left[(3n-3)\left(\frac{r_0}{r}\right)^{6n-3} - (6n-3)\left(\frac{r_0}{r}\right)^{3n-3}\right] \tag{6.2}$$

The Morse potential is

$$u_M(r) = \epsilon(e^{-2\alpha(r-r_0)} - 2e^{-\alpha(r-r_0)}) \tag{6.3}$$

We propose a new form of pair potential given by

$$u_s(r) = \epsilon \left[e^{-2\alpha(r/r_0-1)} \left(\frac{r_0}{r}\right)^{2\beta} - 2e^{-\alpha(r/r_0-1)} \left(\frac{r_0}{r}\right)^{\beta} \right] \tag{6.4}$$

Attractive part of the above potential is chosen inspired by the screening of ions by electrons in metals. Repulsive part is chosen ad-hoc as per mathematical convenience. It can be seen that, by putting $\beta = 0$ in above potential we recover the Morse potential and by putting $\alpha = 0$,it becomes a Lennard-Jones type potential. Since the electron-ion screening term is represented by an exponential term multiplied by the Coulomb term (in the semi-classical picture), we expect that a similar form with the exponents of the exponential term and the Coulomb term being adjusted, would represent the interactions in a better way.

In the case of GLJ potential, r_0, n and ϵ are the parameters. For the Morse potential, ϵ, α and r_0 are parameters and for the modified potential, $\epsilon, \alpha, \beta, r_0$ are the parameters. For all the potentials, the potential is minimum at r_0 and the well depth is ϵ.

6.2.1 Obtaining the Potential Parameters

We use the Energy per particle(U) Vs volume per particle(v) data obtained from ab-initio calculations to obtain the parameters of the potential for various metals. Ab-initio calculations have been done using density functional theory based code VASP[105–108]. Details of the calculations done to obtain the cold curve are given in the appendix A.

The cold curve for each model potential is written as follows

$$U_x = \sum_{i=1}^{m} \frac{\delta_i}{2} u_x(a_i) \tag{6.5}$$

where x can be LJ, M or s. U_x is the energy per particle. a_i is the distance of the i^{th} neighbor from a particle situated at origin. δ_i is the number of i^{th} neighbors. In the present work we have accounted for interaction up to $(m =)10^{th}$ neighbor shell. a_i is related to volume per atom as follows:

In the case of a fcc solid, $a_i = \sqrt{i}a_1$ and $a_1 = a/\gamma$. Where a is the lattice parameter and γ is the structural constant. For fcc solids, volume per atom $v = a^3/4$ and γ is equal to $\sqrt{2}$. For simplicity, we write r_0 as $(4v_0)^{1/3}/\gamma$ without loss of generality. Using this information, Eq.(6.5) can be written in terms of volume per atom v. The equation then becomes

$$U_x = \sum_{i=1}^{m} \frac{\delta_i}{2} u_x(v/v_0) \tag{6.6}$$

For example, using $u_s(r)$ in U,

$$U_s = \sum_{i=1}^{m} \frac{\delta_i \epsilon}{2} \left[\frac{e^{-2\alpha(\sqrt{i}(v/v_0)^{1/3}-1)}}{i^{\beta}} \left(\frac{v_0}{v}\right)^{2\beta/3} - 2\frac{e^{-\alpha(\sqrt{i}(v/v_0)^{1/3}-1)}}{i^{\beta/2}} \left(\frac{v_0}{v}\right)^{\beta/3} \right] \tag{6.7}$$

In the case of a bcc solid, $\gamma = 2/\sqrt{3}$ and $v = a^3/2$. However, the a_i do not hold a general relation with a as for fcc solids and have to be carefully calculated. In this case r_0 has been chosen as $(2v_0)^{1/3}$. Writing $a_i = d_i a$ where d_i has to be calculated using the crystal structure, equation corresponding to $u_s(r)$ is

$$U_s = \sum_{i=1}^{m} \frac{\delta_i \epsilon}{2} \left[\frac{e^{-2\alpha(d_i(v/v_0)^{1/3}-1)}}{d_i^{2\beta}} \left(\frac{v_0}{v}\right)^{2\beta/3} - 2\frac{e^{-\alpha(d_i(v/v_0)^{1/3}-1)}}{d_i^{\beta}} \left(\frac{v_0}{v}\right)^{\beta/3} \right] \tag{6.8}$$

The parameters of each potential model are obtained by fitting the cold curve Eq.(6.6) to the ab-initio cold curve. The fitted zero Kelvin isotherms obtained from various model potentials for Aluminum, Copper, Sodium and Potassium are shown in Figs.(6.2-6.5).

From the figures it can be seen that the cold curve obtained from GLJ potential is deviates significantly from the ab-initio data away from the equilibrium in all the cases, in both compression and expansion regimes.

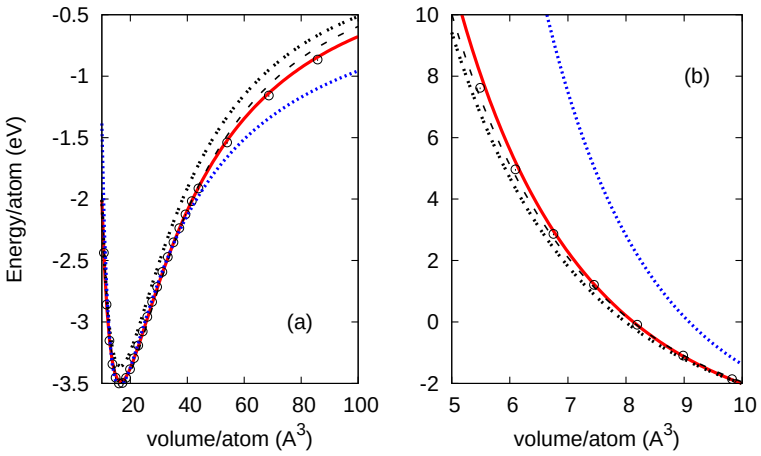

Figure 6.2: Zero Kelvin isotherm of Aluminum obtained using various potentials. (Dotted Line: cold curve from GLJ potential fitted to ab-initio data), (Double dots: Cold curve from Morse potential parametrized by Lincoln et. al.[99]), (Dashes: Cold curve from Morse potential fitted to ab-initio data), (Solid line: Cold curve from modified potential fitted to ab-initio data), (circles: ab-initio data). Panel (a) expansion regime. Panel (b) compression regime.

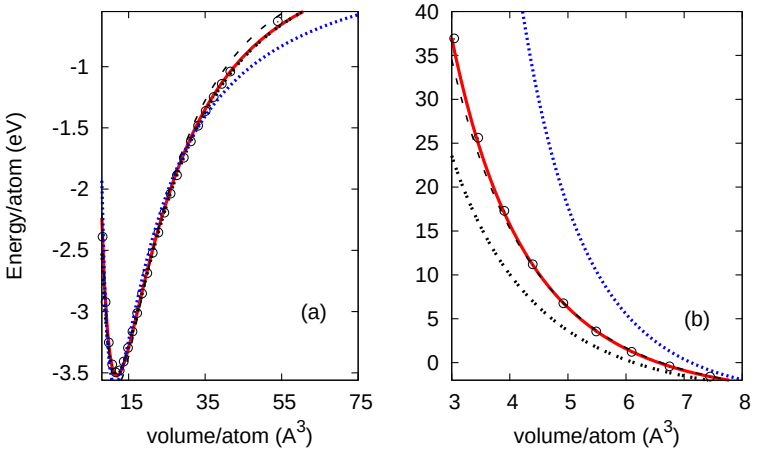

Figure 6.3: Zero Kelvin isotherm of Copper obtained using various potentials. Depiction same as Fig.(6.2).

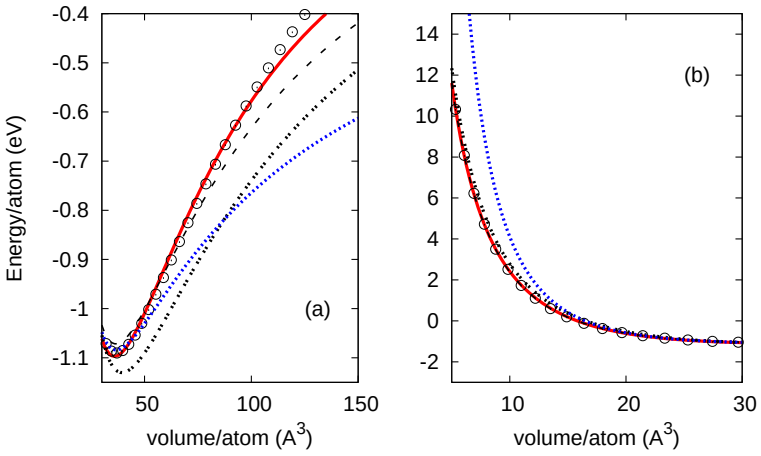

Figure 6.4: Zero Kelvin isotherm of Sodium obtained using various potentials. Depiction same as Fig.(6.2).

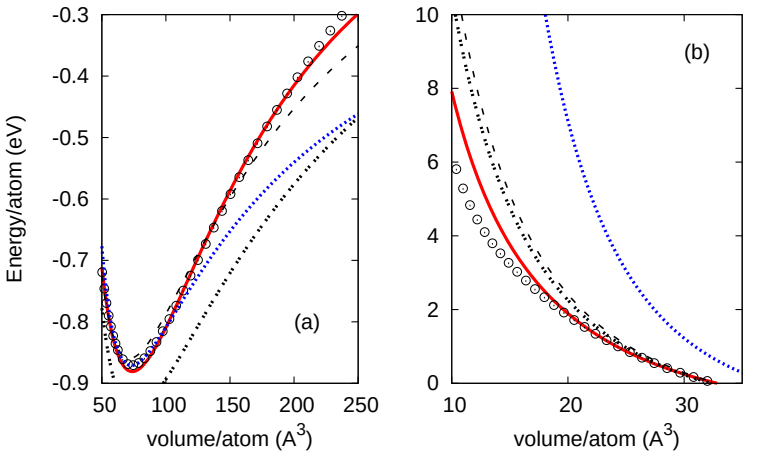

Figure 6.5: Zero Kelvin isotherm of Sodium obtained using various potentials. Depiction same as Fig.(6.2).

In the case of Aluminum, the cold curve obtained from $U_{ML}(v)$ has a quantitative deviation from ab-initio data near equilibrium and away from equilibrium also, as the cohesive energy predicted by ab-initio calculations and that used by Lincoln et. al. differed slightly. On the other hand, $U_M(v)$ and $U_s(v)$ fit the ab-initio data with same accuracy except for a slight deviation of $U_M(v)$ from the ab-initio data away from equilibrium in the expansion regime.

In the case of Copper, $U_{ML}(v)$, $U_M(v)$ and $U_s(v)$ are equally accurate in the expansion phase. But in the compression phase, $U_{ML}(v)$ has a significant deviation from the ab-initio data.

In the cases of Sodium and Potassium, $U_{ML}(v)$ is deviating significantly from ab-initio data. This could be because of improved accuracy of the present ab-initio calculations in predicting the cohesive energies. Also, the $U_M(v)$ is deviating from the ab-initio data in the expansion region far from the equilibrium for both Sodium and Potassium. Whereas in the compression region, $U_M(v)$ is matching reasonably well with ab-initio data in the case of Sodium and is deviating from ab-initio data in the case of Potassium. It can be seen that $U_s(v)$ matched reasonably well with ab-initio cold curve in both the cases.

Above discussion shows that $U_s(v)$ obtained from $u_s(r)$ fitted the ab-initio cold curve with better accuracy than those of other potentials in all the cases discussed. Thus we expect $u_s(r)$ to give an improved liquid-vapor coexistence curve than other potentials.

$u_s(r)$ for Aluminum, Copper, Sodium and potassium is shown in Fig.(6.6). Parameters for the potential $u_s(r)$ obtained using the procedure described above are listed in Table.6.1. For Sodium and Potassium, the parameter β is negative which makes the potential turn down and go to zero close to origin which is un-physical. Thus it has to be cutoff at an appropriate point close to the origin. We found that $0.25r_0$ and $0.4r_0$ can be the cut-off points for Sodium and Potassium respectively. It is assumed that for distances smaller than these, the potential is constant and equal to that at the cutoff point. This should not affect the results as the probability of finding a particle inside the repulsive core is negligible. In order to test the accuracy of modified potential $u_s(r)$ in the fluid phase, we have obtained liquid-vapor phase diagrams (LVPDs) for all these

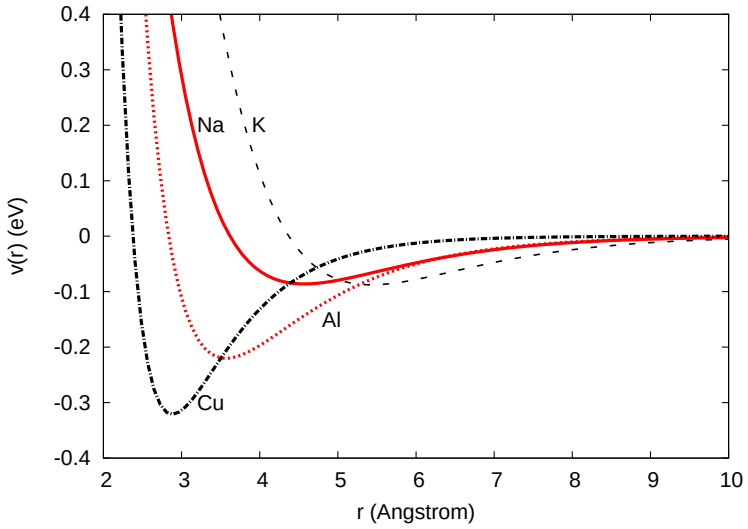

Figure 6.6: Modified pair potentials of Aluminum, Copper, Sodium and Potassium.

metals modeled using $u_s(r)$ from PTMD. Also, for Aluminum and Copper, we have obtained isobars from NPT ensemble simulations.

6.3 Simulation of vapor-liquid phase equilibria

We use the PTMD[101] method, which is a variant of the Gibbs ensemble Monte Carlo(GEMC) method developed by Panagiotopoulos[47], to obtain the liquid-Vapor phase coexistence points. The basic idea of PTMD is to simulate the conditions of liquid-vapor coexistence. The system contains two simulation boxes. Total number of particles in the system is kept constant. However, exchange of particles between boxes is allowed. One box is assumed to be situated in an infinite medium of homogeneous liquid at a (given) constant temperature and the other is assumed to be situated in an infinite medium of homogeneous vapor at the same temperature. Since the idea is to get the thermodynamic properties of a macroscopic system, the interface effects are neglected. The coexistence conditions are simulated by evolving the boxes in such a way that they have same temperature, pressure and chemical potential after equilibration.

Initially, each box is given a guess density(i.e., no. of particles and volume). Equilibration would be faster if the guess densities are closer to the coexisting liquid and vapor densities. Periodic boundary conditions are applied to each box to ensure that they represent the bulk coexisting phases. Temperature fluctuations in each box are controlled by Berendsen thermostat [109] so that they reach the given temperature. Pressures in both the boxes are equalized by controlling their volume fluctuations using a Berendsen barostat[1]. This is done by adjusting the volume of each box such that the instantaneous pressure in one box becomes equal to the instantaneous pressure in the other. The total volume of the two boxes is not restricted to be constant. The particle transfer step to equilibrate chemical potentials in both the boxes is carried out after each five hundred time steps by comparing their chemical potentials. It is done as follows: A particle is chosen randomly from the box where chemical potential is more and is removed from it. Correspondingly a particle is introduced into the other with its potential energy calculated and the velocity taken from the Boltzmann distribution of corresponding temperature. Care is taken so that the introduced particle is not too close to any other particle in the box. With the above three procedures being done during the simulation, the two boxes evolve in time in such away that they have same temperature, pressure and the chemical potential after equilibration. Thus the system may phase separate into liquid in one box and gas in the other with proper choices of initial densities if the temperature of the system is less than the critical temperature. Plots showing the typical evolution of temperature, pressure, density and chemical potential in both the boxes are shown in Fig.(6.7-6.10).

[1]Details of implementation of thermostat, barostat etc. are given in appendix B

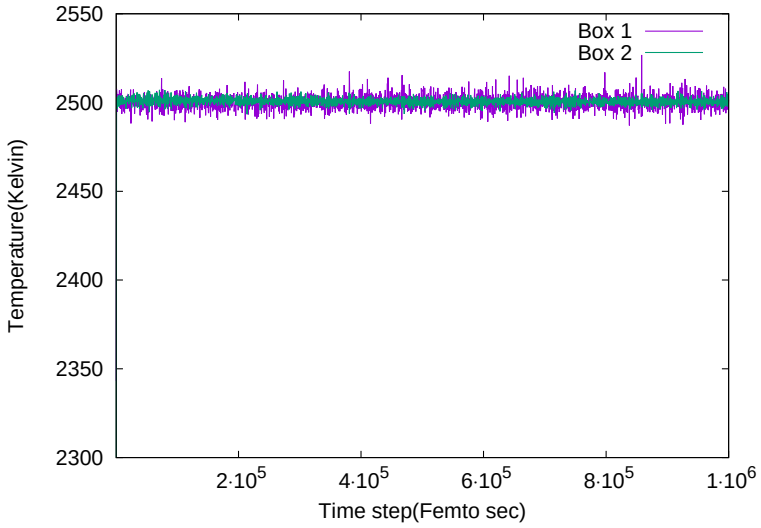

Figure 6.7: Evolution of temperature in Box 1 and Box 2 in PTMD simulation of Sodium at $2500K$ using the modified potential.

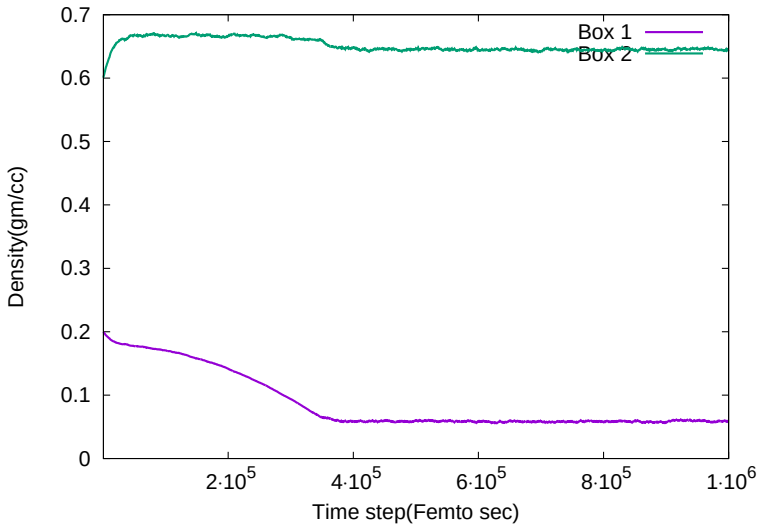

Figure 6.8: Evolution of density in Box 1 and Box 2 in PTMD simulation of Sodium at $2500K$ using the modified potential.

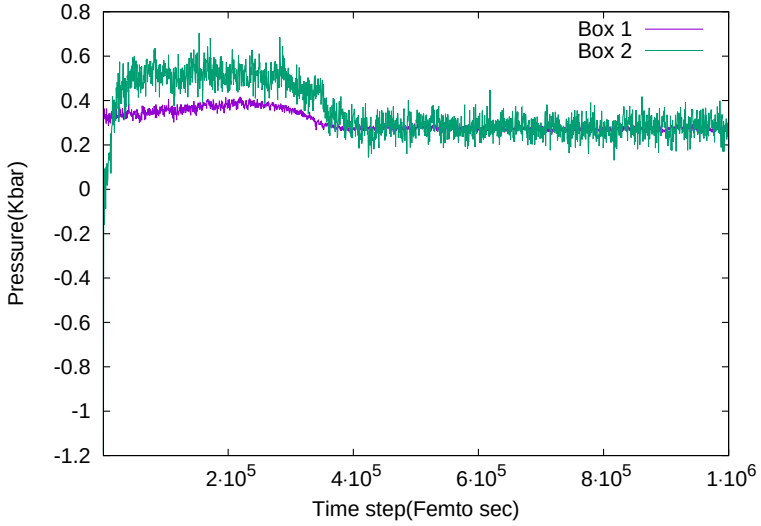

Figure 6.9: Evolution of pressure in Box 1 and Box 2 in PTMD simulation of Sodium at $2500K$ using the modified potential.

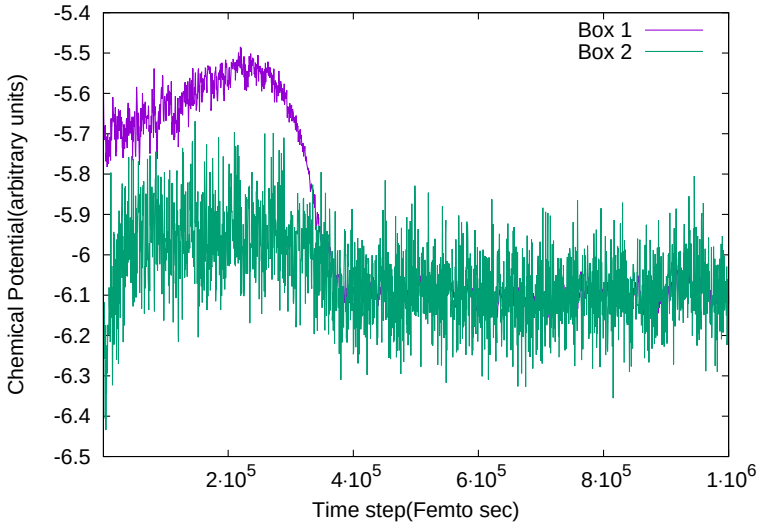

Figure 6.10: Evolution of chemical potential in Box 1 and Box 2 in PTMD simulation of Sodium at $2500K$ using the modified potential.

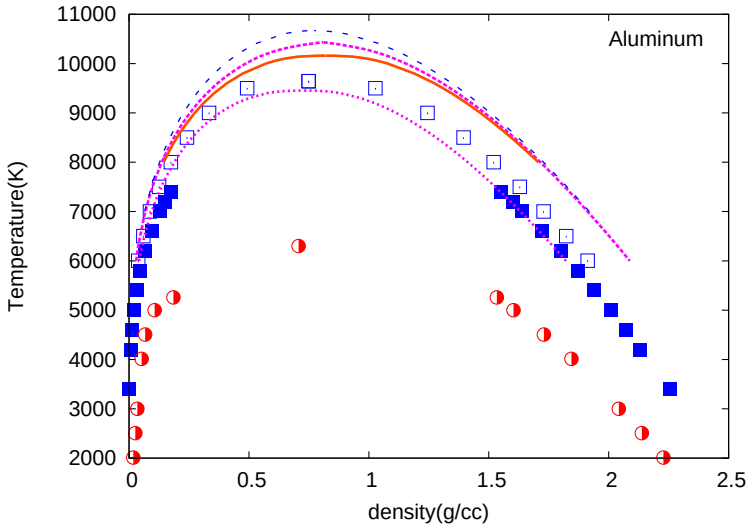

Figure 6.11: Liquid-vapor coexistence curve of Aluminum. Hollow squares: PTMD results using $u_s(r)$, filled squares: Monte Carlo data using $u_{ML}(r)$ from J.K. Singh et. al. [100], half-filled circles: GEMC data using EAM potential from Divesh Bhatt et. al. [112]. Long dashes: I-order S-CPE. Short dashes: S-CPE. Dots: HNC-CPE+GRGT. Solid line: S-CPE+GRGT.

The method described above has been tested for the Lennard-Jones fluid initially. The phase diagram we obtained matched with that of earlier simulations[110] validating the code we developed. Then the code is used to obtain the LVPDs of the metals described above. Time step used in the simulations is 1 femto second and each simulation run has typically 5×10^5 equilibration and production steps. Chemical potential has been evaluated using Widom's test particle insertion method[111]. At each step 200 test particles are inserted and chemical potential is calculated after each five hundred steps. Total number of particles used in the simulation are 1728. The initial densities have been chosen so that after equilibration, both the boxes contain a good number of particles (atleast more than a hundred) so that the averages are reliable and deviations are small.

The Temperature(T) Versus Density(ρ) diagrams for Aluminum, Copper, Sodium and Potassium are shown in Fig.(6.11-6.14). The critical temperature(T_c) and critical density (ρ_c) are obtained by fitting the simulation data to the law

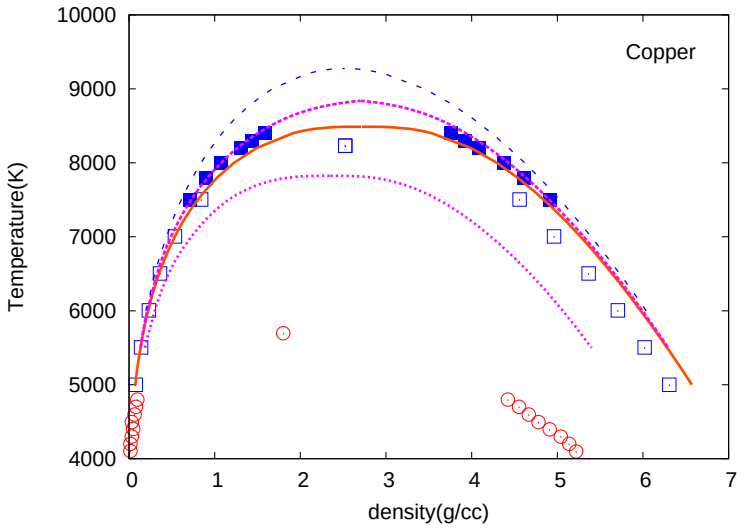

Figure 6.12: Liquid-vapor coexistence curve of Copper. Hollow squares: PTMD results using $u_s(r)$, filled squares: Monte Carlo data using $u_{ML}(r)$ from J.K. Singh et. al. [100], hollow circles: GEMC data using EAM potential from Aleksandrov et. al.[113].Long dashes: I-order S-CPE. Short dashes: S-CPE. Dots: HNC-CPE+GRGT. Solid line: S-CPE+GRGT.

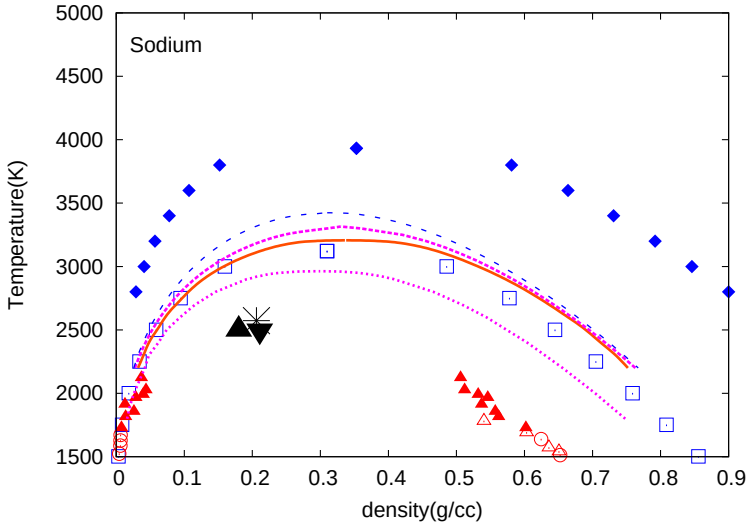

Figure 6.13: Liquid-vapor coexistence curve of Sodium. Squares: PTMD results using $u_s(r)$, diamonds: Monte Carlo data using $u_{ML}(r)$ from J.K. Singh et. al. [100]. Filled up-triangles[114], hollow circles[115] and hollow up-triangles[116] are experimental data. Long dashes: I-order S-CPE. Short dashes: S-CPE. Dots: HNC-CPE+GRGT. Solid line: S-CPE+GRGT.

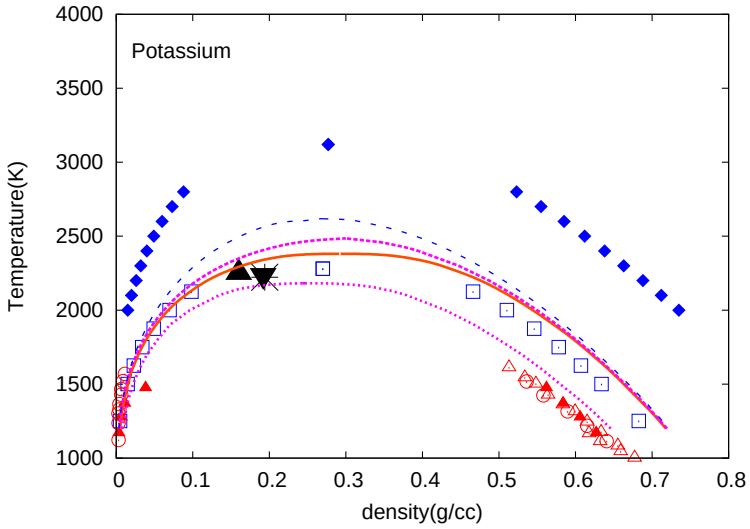

Figure 6.14: Liquid-vapor coexistence curve of Potassium. Squares: PTMD results using $u_s(r)$, diamonds: Monte Carlo data using $u_{ML}(r)$ from J.K. Singh et. al. [100]. Filled up-triangles[114], hollow circles[117] and hollow up-triangles[116] are experimental data. Long dashes: I-order S-CPE. Short dashes: S-CPE. Dots: HNC-CPE+GRGT. Solid line: S-CPE+GRGT.

of rectilinear diameters.

$$\frac{\rho_l + \rho_v}{2} = \rho_c + A(T - T_c) \tag{6.9}$$

and the power law

$$\rho_l - \rho_v = B(T - T_c)^\beta \tag{6.10}$$

where ρ_l and ρ_v are liquid and vapor densities. A and B are fitting constants and $\beta = 0.33$. Critical parameters we obtained are compared with literature data and experiments in table.6.2.

In the case of Aluminum, a large collection of data of T_c and P_c of aluminum obtained from various methods are listed in a recent paper by Morel[118]. The lowest prediction of T_c was $5115K$ by Blairs[119] whereas the highest was $9502K$[120]. Hess[121] estimated the critical point of Aluminum indirectly from various experimental data. Hess' estimates of T_c ranged from $5754K$ to $8944K$. Also the ρ_c predicted by various authors as listed in Morel's paper ranged from $0.3g/cc$ to $1g/cc$ whereas the P_c predictions ranged from $0.18GPa$

to $0.94GPa$. The huge scatter in predictions do not lead to any conclusive estimate. Our estimates of ρ_c and T_c are within the predicted ranges. However, our estimate of T_c was slightly higher than the highest value predicted in literature. In the Fig.(6.12), the GEMC simulation data obtained by Bhatt el. al.[112] using embedded atom model (EAM) potentials and the grand canonical Monte Carlo simulation data obtained by Singh et. al.[100] using $u_{ML}(r)$ are also shown. It can be seen that the LVPDs of our method are close to those of Singh et. al.

In the case of Copper also, the estimates of critical parameters have a huge scatter as can be seen from the table.6.2. Our estimates are within the range of available predictions from literature. In Fig.(6.12), the LVPD of Copper obtained by Alexandrov et. al. [113] using the quantum Sutton-Chen EAM potential from GEMC simulations is depicted. In this case also, the LVPDs we obtained are closer to those obtained by Singh et. al.

For Sodium and Potassium, reliable experimental data of coexistence points and also the critical point is available. Plots of LVPDs obtained using $u_s(r)$ from PTMD along with the data of Singh at. al. using $u_{ML}(r)$ and available experimental data are given in Fig.(6.13) and Fig.(6.14). It can be seen that our estimates of critical parameters are significantly improved over those of Singh et. al.[100] In both the cases of Sodium and Potassium, there is a significant mismatch between $U_{ML}(v)$ and ab-initio data (and hence $U_s(v)$). This is because of the difference in cohesive energies obtained from present ab-initio calculations and earlier values used by Lincoln et. al. [99]. A significant improvement in the LVPDs over those of Singh et. al. reaffirms the accuracy of the ab-initio results.

The results of our simulations for Sodium and Potassium show that, apart from equilibrium data like cohesive energy, bulk modulus etc., the accuracy of the cold curve of a particular potential away from equilibrium plays a major role in determining the accuracy of the thermal properties of fluids obtained from that potential. It can be seen from the Figs.(6.13-ref9ch6) there is still some deviation between our results and experimental coexistence points. The deviation could be because of various reasons. Firstly, the accuracy of potentials we obtained are restricted by the accuracy of the ab-initio calculations.

Secondly, it is unclear whether the potential with fixed parameters could take care of the changes in electronic levels when a liquid-metal transforms into a vapor-insulator. Thirdly, the excitation of electrons to higher levels with temperature would affect the effective potentials. This has not been taken into account. Apart from these, the method we described has been used to obtain parameters of pair potentials for metals keeping in view their utility in theoretical models. However, it can be used with more sophisticated potentials forms including many body effects like EAM potentials also. This may bring down the deviation from experimental results.

6.4 Application of CPE+GRGT to metals

The development of a modified potential and a new way of obtaining its parameters has brought in some improvement in the LVPDs of Sodium and Potassium as obtained from simulations. The LVPDs of Aluminum and Copper did not differ much from those of Morse potential. Now that we have the simulation data for $u_s(r)$ in hand, we apply the CPE+GRGT to $u_s(r)$ to calculate the LVPDs and compare with the simulation data. The implementation of CPE is exactly as explained in chapter 3 and hence is not repeated here. It can be seen from Fig.(6.6) that the range of attractive part and the slope of repulsive part is different for each potential. Since the accuracy of the results of CPE depends on bridge function and the performance of a bridge function depends on the features of the potential like the range of potential, the strength of the repulsive part, which bridge function is to be used for the potentials is unclear. Hence we have done CPE calculations using two closures; the Sarkisov closure[63] and the Hyper-Netted Chain(HNC) closure. The CPE calculations done using Sarkisov closure are referred as S-CPE and those done using HNC are referred as HNC-CPE.

In Fig.(6.15) the calculated RDFs of Sodium at $378K$, $0.928g/cc$ and at $820K$, $0.82g/cc$ are compared with available experimental data. At $378K$, the S-CPE did not have a solution whereas the RDF obtained using the HNC-CPE compares well with the experimental data. At $820K$, solutions could be obtained

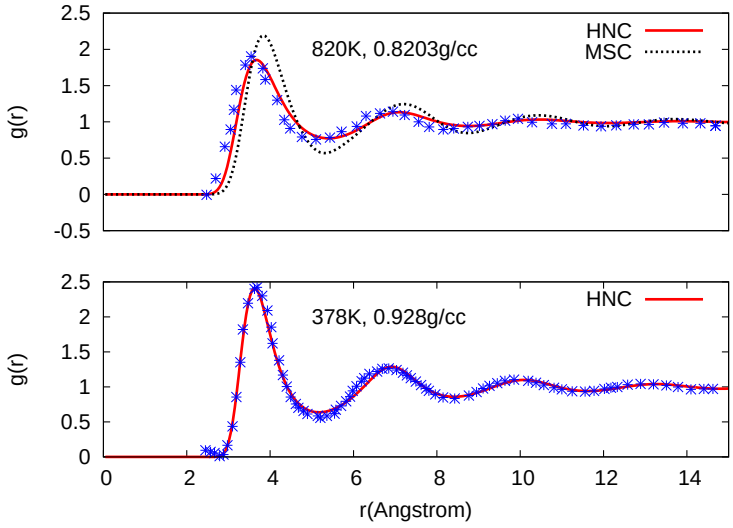

Figure 6.15: RDF of Sodium. Stars: experimental data. Solid lines: HNC-CPE. Dots: S-CPE.

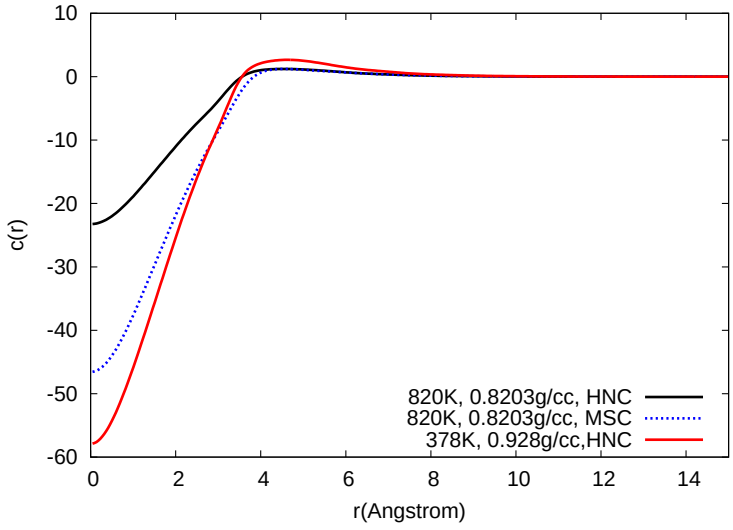

Figure 6.16: DCF of Sodium. Depiction same as in Fig.(6.15)

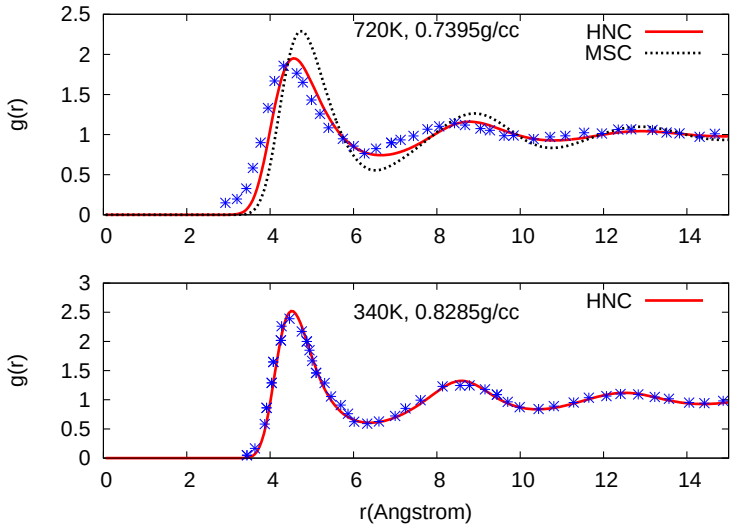

Figure 6.17: RDF of Potassium. Stars: experimental data. Depiction same as in Fig.(6.15).

using both the methods. However, the RDF obtained using HNC-CPE matched better with experiment than that of S-CPE. In Fig.(6.16) DCFs of Sodium corresponding to the temperatures and densities mentioned above are shown. In Fig.(6.17), the calculated RDFs of potassium are plotted against experimental data. In this case also, the HNC-CPE results are more accurate than the S-CPE results.

In Figs.(6.11 - 6.14), vapor-liquid coexistence curves obtained using the S-CPE+GRGT and HNC-CPE+GRGT methods are compared with the PTMD results obtained above, available experimental data and simulation data of other potentials. We also depict the results of S-CPE and I-order S-CPE calculations. It can be seen from the figures that the LVPDs obtained using S-CPE+GRGT are closer to PTMD results than those obtained with HNC-CPE+GRGT for Sodium, Potassium and Copper. Whereas in the case of Aluminum, the HNC-CPE+GRGT results are more in agreement with PTMD results than those of S-CPE+GRGT.

Overall, a decent agreement of results of CPE+GRGT with the simulation data has been observed. However, the following points are to be noted. From the above applications, it is clear that the CPE plays a major role in deciding the

accuracy of the calculations in the whole phase diagram. The improvement by GRGT is mostly limited to the critical region. The accuracy of the CPE depends on the bridge function used in the calculation. The present calculations show the significant role played by the bridge function and the need for an accurate bridge function.

6.5 Summary and Conclusion

In this chapter, we described a simple way of obtaining parameters of inter-particle potentials using ab-initio cold curve. We also proposed a modified form of empirical pair potential for metals. Using this potential, the LVPDs of Aluminum, Copper, Sodium and Potassium are determined using PTMD simulations. In the case of Sodium and Potassium, the present phase diagrams are significantly improved over those obtained from existing Morse potential when compared with experimental data. In the cases of Aluminum and Copper, we got a new set of LVPDs and critical points which are closer to those obtained using the existing Morse potentials.

We applied the CPE+GRGT to modified potentials. The RDFs obtained using HNC-CPE method close to melting compared well with experimental data. The LVPDs obtained using S-CPE+GRGT are in close agreement with our simulation results for Copper, Potassium and Sodium whereas in the case of Aluminum the LVPD obtained using HNC-CPE+GRGT is in close agreement with present simulation results. Overall, a notable improvement in the LVPDs obtained using the S-CPE+GRGT over those obtained using just I-order S-CPE and S-CPE can be observed. The effect of GRGT is to flatten the LVPD close to the critical region and also to flatten the isotherms in the two phase region. The deviation of the results of present theory from those of simulations is due to the approximate bridge function used in the CPE.

Table 6.1: Parameters for $u_s(r)$

metal	$\epsilon(eV)$	$r_0(A^o)$	α	β
Al	0.220	3.568	2.499	0.7808
Cu	0.321	2.881	3.095	0.792
Na	0.086	4.567	3.968	-0.5573
K	0.088	5.425	5.172	-1.439

Table 6.2: Critical Point Data

metal	$T_c(K)$	$\rho_c(g/cc)$	$P_c(GPa)$	Reference
Al	9643	0.75	0.81	This work
	7963	0.44	0.35	Faussurier[122]
	8860	0.28	0.31	Likalter[123]
	8387	0.38	0.45	Vinayak[124]
	8472	0.79	0.51	Singh[100]
	5115	–	–	Blairs[119]
	5754-8944	0.43	0.47	Hess[121]
	9502	0.90	0.94	Boissiere[120]
Cu	8231	2.05	0.73	This work
	5696	1.8	0.11	Aleksandrov[113]
	8650	2.6	0.95	Singh[100]
	7696	1.93	0.58	Hess(Exp.)[121]
	8900	1.04	–	Cahill(Exp.)[125]
	5140	–	0.4	Martynyuk(Exp.)[126]
Na	3121	0.31	0.109	This work
	2497	0.21	0.025	Ohse(Exp.)[127]
	3932	0.35	0.129	Singh[100]
	2500	0.18	0.037	Vargaftik(Exp.)[128]
	2573	0.21	0.035	Dillon(Exp.)[114]
K	2280	0.27	0.037	This work
	2280	0.19	0.016	Ohse(Exp.)[127]
	3120	0.28	0.053	Singh[100]
	2250	0.16	0.016	Vargaftik(Exp.)[128]
	2223	0.19	0.016	Dillon(Exp.)[114]

CHAPTER 7

Summary and future scope

7.1 Summary of thesis

In this thesis, an improved method to obtain the Helmholtz free energy of a simple classical fluid has been developed which includes the physics of liquid-vapor phase transition in a more rigorous way. The new method is applied to model fluids like square-well fluid, Lennard-Jones fluid and liquid metals modeled using empirical potentials with considerable success. Apart from the development of the theoretical method, molecular dynamics simulations have been done to obtain vapor-liquid equilibria. Also, density functional theory calculations of zero Kelvin isotherms of various simple metals has been done. The following is a summary of the work done in the thesis

1. **Derivation of a generalized version of global renormalization group theory**

   The starting point of our study was the global renormalization group theory (GRGT) originated by White. We have derived a generalized version of GRGT using the Wilson's method of functional integration starting from the square-gradient functional for Helmholtz free energy. The new method has been applied to square-well fluids of ranges 1.5 and 3.0 in reduced units. It is observed that the isotherms below critical point become flat after the GRGT correction indicating an improved description of physics in the two phase region. The liquid vapor phase diagrams(LVPDs) obtained are compared with simulation data and a good improvement in the critical region has been observed for the fluid with range 3.0. However, for the fluid with range 1.5 the GRGT correction was not adequate. We found that the mean field Helmholtz free energy

calculated using first order perturbation theory and the direct correlation function used in the GRGT were too erroneous for short-range potentials.

2. **Coupling parameter expansion(CPE) method**

   We have developed a new way of obtaining the terms of perturbation series for mean field Helmholtz free energy of a simple fluid by combining the thermodynamic perturbation theory with integral equation theory. Initial version of the method assumed reference hyper-netted chain(RHNC) closure. Later the method has been generalized to use any closure. The CPE method, with terms calculated up to seventh order, has been applied to square-well fluids of various ranges and Lennard-Jones fluid. A significant improvement in accuracy of calculated LVPDs against simulation data over those of existing methods is observed. The radial distribution function(RDF), direct correlation functions (DCF) and surface tension obtained using CPE[1] compared well with the available simulation data.

   Overall, the results of CPE method has been a significant improvement over those of existing theories. The accuracy of the results of CPE away from the critical region is limited only by the accuracy of the bridge function used in the calculations. However, the CPE method being a mean field theory requires an improvement close to the critical region.

   In addition, we showed that for a fluid with interaction potential having a repulsive core, the terms of CPE for RDF and DCF also scale with temperature in addition to the terms of Helmholtz free energy series.

3 **Combination of CPE method with GRGT**

   The improved mean field Helmholtz free energy and the DCF obtained from the CPE are used in GRGT and the improvement in its performance is studied through application to square-well fluids of various ranges. The combined method (CPE+GRGT) showed a significant improvement globally. The combined method could accurately predict the LVPDs of square-well fluid of range 1.25 and above in reduced units. We also stud-

[1] By CPE we mean the seventh order version of it unless specified.

ied the critical scaling laws and Yang-Yang anomaly in square-well fluids. Our method predicted the critical scaling constants conforming to the Ising universality class. The method could also predict the Yang-Yang anomaly.

4 Vapor-liquid equilibria of metals

We proposed a modified form of inter-atomic pair potential for metals and obtained its parameters for Copper, Aluminum, Sodium and Potassium by fitting to the corresponding zero Kelvin isotherm. We performed the particle transfer molecular dynamics simulations in order to obtain numerically exact LVPDs predicted by these potentials. The results showed a significant improvement in LVPDs of Sodium and Potassium over available simulation data using Morse potential when compared with experimental data. We then applied the CPE+GRGT to theses potentials. Two sets of calculations were done; one using the hypernetted chain closure and other using Sarkisov closure. The LVPDs obtained using CPE+GRGT with Sarkisov closure are in excellent agreement with simulation data for Sodium, Potassium and Copper whereas in Aluminum's case, LVPDs obtained using CPE+GRGT with with HNC closure are in close agreement. Overall, a notable improvement in accuracy of seventh order CPE+GRGT results over first order CPE results has been observed when compared against simulation data. However, the calculations show the sensitivity of results to the bridge function used in the calculations. To get accurate results, a proper choice of bridge function is necessary.

7.2 Future work

1 Extension of CPE+GRGT to molecular fluids, associating fluids etc.

2 A study of variation of bridge function with temperature and density using simulations and its implementation in calculations of CPE.

3 Implementation of CPE in classical density functional theory of in-homogeneous fluids.

4 Combining the CPE with density functional theory to obtain equation of state of warm dense plasma.

Bibliography

[1] J P HANSEN AND I R MCDONALD. *Theory of Simple Liquids* (Academic press, London, 2006).

[2] M. BORN AND M. S. GREEN. *A General Kinetic Theory of Liquids* (Cambridge University Press, Cambridge, 1949).

[3] J G KIRKWOOD. *The Journal of Chemical Physics*, **3**, 300 (1935).

[4] D LEVESQUE. *Physica*, **32**, 1985 (1966).

[5] J. M. BOMONT. *Advances in Chemical Physics*, **139**, 1–80 (2008).

[6] J. S. ROWLINSON. *Reports of Progress in Physics*, **28**, 169 (1965).

[7] J. K. PERCUS AND G. J. YEVICK. *Physical Review*, **110**, 1 (1958).

[8] D. PINI, G. STELL, AND J. S. HYE. *Int. J. Thermophys.*, **19**, 1029 (1998).

[9] R W ZWANZIG. "Hightemperature equation of state by a perturbation method. I. nonpolar gases". *The Journal of Chemical Physics*, **22**, 1420–1426 (1954).

[10] J A BARKER AND D HENDERSON. "What is "liquid"? Understanding the states of matter". *Rev. Mod. Phys.*, **48**, 587 (1976).

[11] J L BRETONNET. *Thermodynamics-Interaction studies-Solids, Liquids and Gases* (2011).

[12] J A BARKER AND D HENDERSON. *J. Chem. Phys.*, **47**, 2856 (1967).

[13] J LARGO AND J R SOLANA. *Mol. Simul.*, **29**, 363 (2003).

[14] E PRAESTGAARD, S TOXVAERD. *J. Chem. Phys.*, **51**, 1895 (1969).

[15] N F CARNAHAN AND K E STARLING. *J. Chem. Phys.*, **51**, 635 (1969).

[16] J A BARKER AND D HENDERSON. *J. Chem. Phys.*, **47**, 4714 (1967).

[17] J D WEEKS, D CHANDLER AND H C ANDERSEN. *J. Chem. Phys.*, **54**, 5237 (1971).

[18] F LADO. *Mol. Phys.*, **52**, 871 (1984).

[19] D BEN AMOTZ AND G STELL. *J. Phys. Chem. B*, **108**, 6877 (2004).

[20] G A MANSOORI AND F B CANFIELD. *J. Chem. Phys.*, **51**, 4958 (1969).

[21] J C RASAIAH AND G STELL. *Mol. Phys.*, **18**, 249 (1970).

[22] G I KERLEY. *J. Chem. Phys.*, **73**, 469 (1980).

[23] S ZHOU. *Phy. Rev. E*, **74**, 031119 (2006).

[24] S ZHOU. *Phy. Rev. E*, **77**, 041110 (2008).

[25] S. V. G. MENON. *Renormalization group theory of critical phenomena* (IPA Monographs in Physics, Wiley Eastern Ltd, 1995).

[26] KERSON HUANG. *Statistical Mechanics* (John Wiley and Sons(Asia) Pte. Ltd, 2004).

[27] K G WILSON. *Rev. Mod. Phys.*, **55**, 583 (1983).

[28] W. L. BRAGG AND E. J. WILLIAMS. *Proc. Soc. London Ser. A*, **145**, 699 (1934).

[29] R K PATHRIA, P D BEALE. *Statistical Mechanics, Third edition* (Butterworth-Heinemann,The Boulevard, Langford Lane, Kidlington, Oxford, 0X5 1GB, UK, 2011).

[30] D. TER HAAR. *Collected Papers of L. D. Landau,p. 193.* (Pergamon, London, 1965).

[31] L. P. KADANOFF. *Physics*, **2**, 263 (1966).

[32] MEHRAN KARDAR. *Statistical Physics of Fields* (Cambridge Univresity Press, 2007).

[33] J. A. WHITE. *J Chem. Phys.*, **112**, 3236 (2000).

[34] J. A. WHITE AND S ZHANG. *J Chem. Phys.*, **99**, 2012 (1993).

[35] J. A. WHITE AND S ZHANG. *J Chem. Phys.*, **113**, 1580 (2000).

[36] Y. TANG. *J Chem. Phys.*, **109**, 5935 (1998).

[37] J. MI, C. ZHONG, Y. G. LI AND Y. TANG. *AIChE Journal*, **52**, 342 (2006).

[38] L. LUE AND J. M. PRAUSNITZ. *J. Chem. Phys.*, **108**, 5529 (1998).

[39] A. PAROLA AND L. REATTO. *Adv. Phys.*, **44**, 211 (1995).

[40] J. BERGES, N. TETRADIS, C. WETTERICH. *Phys. Rep.*, **363**, 223 (2002).

[41] D. PINI, G. STELL AND N. B. WILDING. *J. Chem. Phys.*, **115**, 2702 (2001).

[42] A. SAI VENKATA RAMANA AND S. V. G. MENON. *Phys. Rev. E*, **85**, 041108 (2012).

[43] R. EVANS. *Adv. in Phys.*, **28**, 143 (1979).

[44] G. R. GOLNER. *Phys. Rev. B*, **8**, 339 (1973).

[45] G. ORKOULAUS AND A. Z. PANAGIOTOPOULOS. *J. Chem. Phys.*, **110**, 1581 (1999).

[46] A. LOFTI, J. VRABEC AND J. FISHER. *Mol. Phys.*, **76**, 1319 (1992).

[47] A. Z. PANAGIOTOPOULOS. *Mol. Phys.*, **61**, 813 (1987).

[48] L.W. SALVINO AND J. A. WHITE. *J. Chem. Phys.*, **96**, 4559 (1992).

[49] ESTHER FORTE, FELIX LLOVELL, LOURDES F. VEGA, J. P. MARTIN TRUSLER AND AMPARO GALINDO. *J. Chem. Phys.*, **134**, 154102 (2011).

[50] P. M. W. CORNELISSE, C. J. PETERS AND J. DE SWAAN ARONS. *J. Chem. Phys.*, **106**, 9820 (1997).

[51] A. SAI VENKATA RAMANA AND S. V. G. MENON. *Phys. Rev. E*, **87**, 022101 (2013).

[52] Y. ROSENFELD AND N. W. ASHROFT. *Phys. Rev. A*, **20**, 1208 (1979).

[53] A. SAI VENKATA RAMANA AND S. V. G. MENON. *J. Chem. Phys.*, **139**, 044106 (2013).

[54] D.HENDERSON AND E.W.GRUNDKE. *J. Chem. Phys.*, **63**, 601 (1975).

[55] R.D.GROOT, J.P.VAN DER EERDEN AND N.M.FABER. *J. Chem. Phys.*, **87**, 2263 (1987).

[56] A.MALIJVESKY AND S. LABIK. *Mol. Phys.*, **60**, 663 (1987).

[57] S. LABIK, A.MALIJVESKY AND P.VONKA. *Mol. Phys.*, **56**, 707 (1985).

[58] J. LARGO, J. R. SOLANA, S. B. YUSTE AND A. SANTOS. *J. Chem. Phys.*, **122**, 84510 (2005).

[59] S. HLUSHAK, A. TROKHYMCHUK AND S. SOKOLOWSKI. *J. Chem. Phys.*, **130**, 234511 (2009).

[60] L. VEGA, E. DE MIGUEL, L. F. RULL, G. JACKSON AND I. A. MCLURE. *J. Chem. Phys.*, **96**, 2296 (1992).

[61] FERNANDO D. RIO, E. AVALOS, R. ESPINDOLA, L. F. RULL, G. JACKSON AND S. LAGO. *Mol. Phys.*, **100**, 2531 (2002).

[62] B. H. PATEL, H. DOCHERTY, S. VARGA, A. GALINDO AND G. C. MAITLAND. *Mol. Phys.*, **103**, 129 (2007).

[63] G. SARKISOV. *J. Chem. Phys.*, **114**, 9496 (2001).

[64] E. B. EL MENDOUB, J. F. WAX, I. CHARPENTIER, N. JAKSE. *Mol. Phys.*, **106**, 2667 (2008).

[65] C. EBNER, W. F. SAAM, AND D. STROUD. *Phys. Rev. A*, **14**, 2264 (1976).

[66] E. SCHOLL-PASCHINGER, A. L. BENAVIDES AND R. C. PRIEGO. *J. Chem. Phys.*, **123**, 234513 (2005).

[67] S. ZHOU, J.R. SOLANA. *Phys. Chem. Chem. Phys.*, **11**, 11528 (2009).

[68] A. GIL VILLEGAS, F. DEL RIO AND A. L. BINAVIDES. *Fluid Phase Equilibria*, **119**, 97 (1996).

[69] ARTHUR J. M. YANG, PAUL D. FLEMING AND JULIAN H. GIBBS. *J. Chem. Phys.*, **63**, 3732 (1976).

[70] JAYANT K. SINGH, DAVID A. KOFKE AND JEFFREY R. ERRINGTON. *J. Chem. Phys.*, **119**, 3405 (2003).

[71] R. LOPEZ-RENDON, Y. REYES, AND P. OREA. *J. Chem. Phys.*, **125**, 084508 (2006).

[72] L. VERLET. *Phys. Rev.*, **165**, 201 (1968).

[73] S. ZHOU. *AIP Advances*, **1**, 040703 (2011).

[74] S. ZHOU. *J. Chem. Phys.*, **138**, 244115 (2013).

[75] S. ZHOU AND J.R. SOLANA. *J. Phys. Chem. B*, **117**, 9305 (2013).

[76] S. ZHOU. *J. Chem. Phys.*, **139**, 124111 (2013).

[77] S. ZHOU AND J. R. SOLANA. *AIP advances*, **3**, 102103 (2013).

[78] A. SAI VENKATA RAMANA. *J. Chem. Phys.*, **140**, 154106 (2014).

[79] A. JEFFREY AND D. ZWILLINGER(EDS.). *Table of integrals, series, and products* (Academic Press, 2007).

[80] C. N. YANG AND C. P. YANG. *Phys. Rev. Lett.*, **13**, 303 (1964).

[81] M. E. FISHER AND G. ORKOULAS. *Phys. Rev. Lett.*, **85**, 696 (2000).

[82] G. ORKOULAS, M. E. FISHER AND A. Z. PANAGIOTOPOULOS. *Phys. Rev. E*, **63**, 051507 (2001).

[83] A. F. GHOBADI, J. R. ELLIOTT. *Ind. Eng. Chem. Res.*, **52**, 7030 (2013).

[84] X. TANG, J. GROSS. *J. Supercritical Fluids*, **55**, 735 (2010).

[85] J. R. ELLIOTT AND L. HU. *J. Chem. Phys.*, **110**, 3043 (1999).

[86] C. J. THOMPSON. *Progress of Theoretical Physics*, **87**, 535 (1992).

[87] A. F. GHOBADI, J. R. ELLIOTT. *J. Chem. Phys.*, **139**, 234104 (2013).

[88] C. AVENDANO, T. LAFITTE, A. GALINDO, C. S. ADJIMAN, G. JACKSON AND E. A. MULLER. *J. Phys. Chem. B*, **115**, 11154 (2011).

[89] A. PELISSETTO AND E. VICARI. *Phys. Rep.*, **368**, 549 (2002).

[90] G. S. RUSHBROOKE. *J. Chem. Phys.*, **39**, 842 (1963).

[91] R. B. GRIFFITHS. *J. Chem. Phys.*, **43**, 1958 (1965).

[92] Y. C. KIM. *Phys. Rev. E*, **71**, 051501 (2005).

[93] A PAROLA AND R. REATTO. *Mol. Phys.*, **110**, 2859 (2012).

[94] R. P. DRAKE. *High Energy Density Physics: Fundamentals, Inertial Fusion, and Experimental Astrophysics* (Springer, 2006).

[95] J. X. SUN, H. C. YANG,Q. WU AND L. C. CAI . *J. Phys. Chem. Solids*, **63**, 113 (2002).

[96] P. M. MORSE. *Phys. Rev.*, **34**, 57 (1929).

[97] SUN JIUXUN. *J. Phys.: Condens. Matter*, **17**, L103 (2005).

[98] A. S. V. RAMANA. *arXiv preprint*.

[99] R. C. LINCOLN, K. M. KOLIWAD AND P. B. GHATE. *Phys. Rev.*, **157**, 463 (1967).

[100] J. K. SINGH , J. ADHIKARI , S. K. KWAK. *Fluid Phase Equilibria*, **248**, 1 (2006).

[101] Z.-Y. LU AND R. HENTSCHKE. *Phys. Rev. E*, **63**, 051801 (2001).

[102] Z.-Y. LU AND R. HENTSCHKE. *Phys. Rev. E*, **65**, 041807 (2002).

[103] Z.-Y. LU AND R. HENTSCHKE. *Phys. Rev. E*, **67**, 061807 (2003).

[104] A. S. V. RAMANA. *Fluid Phase Equilibria*, **361**, 181 (2014).

[105] G. KRESSE, J. HAFNER. *Phys. Rev. B*, **47**, 558 (1993).

[106] G. KRESSE, FURTHMULLER. *J. Computat Mater Sci*, **6**, 15 (1996).

[107] G. KRESSE, FURTHMULLER. *Phys. Rev. B*, **54**, 11169 (1996).

[108] G. KRESSE,D. JOUBERT. *Phys. Rev. B*, **59**, 1758 (1999).

[109] H. J. C. BERENDSEN, J. P. M. POSTMA, W. F. VAN GUNSTEREN, A. DINOLA, AND J. R. HAAK. *J. Chem. Phys.*, **81**, 3684 (1984).

[110] A. Z. PANAGIOTOPOULOS, N. QUIRKE, M. STAPLETON, D. J. TILDESLEY. *Mol. Phys.*, **63**, 527 (1988).

[111] B. WIDOM. *J. Chem. Phys.*, **39**, 2808 (1963).

[112] DIVESH BHATT, A. W. JASPER, N. E. SCHULTZ, J. I. SIEPMANN, AND D. G. TRUHLAR.

[113] T. ALEKSANDROV, C. DESGRANGES, J. DELHOMMELLE. *Fluid Phase Equilibria*, **287**, 79 (2010).

[114] I. G. DILLON, P. A. NELSON, B. S. SWANSON. *J. Chem. Phys.*, **44**, 4229 (1966).

[115] J.P. STONE, C.T. EWING, J.R. SPANN, E.W. STEINKULLER, D.D. WILLIAMS, R.R. MILLER. *J. Chem. Eng. Data*, **11**, 309 (1966).

[116] E.I. GOLTSOVA. *High Temperature*, **4**, 348 (1966).

[117] J.P. STONE, C.T. EWING, J.R. SPANN, E.W. STEINKULLER, D.D. WILLIAMS, R.R. MILLER. *J. Chem. Eng. Data*, **11**, 314 (1966).

[118] V. MOREL, A. BULTEL, B. G. CHERON.

[119] S. BLAIRS, M. H. ABASSI. *J. Colloid Interface Sci*, **304**, 549 (2006).

[120] C. BOISSIERE, G. FIORESE.

[121] H. HESS. *Z. Metallkd*, **89**, 388 (1998).

[122] G. FAUSSURIER, C. BLANCARD, AND P. L. SILVESTRELLI. *Phys. Rev. B*, **79**, 134202 (2009).

[123] A. A. LIKALTER. *Physica A*, **311**, 137 (2002).

[124] V. MISHRA, S. CHATURVEDI. *Physica B*, **407**, 2533 (2012).

[125] J. A. CAHILL, A. D. KRISHENBAUM. *J. Phys. Chem.*, **66**, 1080 (1962).

[126] M.M. MARTYNYUK, O.G. PANTELEICHUK. *High Temperature*, **14**, 1201 (1976).

[127] R. W. OHSE, J. F. BABELOT, J. MAGILL, M. TENENBAUM. *Pure & Appl. Chem.*, **57**, 1407 (1985).

[128] N. B. VARGAFTIK. *Tables on thermodynamic properties of liquids and gases* (John Wiley & Sons, Inc., 1975).

[129] R. G. PARR AND W. YANG. *Density-functional theory of atoms and molecules (Vol. 16)* (Oxford university press., 1989).

[130] E. K. GROSS AND R. M. DREIZLER(EDS.). *Density functional theory (Vol. 337)* (Springer Science and Business Media., 2013).

[131] R. M. MARTIN. *Electronic structure: basic theory and practical methods.* (Cambridge university press., 2004).

[132] W. KOHN. *Reviews of Modern Physics*, **71**, 1253 (1999).

[133] A. D. BECKE. *J. Chem. Phys.*, **140**, 18A301 (2014).

[134] K. BURKE. *J. Chem. Phys.*, **136**, 150901 (2012).

[135] P. HOHENBERG AND W. KOHN. *Physical Review*, **136**, B864 (1964).

[136] M. LEVY. *Proc. Natl. Ac. Sci. USA*, **76**, 6062 (1979).

[137] W. KOHN AND L.J. SHAM. *Phys. Rev.*, **140**, A1133 (1965).

[138] P. A. M. DIRAC. *Proc. Cambridge Phil. Soc.*, **26**, 376 (1930).

[139] L. SPRUCH. *Rev. Mod. Phys.*, **63**, 151 (1991).

[140] E. P. WIGNER. *Trans. Faraday Soc.*, **34**, 678 (1938).

[141] O. GUNNARSSON AND B. I. LUNDQVIST. *Phys. Rev. B*, **15**, 6006 (1977).

[142] S. H. VOSKO, L. WILK AND M. NUSAIR. *Can. J. Phys.*, **58**, 1200 (1980).

[143] J. P. PURDUE. *Electronic Structure of Solids 91, edited by P. Ziesche and H. Eschrig, p. 11* (Akademie Verlag, Berlin., 1991).

[144] J. P. PURDUE, K. BURKE, M. ERNZERHOF. *Phys. Rev. Lett.*, **77**, 3865 (1996).

[145] C. HERRING. *Phys. Rev.*, **57**, 1169 (1940).

[146] N. W. ASCHROFT AND N. D. MERMIN. *Solid state physics, third edition* (Thomson Asia Pte Ltd., Singapore, 2005).

[147] P. E. BLOCHL. *Phys. Rev. B*, **50**, 17953 (1994).

[148] L. VERLET. *Phys. Rev.*, **159**, 98 (1967).

APPENDIX A

Calculation of zero Kelvin isotherm from density functional theory

We used the Vienna Ab-initio Simulation Package(VASP)[105–108] to calculate the zero Kelvin isotherm. VASP employs density functional theory(DFT) for electronic structure calculations and Born-Oppenheimer molecular dynamics. Here we are concerned with the DFT part of it. Vast amount of reviews and books exist[129–134] which explain DFT in great details and hence is not repeated here. However, the basic ideas of DFT to the extent used in our work and its implementation below is briefly mentioned below.

A.1 Density functional theory in nutshell

DFT is a powerful tool for electronic structure calculations in which the electron density ($\rho(\vec{r})$)[1] is used as the basic variable to describe the system instead of wave-function. That the $\rho(\vec{r})$ can be used as a basic variable to describe the system has been proved by Hohenberg and Kohn[135] by showing that the $\rho(\vec{r})$ and the external potential ($v_{ext}(\vec{r})$), which uniquely fixes the Hamiltonian of a many-electron system interacting with external field sources like Nuclei etc., are uniquely related except for an additive constant. Hohenberg and Kohn also proved that the $\rho(r)$ which minimizes the the energy functional is the ground electron density. These two theorems form the basis of density functional theory. In the proof of the variational principle, Hohenberg and Kohn assumed that the trial density is a density corresponding to some external potential (called $v - representable$ density). The conditions satisfied by

[1]This notation is only valid for this Appendix. Also, Hartree atomic units are used in this appendix.

such density are unknown and hence it is impractical to implement. Levy[136] later devised a variational principle which just requires that the density should give the total number of particles in the system upon integration over its volume (called $N-representalbe$ density) which is a looser restriction that can be handled.

The practical implementation of DFT became possible after the algorithm developed by Kohn and Sham[137] in which the system containing interacting electrons and nuclei(or ions etc.) is mapped onto a system of non-interacting electrons in an effective external field. The effective potential looks as follows:

$$v_{eff}(\vec{r}) = v(\vec{r}) + \int \frac{\rho(\vec{r'})}{|\vec{r} - \vec{r'}|} + v_{xc}(\vec{r}) \tag{A.1}$$

In the above, $v(\vec{r})$ is the external potential due to nuclei etc., second term is the Hartree interaction term and the third term is called the exchange correlation potential in which all the effects due to the exchange interaction of electrons and correlations between electrons are dumped. The approximations in DFT appear in modeling the $v_{xc}(\vec{r})$.

The simplest form of approximation is the local density approximation (LDA) in which

$$v_x(\vec{r}) = -\left(\frac{3\rho(\vec{r})}{\pi}\right)^{1/3} \tag{A.2}$$

is the exchange contribution and

$$v_c(\vec{r}) = -\frac{0.44}{r_s + 7.8} \tag{A.3}$$

where $r_s = \left(\frac{3}{4\pi\rho(\vec{r})}\right)^{1/3}$ is the correlation potential. $v_{xc} = v_x + v_c$. In obtaining the above forms it is assumed that the electron gas is locally homogeneous. The $v_x(\vec{r})$ is derived by Dirac[138] (as an extension of Thomas Fermi method[139] to include exchange) and $v_c(\vec{r})$ is obtained by Wigner[140] using Monte Carlo simulations. If the densities of the up and down spins are considered separately, then it is called local spin density approximation(LSDA). There are various functionals which include the exchange and correlation contributions within the LSDA like the Gunnarsson-Lundqvist functional[141], Vosko-Wilk-

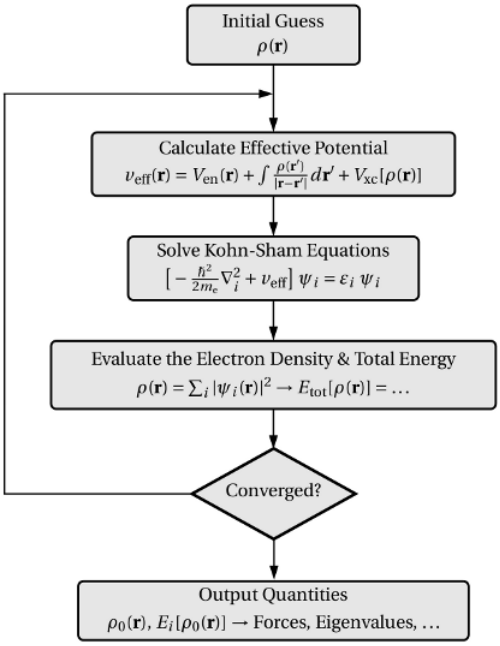

Figure A.1: Flow-chart for Kohn-Sham algorithm

Nusiar[142] functional etc.

The validity of local density approximation is accurate when the variation of density is slow compared to the Fermi wavelength. In an atom, this condition is not valid close to the nucleus and also asymptotically. In a molecule, cluster or a solid the condition is seriously violated. However, the calculations done using LDA are seen to predict the energies of the systems within $10-20\%$ deviation[132]. The big success of this method is that it predicts some quantities like the bond length in molecules, geometries within an accuracy of 1%. This has been observed as a consequence of cancellation of errors and the exchange hole sum rule being satisfied by LDA.

The exchange correlation functionals which go beyond the LDA are the generalized gradient approximation (GGA) functionals. The GGA functionals allow for local variation of density and their general form is

$$E_{xc}^{GGA}[\rho] = \int f(\rho(\vec{r}), |\nabla\rho(\vec{r})|)\rho(\vec{r})dr \tag{A.4}$$

Various parametrizations of GGA are available in literature. The VASP code incorporates the Purdue-Wang(PW)[143] functional, Purdue-Burke-Ernzerhof(PBE)[144]

functional and its revised forms. The PW and PBE analytical functionals are constructed satisfying some physical constraints. We have used the PBE functional for our calculation.

A flow-chart for Kohn-Sham algorithm is shown in Fig.(A.1).

A.2 Pseudopotential and projector augmented wave methods

Any system (an atom, a molecule or a solid) will have core-electrons which are tightly bound to the nuclei and valence-electrons which are loosely bound. The wavefunction of a core-electron ($\psi^c(r)$) is localized around the nucleus and rapidly varying with rapid oscillations because of high kinetic energy. The wavefunction of a valence electron ($\psi^v(r)$) is spreadout away from the nucleus but close to the nucleus there are again rapid oscillations because of high kinetic energy of the electron. The wiggles in the $\psi^v(r)$ close to nucleus can also be inferred from the orthogonality of the $\psi^v(r)$ with each of $\psi^c(r)$. The spreadout part of the $\psi^v(r)$ can be represented by smaller number of plane waves but the the part of it close to the nucleus having rapid oscillations requires a huge number of plane waves to be represented in plane wave basis. This makes the problem complicated and renders the plane wave basis inadequate. A workaround for this problem is the orthogonalized plane wave(OPW) method due to Herring[145]. In the OPW method, the $\psi^v(r)$ is expanded in a basis of OPWs instead of simple plane waves. An OPW is written as [146]

$$\phi_k(r) = e^{i\vec{k}\cdot\vec{r}} + \sum_c A_c {\psi^c}_k(\vec{r}) \tag{A.5}$$

The sum is over all core states ${\psi^c}_k(r)$ which are assumed to be known (for e.g., from tight binding calculation). The unknown A_c are obtained using the orthogonality of the valence state with each of the core states. The valence electron wavefunction $\psi^v(r)$ when expanded in terms of OPWs will contain a smooth part expanded in a plane wave basis and a rapidly oscillating part containing the core-electron wavefunctions.

The pseudopotential(PP) method and the projected augmented-wave (PAW) method have their origins the OPW method. The basic idea is that for most of the purposes the core- electrons are inert while valence electrons play an active role. Hence, if the singular Coulomb potential close to the nucleus is replaced by a smoother potential such that the valence electron wavefunctions outside the core region and their energies are not disturbed, the problem gets simplified and the calculations can be done using lesser number of plane waves. The ab-initio PPs are those which are obtained with atom as reference state and does not have any fitting parameters. The main advantage of the PP and PAW methods is the transferability. The PPs or PAWs obtained with atom as reference state are useful in other environments like a solid etc.

An elementary description of the PP method is as follows. In this method, the single electron Schrodinger equation (in this case the Kohn-Sham equation) for valence electrons is re-written in terms of the smooth part in the OPW expansion of the valence electron wavefunction ($\tilde{\psi}^v(r)$). In doing so, the complicated rapidly oscillating part involving the core-electrons energy levels and their eigenfunctions is absorbed into an additional term $V_R(r)$ in the potential which turns out to be always repulsive and thus smooths out the rapidly varying Coulomb potential in the core region of the nucleus and removes the singularity of Coulomb potential. The PP is

$$v_{PS}(\vec{r}) = v_{eff}(\vec{r}) + v_R(\vec{r}) \tag{A.6}$$

Because of the presence of core-electron wavefunctions, the v_R and hence the v_{PS} are non-local[1] There are various types of ab-initio PPs. The ultrasoft-pseudopotentials(USPP) and the norm-conserving pseudopotentials(NCPP) are the mostly used ones[131]. The NCPP are generated imposing stricter constraints like conserving the norm of pseudo and all electron wavefunctions etc. and hence are more transferable to other systems. However, for transition metals with highly localized orbitals, the cutoff radius for $\tilde{\psi}^v(r)$ becomes very small and the pseudo-potentials become "hard" requiring large number

[1]Both v_{PS} and v_R depend on angular momentum quantum number. They also called semi-local in the sense that the radial part is local.

of plane waves to expand. The USPP relax the norm conservation by include augmentation charges to balance the charge difference between all electron and pseudo wavefunctions. However, in this case, the transferability becomes less and more number of parameters are to be chosen.

The disadvantages of the PPs are to some extent avoided by the PAW method [147]. The PAW method basically introduces a transformation from the pseudo wavefunction to the all electron wavefunction. Using the transformation in a manner similar to changing the representation from Schroedinger picture to Heisenberg picture, all the expectation values of operators corresponding to the physical quantities can be obtained as expectation values of transformed operators in the space of pseudo wavefunctions. The Kohn-Sham equation is also re-written in terms of the pseudo wavefunctions and the transformation operator. Thus, the averages are equivalent to all electron averages and hence the accuracy of calculations is more than that of PPs.

The VASP code has the options to use NCPP, USPP and the PAW methods. In our calculations, we used the PAW data sets. The k-point grid is chosen by inspecting the convergence of total energy for each case. The energy cutoff typically used is $400eV$ and the energy convergence criterion is set to $10^{-6}eV$. The energy of an isolated atom has been obtained by taking a large unit cell. The obtained energy of an isolated atom is subtracted from total energy to get the cohesive energy.

APPENDIX B

Algorithms used in classical molecular dynamics

B.1 Velocity Verlet Algorithm

Let the simulation box contain N particles interacting with a pairwise additive potential $u(r)$. The position and velocity of each particle is advanced according to the following equations[148]

$$\begin{aligned} \vec{r}(t+\Delta t) &= \vec{r} + \vec{v}(t)\Delta t + \frac{1}{2}\vec{a}(t)(\Delta t)^2 \\ \vec{v}(t+\Delta t) &= \vec{v}(t) + \frac{1}{2}(\vec{a}(t) + \vec{a}(t+\Delta t))\Delta t \end{aligned} \tag{B.1}$$

where $\vec{r}(t)$, $\vec{v}(t)$ and $\vec{a}(t)(= \vec{F}_i/m)$ are position, velocity and acceleration at time t. $\vec{F}_i(= -\frac{\partial U}{\partial r_i})$ is the force on i^{th} particle.

$$U = \sum_i \sum_j u(r_{ij}) \ (i > j) \tag{B.2}$$

is the total potential energy. m is the mass of the particle. Δt is the time step which is generally chosen to be smaller than the fastest timescale in the system. The typical time step is $10^{-15}s$ (1 femto second). The velocity Verlet algorithm satisfies the basic qualities required for a molecular dynamics algorithm such as i) stability (allows for larger time step), ii) satisfying the laws of conservation of energy and momentum, iii) time reversibility, iv) fastness and ease of programming.

B.2 Berendsen Thermostat

The system is assumed to be weakly coupled to the thermal bath maintained at required temperature (T_{req})[109]. The system is evolved in such a way that

the instantaneous temperature T settles down to (T_{req}) at an exponential rate with time constant (τ). The temperature evolution is according to the following equation

$$\frac{dT}{dt} = \frac{T - T_{req}}{\tau} \tag{B.3}$$

Finite differencing the above equation, we get,

$$T(t + \Delta t) = T(t) + (\Delta t)\frac{T - T_{req}}{\tau} \tag{B.4}$$

The velocity of each particle at each step is scaled as below to implement the thermostat

$$\begin{aligned} v(t + \Delta t) &\rightarrow \sqrt{\frac{T(t + \Delta t)}{T(t)}} v(t + \Delta t) \\ &= \sqrt{1 + \frac{\Delta t}{\tau}\left(1 - \frac{T_{req}}{T}\right)} v(t) \end{aligned} \tag{B.5}$$

The Berendsen thermostat doesn't exactly simulate the trajectories of canonical ensemble. However, it yields the correct canonical ensemble averages. The value of τ is chosen to be a value much larger than Δt

B.3 Berendsen barostat

Analogous to Berendsen thermostat, the Berendsen barostat[109] also assumes that the system is weakly coupled with the pressure bath which is mimicked by the following equation

$$\frac{dP}{dt} = \frac{P - P_{req}}{\tau_p} \tag{B.6}$$

which is rewritten as

$$\frac{dV}{dt} = B\frac{P - P_{req}}{\tau_p} V \tag{B.7}$$

In the above equation, $V(t)$ is the volume of the box at time t and B is the bulk modulus. Finite differencing the above equation we get the scaling factor for

volume of the simulation box to be

$$\frac{V(t+\Delta t)}{V(t)} \approx \left(1 + B\frac{P - P_{req}}{\tau_p}\right)\Delta t \tag{B.8}$$

The coordinates of each particle are also scaled as follows

$$\vec{r}(t+\Delta t) \rightarrow \left(1 + B\frac{P - P_{req}}{\tau_p}\right) \tag{B.9}$$

Generally B is absorbed in τ_p and τ_p is chosen to be a value much larger than Δt.

B.4 Calculation of Thermodynamic Averages

B.4.1 Average energy

$$E = \left\langle \sum_i \frac{p_i^2}{2m} + \frac{1}{2}\sum_i \sum_j u(r_{ij}) \right\rangle \ (i \neq j) \tag{B.10}$$

where p is momentum. Angular brackets indicate time averaging. $r_{ij} = |\vec{r}_i - \vec{r}_j|$

B.4.2 Temperature

Instantaneous temperature T is calculated using

$$\sum_i \frac{p_i^2}{2m} = \frac{3}{2} N k_B T \tag{B.11}$$

Average is calculated by taking the time average of the above equation.

B.4.3 Pressure

Instantaneous pressure is calculated using the virial expression

$$P = \rho k_B T + \sum_i \vec{r}_i \cdot \vec{F}_i \tag{B.12}$$

where ρ is the number density.

B.4.4 Chemical potential

Chemical potential(μ) is the change in the Helmholtz free energy when a particle is added to or removed from the system. Chemical potential is calculated using Widom's test particle insertion method[111] according to which

$$\mu = -k_B T ln \left(\frac{\left\langle exp\left(\frac{-U_i}{k_B T}\right)\right\rangle}{\rho \lambda_D^3} \right) \tag{B.13}$$

In the above equation U_i is potential energy of the test particle. λ_D is the de-Broglie wavelength of the particle.